European Research Community On Flow, Turbulence And Combustion

www.ercoftac.org

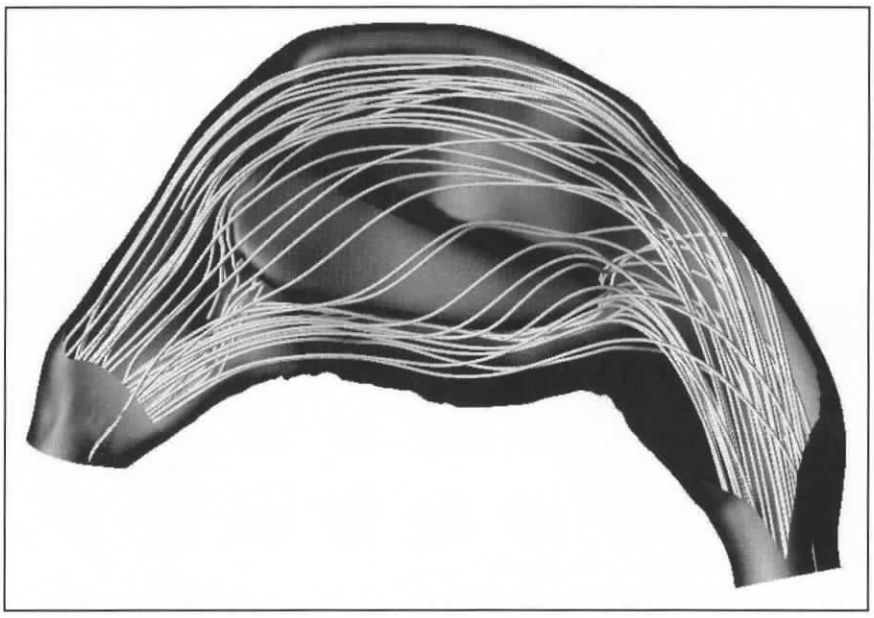

THEME - BIO FLUIDS

ERCOFTAC bulletin

68

MARCH 2006

ERCOFTAC

Honorary Presidents

Mathieu J., Spalding D.B., Vittoz B., Zienkiewicz O.

Managing Board Members

Executive Committee:

Oliemans R.V.A.	***Chairman*** — Multiphase Flow B.V., Bilthoven, NL Tel.: +31.30.229.1719, Fax: +31.15.278.2838
Rodi W.	***Deputy Chairman*** — Universität Karlsruhe, Karlsruhe, D
Hirsch Ch.	***Deputy Chairman*** —NUMECA, Brussels, B
Duursma R.P.J.	***Treasurer*** — CORUS, Amsterdam, NL
Ooms G.	***Deputy Treasurer*** — J.M. Burgers Centre, Delft, NL
Hunt J.	University College — London, UK
Hutton A.G.	QinetiQ — Farnborough, GB
Jacquin L.	ONERA-DAFE — Meudon, F
Laurence D.	UMIST — Manchester, UK / EDF — Chatou, F
Leschziner M.	Imperial College — London, UK

Anderson H.	NTNU — Trondheim, N
Binninger B.	ITM, RWTH — Aachen, D
Bonnet J.P.	Univ. de Poitiers — Poitiers, F
Bontoux P.	Univ. de Aix-Marseille — Marseille, F
Cambon C.	ECL/LMFA — Ecully, F
Carey Ch.	Fluent Europe Ltd — Sheffield, UK
Castilla R.	UPC — Barcelona
Chmielniak T.	Silesian Tech. Univ. — Gliwice, PL
Courty J.-C.	Dassault Aviation — Saint Cloud, F
Doerffer P.	Polish Academy of Sciences — Gdansk, PL
Eggels R.	Rolls Royce Deutschland — Dahlewitz, D
Haas J.-F.	CEA-DIF — Bruyères-le-Châtel, F
Kozel K.	CTU — Prague, CZ
Knörzer D.	CEC — Brussels, B
Kuhlmann H.	TU Wien — Vienna, A
Macek J.	CTU — Prague, CZ
Martelli F.	University of Florence — Florence, I
Menter F.	AEA Technology — Otterfing, D
Monkewitz P.	EPFL-LMF — Lausanne, CH
Redondo J.M.	UPC — Barcelona, E
Sick M.	VATECH — Zurich, CH
Spathopoulos T.	Hellenic Aerospace Industry — Schmitari, GR
Torre A.	Ansaldo Energia — Genova, I
Tatschl R.	AVL List GmbH — Graz, A
Van den Braembussche R.	VanKarman Institute — Rhode-St-Genèse, B
Vlachos N.	University of Thessaly — Volos, GR
Wagner C.	DLR — Göttingen, D
Wallin S.	FOI — Stockholm, S

Secretary	***Ursenbacher T.*** — ERCOFTAC Coordination Centre

Industrial Advisory Committee

Hutton A.G.	***Chairman*** — QinetiQ, Farnborough, GB Tel.: + 44 (0) 1252.395.568 Fax: +44 (0) 1252.395.322 E-mail: aghutton@QinetiQ.com
Laurence D.	***(Deputy Chairman),*** UMIST — Manchester, GB

The members of the IAC are the representatives of industrial members of ERCOFTAC.

Scientific Programme Committee

Leschziner M. ***(Chairman)***
Imperial College — London, UK

Tel.: + (0) 44.20.7594.5061
Fax: + (0) 44.20.7584.8120

Andersson H. — NTNU, Trondheim, N
Aupoix B. — ONERA, Toulouse, F
Braza M. — IMFT-CNRS, Toulouse, F
Cambon C. — ECL/LMFA, Ecully, F
Carey Ch. — Fluent Europe, Sheffield, UK
Cartage T. — Solvay S.A., B
Castro I. — Univ. of Southampton, UK
Choi K.S. — Univ. of Nottingham, UK
Courty J.-C. — Dassault Aviation, F
Dick E. — Universiteit, Gent, B
Doerffer P. — Polish Academy of Sciences, Gdansk, PL
Drobniak S. — TU-Czestochowa, PL
Duursma R.P.J. — CORUS, NL
Flohr P. — ALSTOM Ltd., Baden-Daettwil, CH
Geurts B.J. — Univ. Twente, Enschede NL
Haas J.F. — CEA, Bruyères-le-Châtel, F
Haase W. — EADS, München, D
Hanjalic K. — TU - Delft, NL
Hirsch Ch. — NUMECA, Brussels, B
Hunt J.C.R. — Univ. College London, UK
Kozel K. — CTU, Prague, CZ
Kuhlmann H. — TU Wien, Vienna, A
Menter F. — AEA Technology, D
Métais O. — IMG-LEGI, Grenoble, F
Monkewitz P. — EPFL-LMF, Lausanne, CH
Morvan H. — Univ. of Nottingham, UK
Oliemans R.V.A. — Multiphase Flow B.V., NL
Ooms G. — JMBC, Delft, NL
Orlandi P. — Universita di Roma, I
Peters B. — AVL GmbH, Graz, A
Peters N. — RWTH, Aachen, D
Redondo J. — UPC, Barcelona, E
Rodi W. — Universität Karlsruhe, D
Savill A.M. — Cranfield Univ. Cranfield, UK
Stelling G.S. — TU Delft, Delft, NL
Turan A. — UMIST, Manchester, UK
Van Steenhoven A. — TUE, Eindhoven, NL
Wagner C. — DLR, Göttingen, D

Secretary: Ursenbacher T.
Director : Monkewitz P.A.
ERCOFTAC Coordination Centre

LISTE OF CONTENTS

PAGE

THEME: BIO FLUIDS

Editorial 5
A.A. Van Steenhoven

Biomechanics of aquatic micro-organisms
T. J. Pedley 7

On The Geometry Dependence of the Nose Flow
I. Hoerschler, W. Schröder 13

Blood flow Measurements in Micro-Vessels
P. Vennemann, M. Pourquie, J. Westerweel 17

Geometrical Multiscale Modeling of the Cardiovascular System
A. Veneziani 21

Left Ventricular Fluid Dynamics
G. Pedrizzetti 25

Flow in Artificial Valves and Pulsatile Blood Pumps
U. Kertzscher, L.Goubergrits, K. Affeld 29

Thermal Problems in Hard and Soft Tissue Biomechanics
M. Stanczyk 33

Coupled Heat Transfer Processes in a Double Wall Infant Incubator
A.J. Nowak, M.K. Ginalski, L.C. Wrobel 39

Modelling Heat Transfer in Humans
A.J.H. Frijns, G.M.J. van Leeuwen, A.A. van Steenhoven 43

BULLETIN THEMES AND PC REPORTS 49
Past and Futur

ERCOFTAC SPECIAL INTEREST GROUPS 50
Contacts E-mails, Faxes and Phone Numbers

ERCOFTAC PILOT CENTRES AND OFFICES 51
Addresses, E-mails and Phone Numbers

EDITORIAL BOARD

Editor - T. Ursenbacher
EPF-Lausanne

E. Dick, ***Chairman***
Univ. of Gent

B.J. Geurts
Univ. of Twente

W. Elsner
TU Czestochowa

ADDRESS:
ERCOFTAC BULLETIN
ERCOFTAC C.C.
EPFL STI ISE ERCOFTAC
ME B2 495, Station 9
CH-1015 Lausanne
Tel: +41.21.693.5305
Fax: +41.21.693.5307
E-Mail: ercoftac@epfl.ch
http://www.ercoftac.org

SUBSCRIPTION FEE:
ERCOFTAC members: Free*
Non-members in Europe: € 140.-
Institutes outside Europe: € 75.-
*€ 60.- after first ten subscriptions per member organisation.
Libraries: enquiries to the above address.

The reader should note that the Editorial Board cannot accept responsibility for the accuracy of statements made by individual contributing authors.

CIRCULATION: 850 copies

TEXT PROCESSING AND LAYOUT:
Ruth Fiaux

FRONT COVER PICTURE:

Numerical prediction of the flow field streamlines inside the nose at expiration (flow from right to left) for nasal cavity geometry without spurs and with lower turbinate. Courtesy I. Hörschler and W. Schröder, Aerodynamisches Institut, RWTH Aachen (see paper "On the Geometry Dependence of the Nose Flow", pp. 13-16 in this Special Issue).

Deadline for submission of papers, announcements, letter to the editor

May 1st, 2006

Next issue scheduled for June 2006

THE PROCEEDINGS OF THE

10TH JOINT ERCOFTAC (SIG-15)/IAHR/QNET-CFD WORKSHOP ON REFINED TURBULENCE MODELLING

POITIERS, OCTOBER 10-11, 2002

Laboratoire d'études aérodynamiques
UMR 6609 CNRS/Université de Poitiers/ENSMA, France
Editors : R. Manceau, J.-P. Bonnet, M. A. Leschziner, F. Menter

Are Now Available in Electronic Form at

http://labo.univ-poitiers.fr/informations-lea/Workshop-Ercoftac-2002/Index.html

The proceedings include new results, detailed comparisons and comments written by R. Manceau, M. A. Leschziner and F. Menter

Further information: Remi.Manceau@lea.univ-poitiers.fr

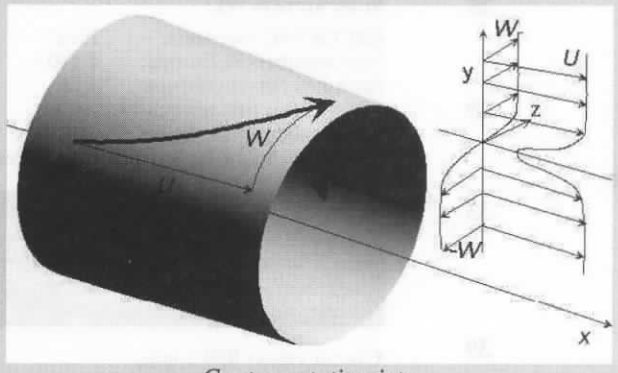

Contra-rotating jets (wake/mixing layer interaction)

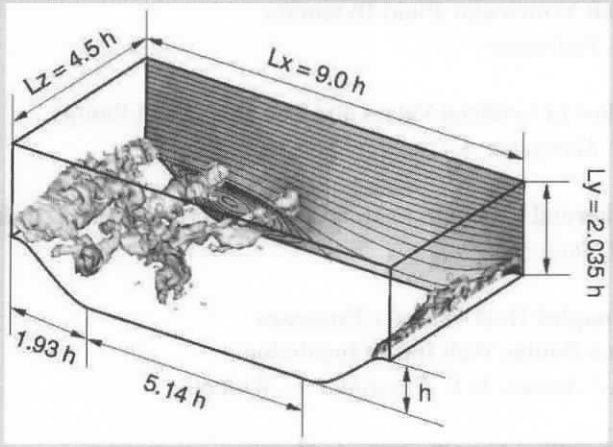

Periodic flow over a 2-D hill

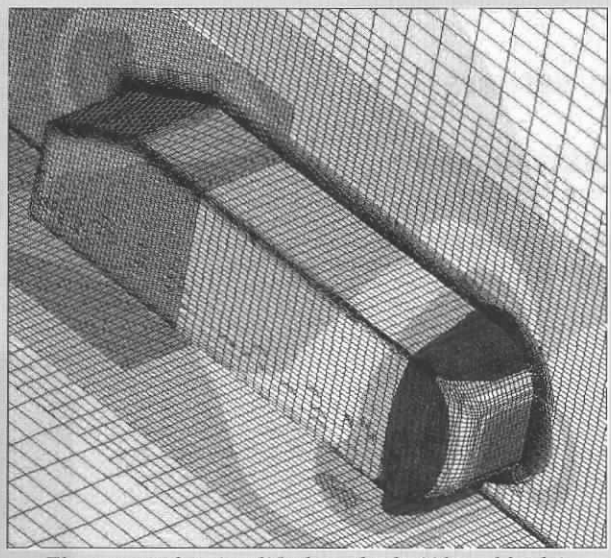

Flow around a simplified car body (Ahmed body)

THEME : BIO FLUIDS

EDITORIAL

A.A. van Steenhoven
J.M. Burgers Centre
Eindhoven University of Technology
The Netherlands
a.a.v.steenhoven@tue.nl

Most biological organisms live in a flowing medium (air or water). During evolution natural selection has found solutions for fluid mechanical problems regarding aquatic and aerial locomotion by organisms ranging in size from single cells to the blue whale. Similarly fluid flow is essential inside the human body, where the blood is pumped around and the air is inhaled. Atherosclerotic plaque formation at well-determined positions in arteries and veins, and gene activation at cellular levels are all influenced by fluid mechanic processes. Diagnostic and therapeutic techniques make use of fluid mechanic and heat transfer knowledge. Examples of the latter are the development of heart valves and the monitoring of temperatures inside the body during surgery.

The complicated geometrical structures in biology and the combination of phenomena (for example the transitional flow of non-Newtonian media in elastic bifurcating channels like blood vessels) form an exciting new area for the development of advanced modelling and experimental techniques. For example, micro- PIV systems are needed to analyse the flow field in micro-vessels and physical models of the fluid flow in the body may also lead to new concepts for non-invasive diagnostic and therapeutic techniques. Also the settlement and growth of settlements in aquatic ecosystems require the combination of advanced flow and mass transport models.

This issue of the Ercoftac Bulletin on Bio-fluid Mechanics and Heat Transfer offers an overview of ongoing research projects in this challenging field. The 8 articles, originating from 5 countries, describe problems ranging from external aquatic flow and flow in the nasal cavity to several analyses of blood flow in the cardiovascular system and of biological topics where temperature plays a major role.

I hope you will enjoy reading and at the end agree with me that this theme is an excellent area for collaboration between research groups from inside and outside the fluid-mechanics community. Besides, the evolutionary solutions found in biological systems are intriguing to understand and may lead to new solutions for technical problems!

ERCOFTAC

Design Optimisation:

Methods & Applications

Las Palmas de Gran Canaria, Spain

April 5 –7, 2006

http://ceani.ulpgc.es/ercoftac06

Backround

The goal of the conference is to foster the spread of single and multidisciplinary design optimisation technology in Europe. It is intended to be a platform for information exchange between research, science and industry. An important goal is to provide large and small scale companies not currently engaged in computer optimisation with an overview over existing methodologies and tools. Thus the conference is organised to:

- Present scientific ideas aiming at supporting design optimisation needs.
- Communicate the experience in the application of optimisation technology.
- Foster communication between industry and academia.
- Discuss new concepts.
- Give an overview over existing methods and associated software.

The conference targets all applications dealing with CFD, CSM, CEM, Power Generation and Environmental Optimisation problems.

A participation of "non-experts" as well as young technologists and scientists recently involved in the field of optimisation is strongly encouraged.

In order to 'close the gap between theory and application', code-vendors are solicited to join in. They will receive the opportunity to present their software tools at own stands.

Organisation

- Las Palmas de Gran Canaria University
- Lab. of Evolutionary Computation and Applications (CEANI) of the IUSIANI Research Institute
- ERCOFTAC Special Interest Group in Design Optimisation

The conference will be chaired by

Chairman:	Prof. G. Winter (IUSIANI)
Co-chairman:	Dr. W. Haase (EADS-M)
Co-chairman:	Dr. J. Periaux (IUSIANI/ULPGC Consultant)

Local and Scientific Organising Committee

Prof. J. Emperador, ULPGC, IUSIANI
Prof. B. Galvan, ULPGC, Director of CEANI
Dr. B. Gonzalez, ULPGC, CEANI
Dr. D. Greiner, ULPGC, CEANI
Prof. J. Periaux, IUSIANI/ULPGC Consultant
Prof. G. Winter, ULPGC, Director of IUSIANI

Call for Papers

A 'Call for Papers', is available on the ULPGC site: http://ceani.ulpgc.es/ercoftac06

Important Dates

15 September 2005	Call for Abstracts
30 December 2005	Abstract deadline
15 February 2006	Acceptance notification
5-7 April 2006	Conference

INSTITUTE OF INTELLIGENT SYSTEMS AND NUMERICAL APPLICATIONS IN ENGINEERING (IUSIANI)

Campus Tafira, 35017 LAS PALMAS, SPAIN
Tel: +34 928 45 4599 / -1925, Fax: -1921

BIOMECHANICS OF AQUATIC MICRO-ORGANISMS

T.J. Pedley
Department of Applied Mathematics and Theoretical Physics
University of Cambridge
t.j.pedley@damtp.cam.ac.uk

1 Introduction

Aquatic micro-organisms, many of which are active swimmers, play a vital role in life on earth. Phytoplankton (algae, diatoms, etc: length scale 10-100μm, are the bottom link of the food chain in oceans and lakes, absorbing energy from sunlight and elementary nutrients from the water. They contain and are surrounded by even smaller bacteria (2-10μm) which break down metabolites and detritus into those elementary nutrients and no doubt have many other effects which have not been described. The phytoplankton are themselves the prey for somewhat larger micro-organisms (zooplankton such as ciliates and heterotrophic flagellates)which in turn are eaten by larger zooplankton such as copepods (small crustacea) which are eaten by fish larvae and adult fish, and so on. The phytoplankton absorb CO_2 from the water, most of which comes from the atmosphere via complex mixing processes, and thus they play an important role in the global carbon cycle and hence in phenomena such as global warming. Every spring, in every ocean, there are massive phytoplankton blooms (population explosions) which underlie the ecology of all aquatic species and need to be understood for fisheries prediction, for example. Harmful algal blooms also occur in coastal waters ('red tides') and can lead to economic damage to coastal communities that rely on shellfish. Some micro-organisms are used by biotechnologists to make chemicals, or are used as a direct source of biomass in large bioreactors. Thus the study of micro-organism behaviour is a proper subject for scientific investigation.

The complex food web of an oceanic ecosystem does not lend itself readily to comprehensive computational simulation; the number of species is far too large, as is the number of ways in which they can interact. In order to get a feel for the sort of effects that can arise in such a web, idealised models have been proposed. One such is outlined in figure 1 [1]. Organisms are arranged in two rows of three categories each. Members of the lower row consume nutrients and are themselves consumed by members of the top row which are also linked by predator-prey interactions. A model of the interactions consists of a set of nonlinear ordinary differential equations. For example, the population density of ciliates (C) is governed by an equation of the form:

$$\frac{dc}{dt} = Y_c(g_{CA} + g_{CH})C - g_{ZC}Z \quad , \qquad (1)$$

where Y_C is the ciliate yield and the g's are functions in which g_{PQ} means the rate at which species P grazes on species Q (the symbols A,H,Z are defined in figure 1). Examples of the sort of functions involved are:

$$\begin{aligned} g_{CA} &= \frac{\lambda_c A^2}{\mu_c(A+H)+A^2+H^2} \\ g_{BN} &= \frac{\lambda_B N}{\mu_B + N} \end{aligned} \qquad (2)$$

where the λs and μs are constants.

These are standard models, but it is worth asking where the functional forms and constants come from. In other words, how should the macroscopic, population-level model be derived from individual behaviour, which itself can be investigated in detail? This article will outline briefly some of the fluid mechanical aspects which have been or are being investigated to shed light on both the individual and the collective behaviour of swimming micro-organisms. There will be a natural but perhaps undesirable emphasis on work in which the writer has been involved; readers should take these as examples of the sort of research that may be of interest rather than an exclusive definition of the field.

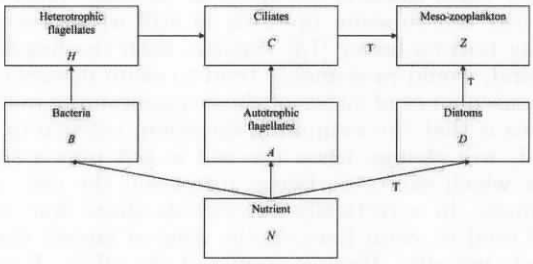

Figure 1: A "minimum model" for plankton population dynamics. Arrows between boxes represent predator-prey interactions; the letter T by an arrow means that turbulence may have an influence [1, 2].

2 Individual behaviour

The question of how micro-organisms swim has attracted fluid dynamicists for over 50 years, the pioneers being G.I. Taylor [3] and James Lighthill [4]. The Reynolds numbers of the cells in question, and of their moving appendages, are very small so inertia is negligible. It follows that the appendages cannot execute purely reversible motions if the cells are to make progress. Biflagellate algae such as *Chlamydomonas spp* execute a sort of low-Reynolds-number breaststroke; monoflagellates and sperm send unidirectional waves along their flagella; bacteria generate thrust from a bundle of *rotating*, fairly rigid flagella; ciliates beat large numbers of cilia in the form of co-ordinated waves. The hydrodynamics of such propulsive devices was first investigated using the rather crude (but extremely useful) *resistive force theory* [5,6], according

to which the normal and tangential components of the force exerted on the fluid by one short segment of a beating flagellum are directly proportional to the normal and tangential components of the velocity of that segment relative to the fluid far away, but with different, constant, coefficients of proportionality K_N and K_T(K_N is nearly twice as large as K_T for a segment of a circular cylinder). The next level of sophistication is to use slender body theory [4,7,8,9], and these days it is feasible to do complete simulations using the boundary element method [10].

If an organism is neutrally buoyant then the net force acting on the whole organism is zero, an important constraint in the theory. If it is homogeneous, then the net torque on the organism must also be zero. However, most micro-organisms are denser than water and tend to sediment, though at a speed that is much smaller than their swimming speed. For example, dead *Chlamydomanas nivalis* sediment at about $3\mu m\ s^{-1}$ while live ones swim at over $50\mu m\ s^{-1}$. In addition, *C. nivalis* naturally tend to swim upwards, on average, against gravity (though individual trajectories are very erratic). This is probably not because they have a sophisticated molecular "gravi sensor": there are at least two passive mechanical mechanisms that can cause them to do so.

The first and most popular is that they are bottom-heavy, so a deviation from the vertical generates a gravitational torque that rotates them back towards the vertical again (albeit slowly, against the viscous torque set up by such rotation) [11, 12]. An alternative proposed mechanism, that has the same effect, is based on a cell's asymmetric shape rather than its asymmetric mass distribution: as *C. nivalis*, for example, sediments slowly relative to the fluid, the drag on its (beating)flagella will exert a torque to rotate them towards the upwards vertical, thus causing the cell to swim upwards in still water without being bottom-heavy [13]. Sperm, with the flagellum behind, would presumably tend to swim downwards. A consequence of either of these upswimming mechanisms is that the swimming direction, relative to the fluid, will change when the cell is put into a shear flow which exerts a viscous torque on the cell. For example, in a vertically downwards shear flow, cells will tend to swim towards the zone of largest downwards velocity. Having predicted the effect, Kessler observed it in a downwards pipe flow, in which cells were focused in a thin green line on the axis [11].

As stated above, bacteria generate thrust and thereby swim in a roughly straight line, by rotating a sort of corkscrew behind them. This corkscrew is formed from a number of individual flagella each of which rotates in its socket in the cell membrane. They come together when the rotation is counter clockwise. From time to time (stochastically) the flagellar motors turn clockwise. Then the flagella can no longer fit together; they fly apart, and the cell tumbles, setting off on a run in a new direction [14]. The details of this process have been thoroughly investigated only for *Escherichia coli* (a gut bacterium) but it is presumed that other bacteria behave similarly. How the rotating flagella come together in a bundle when rotating counter clockwise is itself a fluid mechanical problem. Recent studies suggest that bundling could occur passively if the flagella were slightly flexible [15,16], but there is more detailed work to be done.

It is known that bacteria exhibit chemotaxis - a tendency to swim up gradients of chemoattractant (food). However, they are too small to be able to measure concentration gradients directly [17], so how do they know to swim up the gradient? The mechanism (in *E. coli at least*) requires (a) that they can measure concentration (i.e. "knowing" how many chemoreceptors on their surface are occupied), (b) they they can remember it for a short time, so that they can tell whether the concentration is rising or falling with time, and (c) they can, in consequence, alter the probability of tumbling according to the answer to (b). In fact this is what they do: the tumbling rate falls when they are swimming up a gradient, and rises when they are swimming down it [18]. How the chemotaxis process is affected when the bacteria are in a shear flow, which will rotate them, has not been investigated experimentally, but has been analysed theoretically [19,20]. It is predicted that there are circumstances in which they swim the wrong way!

The functions of equation (2) require that we know the rate at which organisms take up nutrient from the water (an equivalent problem concerns the output of unwanted metabolites, or mate-attracting pheromones). Even for individual cells, this problem exhibits interesting features which have not all been resolved. If the organism is small enough then adequate nutrient uptake can be achieved, in still water, by pure diffusion. However, larger organisms need to enhance this rate, and can do so by moving through or stirring the fluid around them [21].

A precise analysis of how low-Reynolds-number stirring motions can enhance nutrient uptake has been undertaken for a very simple model of a microorganism: a spherical 'squirmer', which propels itself through th fluid by driving a tangential motion along its surface [22,23]. This model was chosen for its simplicity, not because it was meant to represent a real organism (though it is not too bad a representation of the envelope of cilia tips in certain ciliates, or algal colonies like *Volvox*, or cyanobacteria such as the *Oscillatoriaceae*. The velocity field of a 'steady squirmer' is represented by a two-term series of solutions to the Stokes equations, in which the surface velocity on $r = a$ is given by:

$$\begin{aligned} U_r &= 0, U_\theta = \sum_{n=1}^{2} B_n V_n(\theta); V_n(\theta) \\ &= \frac{2}{n(n+1)} sin\theta P_n'(cos\theta) \end{aligned} \tag{3}$$

where (r, θ) are spherical polar co-ordinates, a is the sphere's radius, and the P_n are Legendre polynomials. In this two-term series, B_1 is proportional to the speed at which the squirmer swims, U, and B_2 is proportional to the force-dipole, or stresslet, that it exerts on the fluid.

In [22] the advection-diffusion equation for solute concentration C, in the velocity field of the squirmer, was solved numerically subject to the boundary conditions $C \to 1$ as $r \to \infty$, $C = 0$ on $r = a$. After non-dimensionalisation the results could be expressed as plot of the Sherwood number Sh as a function of the Péclet number Pe for different values of the 'squirming parameter', $\beta = B_2/B_1$. Here Sh is the ratio of the actual nutrient uptake to the value it would have through pure diffusion in a still fluid ($4\pi aD$), where D is the solute diffusivity); $Pe = Ua/D$ is the ratio of advection to diffusion. Asymptotic solutions can be found for small and for large Pe. The results are compared with those for a rigid sphere driven through the water at the same speed, U, by an external force. The results confirm that squirming has negligible ef-

fect on the mass transport unless $Pe > 0.2$, but as Pe rises the effect of squirming becomes more and more important, as the concentration boundary layer on the body surface becomes thinner. Indeed, for large Pe it is shown that $Sh \propto Pe^{1/2}$, not $Pe^{1/3}$ as for a rigid sphere.

One question that needs to be addressed is whether a constant C boundary condition is appropriate on the surface of a micro-organism? There may be some parts of an organism's surface across which uptake is much faster than others so the surface concentration is non-uniform. Alternatively, it might be more appropriate to consider the organelles within the cell as sinks of solute, consuming it at a rate proportional to its concentration. Then, at high Péclet number, when the resistance to mass transport in the fluid is low, the rate-limiting step would be the rate at which the cell could metabolise the solute. It was shown in [22] that in that case the Sherwood number at high Péclet number does not increase indefinitely but tends to a constant (albeit much greater than 1).

The value of Pe for an algal cell of radius $10\mu m$, swimming at $50\mu ms^{-1}$, with a small solute of diffusivity $10^{-9}m^2s^{-1}$, is only 0.5, so the effect of swimming or stirring is small. However, spherical colonies of *Volvox* can be as big as $150\mu m$ in radius, and generate fluid motions of $100\mu ms^{-1}$, so for them the Péclet number is quite large and the fluid flow driven by their flagella is very important for nutrient uptake[24].

Another aspect of nutrient uptake by small organisms is that of predator-prey dynamics. At what rate do microzooplankton encounter and consume their phytoplankton prey? And how is this affected by turbulence in the ambient fluid? The first coherent models of these processes, in two papers that are already classics, were by Gerritsen & Strickler and by Rothschild & Osborn [25,26]. The model was based on a consideration of the volume of fluid swept out by a swimming predator. If it swims in a straight line at constant speed in still fluid, and if the prey do not swim, then it will encounter all prey within a cylinder of radius R around its trajectory, where R is the "contact radius", the furthest distance at which it perceives its prey. Thus the encounter rate (number of contacts per unit time) is $\pi R^2 V_p N_H$, where V_p is the predator's swimming speed and N_H is the number density of prey. This simple swept-volume model can be modified to account for randomly oriented prey swimming and for turbulence; Rothschild & Osborn obtained the following formula for the contact rate;

$$CR = \pi R^2 N_H (V_p^2 + V_H^2 + 2W^2(r))^{1/2}, \qquad (4)$$

where V_p, V_H are the *average* predator and prey swimming speeds and $W(r)$ is a scale for the difference in turbulent fluid velocities at two points separated by a distance r. It was not clear whether r should be chosen equal to R or not.

There were some over-simplifications in the Rothschild and Osborn model, so Lewis & Pedley [27] set out to modify it and, more importantly, to test the modified model against a numerical simulation. The simulation consisted in placing a number of predator and prey individuals randomly in a periodic box and allowing them to swim with random speeds and orientations (according to specified probability distributions), recording an encounter when they came within a distance R of each other. The fluid was also moving randomly, with a turbulent-like incompressible velocity field specified by a Fourier series, whose terms had randomly selected wave number, frequency and amplitude such that the energy spectrum was the same as for isotropic, homogeneous turbulence. Two-point correlations were not controlled so this velocity field was different from real turbulence. However, that would have required enormous computer resources, for reasonable Reynolds numbers, as can be seen from the corresponding work of Yamazaki [28]. The main result, in the event, was that the modified swept-volume model (with $V = R$ in equation (4)) agreed rather well with the full simulations in predicting encounter rates; the value of the model is that it is analytical and can be used to specify the functional forms required in equation (1).

However, encounter is not the whole story. To predict prey capture it is necessary to specify the probability of capture, given that encounter has occurred. A simple model for this [29] led to the interesting, if not surprising, result that if turbulence is weak or the time taken for capture is small, then it pays the predator to swim in order to catch prey. However, if turbulence is strong or capture efficiency low, there is a tendency for the prey to be swept away before it can be captured, so it does not pay to swim; it is better to stay still (relative to the fluid) and wait for prey to come to you. Examples of both 'cruise' and 'ambush' predators are recorded in the literature.

3 Collective behaviour

We turn now to the fluid dynamic behaviour of populations of swimming micro-organisms, in particular the phenomena of *bioconvection*. Bioconvection patterns are observed in shallow suspensions of randomly, but on average upwardly, swimming micro-organisms which are a little denser than water. Images of typical bioconvection patterns formed by suspensions as single-celled algae and bacteria can be found in [12]. The basic mechanism is analogous to that of Rayleigh-Bénard convection, in which an overturning instability develops when the upper regions of fluid become denser than the lower regions. The reason for the upswimming however depends on the species of micro-organism: some algae are bottom-heavy, (see above) while certain oxytactic bacteria, such as *Bacillus subtilis*, swim on average up oxygen gradients that they generate by their consumption of oxygen.

The rational continuum modelling of bioconvection is dilute suspensions (volume fraction of cells $<$ 0.001) has been fully described in many original papers and, in particular, in two review articles [30,31]. Here we concentrate on aspects of the phenomena or the modelling that are not completely understood.

In a continuum model it is assumed that every volume element, small compared with the scale of the bulk flow, contains very many cells, so that variables such as the cell number density n or the bulk velocity $\mathbf{u}$ can be represented by their averages over the volume element. They can thus be taken to be smooth functions of position and time t.

Averaging has to be done with care, because the cells swim randomly - i.e. each cell undergoes a (biased) random walk, and each random walk is independent of the trajectories of other cells. Data on the trajectories of *C. nivalis* in still fluid are shown in figure 2, from the authors of [32], where the vector from the origin to a cross represents the vertical projection of a 1.1 second segment of a trajectory. The bias to upswimming is clear.

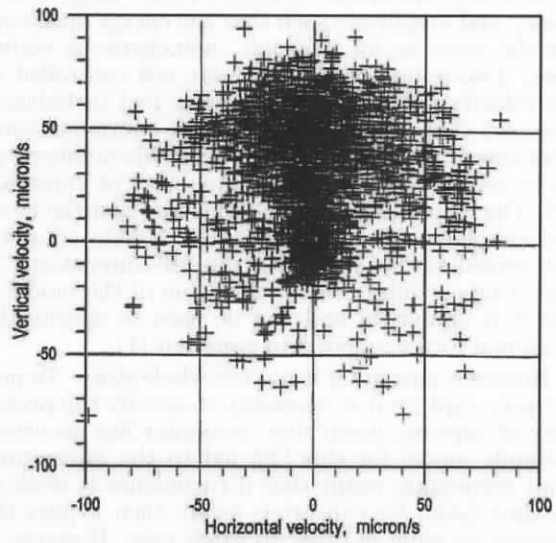

Figure 2: Projections of the velocity vectors of 1.1 sec segments of trajectories of C. nivalis, represented by the vector from the origin to the centre of each cross (see [32]).

Perhaps the most important equation in the continuum model is the cell conservation equation:

$$\frac{\partial_n}{\partial t} = -\nabla \cdot [n(\mathbf{u} + \mathbf{V}_c) - \mathbf{D} \cdot \nabla n], \qquad (5)$$

where $\mathbf{V}_c$ is the average cell swimming speed, representing directed cell swimming, and the last term represents the flux due to random cell swimming, here modelled as a diffusive process. Both $\mathbf{V}_c$ and $\mathbf{D}$ can be calculated if we know the probability distribution for cell swimming velocity, incorporating both magnitude and direction. The data in figure 2 provide information on this distribution, in one case. However, assuming that the cell swimming *speed* was constant, that the random reorientation experienced by a cell was independent of its current orientation and that the time-scale for such reorientation was small compared with any other time-scale of interest, Pedley & Kessler [33] proposed that the p.d.f. f(**p**)for swimming direction **p** (a unit vector) should satisfy a quasi steady Fokker-Planck equation. The solution of that equation for bottom-heavy algae in a still fluid is

$$f(\mathbf{p}) = \mu e^{\lambda \mathbf{k} \cdot \mathbf{p}} \qquad (6)$$

where the unit vector $\boldsymbol{k}$ is vertically upwards, and λ, μ are constants, which is reasonably consistent with figure 2.

When the fluid is moving, the Fokker-Planck equation can still be used to find f **(p)** if it is possible to write down an equation for $(\dot{\mathbf{p}})$, the rate of change of , in the absence of the random reorientations. This is straight-forward for the bottom heavy algae, because $\dot{\mathbf{p}}$ is determined by the balance between gravitational and viscous torques and the latter can be evaluated for any ambient shear flow. However, we do not have an equation for $\dot{\mathbf{p}}$ in the case of chemotactic bacteria, because the chemotaxis process cannot be expressed in terms of a torque balance. In addition, there is no general guarantee that random swimming can be represented as a diffusion process.

In the standard model of chemotaxis in a still fluid, first proposed by Keller and Segel [35], the cell swimming term in (5) is given by $V_c = \chi \nabla C$, where C is the chemoattractant distribution (for which, in general, another conservation equation is required) and χ is a scalar chemotaxis parameter. The main objective of the thesis work of Bearon [19,35] was to see under what circumstances equation (5) can still be used for run-and-tumble, chemotaxis in a shear flow, with some rational choice for V_c. The investigation was highly probabilistic, starting from a master equation for $\Psi(\mathbf{p}, \mathbf{x}, \mathbf{t})$, the number density of cells with swimming direction $\mathbf{p}$ at position $\mathbf{x}$ and time t.

The master equation can be integrated to give an equation of the form

$$\frac{\partial n}{\partial t} = -\mathbf{u} \cdot \nabla n - \nabla \cdot \mathbf{J} \qquad (7)$$

(cf eq.(5)), where $n = \int \Psi d^2\mathbf{p}$ and the flux $\mathbf{J}$ is the first moment of the Ψ distribution ($\mathbf{J} = \int \Psi \mathbf{p} d^2\mathbf{p}$). One can also obtain an equation for $\partial \mathbf{J}/\partial t$ but that involves the second moment, etc. It is a particular closure assumption that the second moment can be represented as a diffusive term; in general this may not be done. The findings of [35], briefly, were that the closure could be performed, and the Keller-Segel model used in a general shear flow, only if the perturbation to isotropic tumbling were small enough and if the vorticity in the flow were much less than the tumble rate. What to do in a general flow is still very unclear.

All the research referred to above has been restricted to dilute suspensions, in which cell-cell interactions are neglected. However, there is an increasing body of experimental evidence that some very interesting hydrodynamic phenomena arise in concentrated suspensions, mainly of swimming bacteria (*B. subtilis*). Mendelson et al [36] observed a population of *B. subtilis* swimming in a thin liquid layer on top of an agar gel, and reported a rich structure of meso-scale motions (by which is meant motions on length-scales intermediate between the population as a whole and the size or spacing of individual cells)which they called "whorls and jets". Dombrowski et al [37] also observed meso-scale motions in three-dimensional concentrated suspensions of *B. subtilis*. These are not yet understood.

One approach to modelling concentrated suspensions is by means of a continuum model in the form of a *mixture theory*, in which the cells and the suspending fluid are regarded as two co-existent continua, interacting via the laws of mechanics. This approach was well-explained in the context of shear flows of suspended rigid spheres by Nott & Brady [38]. A version of the theory was applied to two-dimensional bacterial populations by Lega & Passot [39]. Such theories raise a number of awkward questions, such as what do we mean by the concepts of "pressure" and "viscosity" in the continuum representing particles or cells? Moreover, Lega & Passot triggered the motion of their mixture by applying a random (white noise) external force to the particles, despite the fact that a neutrally buoyant swimming cell experiences zero net force. Nevertheless, the simulation reported by these authors did exhibit meso-scale motions. The mixture-theory approach needs to be followed up in greater depth.

Another approach to modelling suspensions in which hydrodynamic cell-cell interactions are important is being followed by Dr T. Ishikawa and myself. It involves simulations in which each cell is followed as it moves and in which the interaction with other

cells is analysed in a pairwise manner. Real microorganisms are too complicated for their geometry and kinematics to be represented accurately in a simulation of many cells. Instead we have gone back to the "steady squirmer" introduced above. Each 'cell' is an identical spherical squirmer, of radius a, swimming according to equation (3) with a given swimming speed U and squirming parameter β. An additional possibility is to allow the cells to be bottom-heavy, in gravity $\mathbf{g}$. The only distinction between different individuals is their orientation, or swimming direction, $\mathbf{p}$. The first step in the simulation is to calculate the trajectories of pairs of interacting squirmers in the absence of others. This is done by computing the virtual or *effective force* applied to one squirmer by the presence of another, for arbitrary initial orientations and relative position. In the far field the effective force can be calculated analytically, as it can in the very near field, when the squirmers are nearly touching and lubrication theory can be used. In between the calculation is performed numerically, using the boundary element method. A database of the results, covering the space of orientations and relative positions more-or-less uniformly, has been compiled and is used to speed up the simulations of larger numbers of spheres [40]. The macroscopic simulations are performed for random conditions in a cubic domain, extended by the use of periodic boundary conditions to represent an infinite domain. They have been used to compute (a) the effect of squirming on the rheology of a suspension of neutrally buoyant spheres in a simple shear flow [41] and (b) the mean square displacement of individual spheres: is the spreading diffusive or not [42]? In both cases a volume fraction of 0.1 is taken as typical. The answer in (a) is that squirming has a negligible effect on Batchelor's [43] results for the viscosity of a suspension of rigid spheres up to $O(C^2)$, when the squirmers are not bottom-heavy, but a significant effect when they are bottom-heavy, depending on the orientation of the shear flow relative to $\mathbf{g}$. In that case there can also be significant non-Newtonian normal stresses. In (b), the answer is that the spreading apart of non-bottom-heavy squirmers *is* correctly described as a diffusive process (i.e. their mean square displacement increases linearly with time t at large times), despite the fact that all the squirmers' motions are calculated deterministically. However, this is valid only for time-scales greater than about 30 a/U. Current research is extending these and similar results to larger volume fractions.

Bibliography

[1] Metcalfe, A.M., Pedley, T.J. & Thingstad, F. *J. Mar. Syst.* **49**: 105-122,2004

[2] Alcaraz, M., Marrasé, C., Peters, F., Arin, L. & Malits, A. *Mar. Ecol. Prog. Ser.* **242**: 63-71,2002

[3] Taylor, G.I. *Proc. R. Soc. Lond. A* **209**: 447-461, 1951

[4] Lighthill, J. *SIAM Rev.* **18**: 161-230, 1976

[5] Gray, J. & Hancock, G.J. *J. Exp. Biol.* **32**: 802-814, 1955

[6] Jones, M.S., LeBaron, L. & Pedley, T.J. *J. Fluid Mech.* **281**: 137-158, 1994

[7] Higdon, J.J.L., *J. Fluid. Mech* **90**: 685-711, 1979

[8] Blake, J.R. *J. Fluid Mech* **55**: 1-23, 1972

[9] Childress, S. *Mechanics of swimming and flying*, Cambridge, 1981

[10] Phan-Thien, N., Tran-Cong, T. & Ramia, M. *J. Fluid Mech.* **184**: 533-549, 1987

[11] Kessler, J.O., *J. Fluid Mech.* **123**: 191-205, 1985

[12] Pedley, T.J., & Kessler, J.O. *Sci.Prog* **76**: 105-123, 1992

[13] Roberts, A.M. & Deacon, F.M. *J. Fluid Mech.* **452**: 405-423, 2002

[14] Berg, H.C. & Brown, D.A. *Nature* **239**: 500-504, 1972

[15] Kim, M., Bird, J.C., Van Parys, A.J., Breuer, K.S., & Powers, T.J. *PNAS* **100**: 15481-5, 2003

[16] Flores, H., Lobaton, E., Méndez-Diez, S., Tlupova, S. & Cortez, R. *Bull. Math. Biol.* **67**: 137-168, 2005

[17] Berg, H.C. & Purcell, E.M. *Biophys. J.* **20**: 193-219, 1977

[18] Berg, H.C. E Coli *in motion*, Springer, 2004

[19] Bearon, R.N. & Pedley, T.J. *Bull. Math. Biol.* **62**: 775-791, 2000

[20] Locsei, J.T. (personal communication)

[21] Childress, S., Koehl, M.A.R. & Miksis, M.J. *J. Fluid. Mech* **177**: 407-436, 1987

[22] Magar, V., Goto, T. & Pedley, T.J. *Q.J. Mech. Appl. Math.* **56**: 65-91, 2001

[23] Magar, V. & Pedley, T.J. *J. Fluid Mech.* **539**: 93-112, 2005

[24] Solari, C.A., Ganguly, S., Kessler, J.O., Michod, R.E. & Goldstein, R.E. To be submitted, 2005

[25] Gerritsen, J. & Strickler, J.R. *J. Fish Res. Bd.Can.***34**: 73-82, 1977

[26] Rothschild, B.J. & Osborn,, T.R. *J. Plankton Res.* **10**: 465-474, 1988

[27] Lewis, D.M. & Pedley, T.J. *J. Theor. Biol.* **205**: 377-408, 2000

[28] Yamazaki, H., Osborn, T.R. & Squires, K.D. *J. Plankton Res.* **13**: 629-643, 1991

[29] Lewis, D.M. & Pedley, T.J. *J. Thoer. Biol.* **210**: 347-365, 2001

[30] Pedley, T.J. & Kessler, J.O. *Ann. Rev. Fluid Mech.* **24**: 313-358, 1992

[31] Hill, N.A. & Pedley, T.J. *Fluid Dyn. Res* **37**: 1-20, 2005

[32] Vladimirov, V.A., Wu, M.S.C., Pedley, T.J., Denissenko, P.V. & Zakhidova, S.G. *J. Exp. Biol.* **207**: 1203-1216, 2004

[33] Pedley, T.J. & Kessler, J.O. *J. Fluid Mech.* **212**: 155-182, 1990

[34] Keller, E.F. & Segel, L.A. *J. Theor. Biol.* **30**: 235-248, 1971

[35] Bearon, R.N. PhD Thesis, Cambridge University, 2001

[36] Mendelson, N.H., Bourque, A., Wilkening, K., Anderson, K.R. & Watkins, J.C. *J. Bacteriol.* **180**: 600-609, 1999

[37] Dombrowski, C., Cisneros, L., Chatkaew, S., Goldstein, R.E & Kessler, J.O. *Phys. Rev. Lett.* **93**: 098103, 2004

[38] Nott, P.R. & Brady, J.F. *J.Fluid Mech.* **275**: 157-199, 1994

[39] Lega, J. & Passot, T. *Phys. Rev. E* **67**: 031906

[40] Ishikawa, T., Simmonds, M.P., & Pedley, T.J. Submitted to *J. Fluid Mech.*, 2005

[41] Ishikawa, T. & Pedley, T.J. To be submitted to *J. Fluid Mech.*, 2005

[42] Batchelor, G.K. *J. Fluid Mech.* **41**: 545-570, 1970

Recent Tables of Contents of Flow Turbulence and Combustion

An International Journal Published in Association with ERCOFTAC

Board of Editors: J.C.R. Hunt, K. Hanjalic, L. Vervisch & W. Rodi

TABLE OF CONTENTS VOLUME 75 NO 1-4, DECEMBER 2005

Title: 2nd International Workshop on "Trends in Numerical and Physical Modelling of Turbulent Processes in Gas Turbine Combustors and Automotive Engines"

Guest Editor(s): A. Sadiki, L. Vervisch, W. Rodi

A. Sadiki, L. Vervisch, W. Rodi
Preface
pp. 1 - 2

F. Flemming, C. Olbricht, B. Wegner, A. Sadiki, J. Janicka, F. Bake, U. Michel, B. Lehmann, I. Röhle
Analysis of Unsteady Motion with Respect to Noise Sources in a Gas Turbine Combustor: Isothermal Flow
pp. 3 - 27

Johann Wäsle, Anton Winkler, Thomas Sattelmayer
Spatial Coherence of the Heat Release Fluctuations in Turbulent Jet and Swirl Flames
pp. 29 - 50

Martin Freitag and Markus Klein
Direct Numerical Simulation of a Recirculating, Swirling Flow
pp. 51 – 66

J. A. Oijen, R. J. M. Bastiaans, G. R. A. Groot, L. P. H. Goey
Direct Numerical Simulations of Premixed Turbulent Flames with Reduced Chemistry: Validation and Flamelet Analysis
pp. 67 - 84

K. Helbig, A. Alexeev, T. Gambaryan-Roisman, P. Stephan
Evaporation of Falling and Shear-Driven Thin Films on Smooth and Grooved Surfaces
pp. 85 - 104

A. Sadiki, M. Chrigui, J. Janicka, M. R. Maneshkarimi
Modeling and Simulation of Effects of Turbulence on Vaporization, Mixing and Combustion of Liquid-Fuel Sprays
pp. 105 - 130

M. Klein
An Attempt to Assess the Quality of Large Eddy Simulations in the Context of Implicit Filtering
pp. 131 - 147

N. K. Aluri, P. K. G. Pantangi, S. P. R. Muppala, F. Dinkelacker
A Numerical Study Promoting Algebraic Models for the Lewis Number Effect in Atmospheric Turbulent Premixed Bunsen Flames
pp. 149 - 172

Mohammed Seaïd, Axel Klar, René Pinnau
Numerical Solvers for Radiation and Conduction in High Temperature Gas Flows
pp. 173 – 190

E. Schneider, A. Sadiki, J. Janicka
Modeling and 3D-Simulation of the Kinetic Effects in the Post-Flame Region of Turbulent Premixed Flames Based on the G-Equation Approach
pp. 191 – 216

R. Jester-Zürker, S. Jakirlic, C. Tropea
Computational Modelling of Turbulent Mixing in Confined Swirling Environment Under Constant and Variable Density Conditions
pp. 217 – 244

S. Navarro-Martinez, A. Kronenburg, F. Di Mare
Conditional Moment Closure for Large Eddy Simulations
pp. 245 - 274

P. Weigand, W. Meier, X. R. Duan, R. Giezendanner-Thoben, U. Meier
Laser Diagnostic Study of the Mechanism of a Periodic Combustion Instability in a Gas Turbine Model Combustor
pp. 275 – 292

B. Janus, A. Dreizler, J. Janicka
Experimental Study on Stabilization of Lifted Swirl Flames in a Model GT Combustor
pp. 293 - 315

R. Giezendanner-Thoben, U. Meier, W. Meier, M. Aigner
Phase-Locked Temperature Measurements by Two-Line OH PLIF Thermometry of a Self-Excited Combustion Instability in a Gas Turbine Model Combustor
pp. 317 – 333

A. Brandl, M. Pfitzner, J. D. Mooney, B. Durst, W. Kern
Comparison of Combustion Models and Assessment of Their Applicability to the Simulation of Premixed Turbulent Combustion in IC-Engines
pp. 335 - 350

On the Geometry Dependence of the Nose Flow

Ingolf Hörschler, Wolfgang Schröder

Aerodynamisches Institut, RWTH Aachen

Wüllnerstr. zw. 5. u. 7, 52064 Aachen, Germany - www.aia.rwth-aachen.de

office@aia.rwth-aachen.de

1 Introduction

The human nasal cavity has to satisfy a variety of different functions. Besides respiration it is responsible for moistening, tempering, and cleaning the air. These functions are expected to strongly depend on the complex internal geometry of the nasal cavity. Impaired nasal respiration especially under normal breathing conditions, i.e., in everyday life situations, is a common and widespread disease, which makes nose surgery one of the most often performed operations in the western world. Unfortunately, the success rate, i.e., the number of people having no problems after surgery, is by no means satisfactory. To enhance this situation, it is desired to numerically predict the flow field inside the nose and its relation to geometric changes. This can finally lead to a computer assisted surgery (CAS) tool [1], that will help on the one hand, to understand the flow in the extremely complex human nasal cavity and on the other hand, to derive criteria how to better predict the outcome and to improve the success of nose operations.

In the following sections the grid generation is described first, followed by a concise presentation of the numerical method of solution including the boundary conditions. Finally, the results are discussed.

2 Grid Generation

An anatomically correct replica model with inferior and middle turbinate is constructed from the data by Masing [2], [3].

case	geometry
NC_{000}	cavity hull; no spurs, no turbinates
NC_{001}	cavity hull; no spurs, no lower turbinate
NC_{010}	cavity hull; no spurs, no upper turbinate
NC_{011}	cavity hull; no spurs, with turbinates
NC_{111}	cavity hull; with spurs and turbinates

Table 1: Definition of several nasal cavity geometries

The superior turbinate is neglected as it is often vestigial in average human nasal passages. In the following, we will refer to the anatomical middle as upper turbinate and the inferior will be denoted as lower turbinate.

The physical model was scanned using a computer tomograph to obtain by a marching cube algorithm applied to the CT data an unstructured surface representation. The model surface is subdivided into its main components, which are the cartilage spurs at the septum and the turbinates (Fig. 1, left). For each of these surface components two topology modules are constructed,where the first module is defined

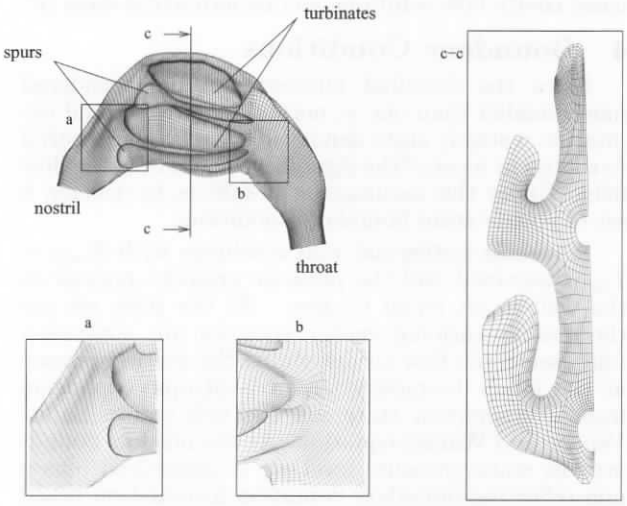

Figure 1: Presentation of the structured multiblock grid for test case NC_{111}; a) b) show enlargements of the tip and tail region of the turbinates, c) illustrates a coronal cross section.

such that a grid around the component can be generated, while the second module represents a topology to create a mesh without the surface component. All topology modules of the different surface components share common boundaries. The modules can be combined arbitrarily thus giving a whole set of different structured multiblock grids for a variety of nasal cavity geometries, which can be used to analyze the influence of the surface components on the flow.

The configurations investigated in this paper are listed in Tab. 1. The grid generation is done using the commercial grid generator GridPro [4]. In Fig. 1 the grid of the NC_{111} case is shown. For each case a mesh is generated with 60,000 and 250,000 cells. Since the flow does not possess a boundary-layer-like character, no special resolution is used in the near-wall regions. The numerical calculations did converge for both resolutions down to an average residuum of 10^{-14}, which can be considered machine accuracy. Although the overall findings do coincide, i.e., the more intricate and more susceptible flow phenomena occur on the 60,000 cell and on the 250,000 cell mesh, the numerical results discussed below are based on the higher resolution since locations of vortex cores and wall shear stress distributions are better resolved on the fine mesh.

3 Method of Solution

To simulate the flow field the dimensionless Navier-Stokes equations are solved using the flow library TFS developed at the Aerodynamisches Institut [5]. An explicit five-step Runge-Kutta method of

second-order accuracy is used for temporal integration and the Runge-Kutta coefficients are optimized for a central scheme. Although the Mach number is fairly small in the flows considered, we solve the compressible equations and do not encounter any convergence problems since no purely one-sided spatial approximation is used. Following the advective upstream splitting method (AUSM) by Liou and Steffen [6] the inviscid fluxes are split into a convective and a pressure term. For the viscous stresses a central discretization is chosen. This numerical method has been successfully validated by comparing numerical nasal cavity flow solutions and experimental data [7].

4 Boundary Conditions

Since the Strouhal number can be considered much smaller than one at normal inspiration and expiration a steady state simulation can be conjectured to represent most of the significant features of the flow field. Under this assumption it suffices to develop a set of steady state boundary conditions.

A no-slip isothermal wall condition with $T_{wall} = T_\infty$ is assumed and the pressure gradient normal to the wall is set equal to zero. At the inlet we use the one-dimensional energy equation for compressible, isentropic flow to determine the static pressure at the inflow boundary for an isentropic expansion from a stagnation state via the well-known Saint-Venant and Wanzel equation. At the outflow boundary the static pressure level p_∞ is prescribed plus a non-reflecting boundary condition formulation based on a sponge layer [8].

5 Results

At inspiration and expiration we assume volume fluxes for respiration at rest of 159.15 ml/sec and 127.32 ml/sec that result in Reynolds numbers of $Re = 500$ and $Re = 400$, respectively. Note that in this study the mean Reynolds number based on the mean channel width for the highest considered volume flux of 318.31 ml/sec is in the range of 1030 to 1400 for all configurations investigated, which is why the flow in the numerical analysis is conjectured laminar. The reference length for the Reynolds number is based on the hydraulic diameter of the throat. Furthermore, as aforementioned the flow can be considered steady since the Strouhal number is much smaller than one.

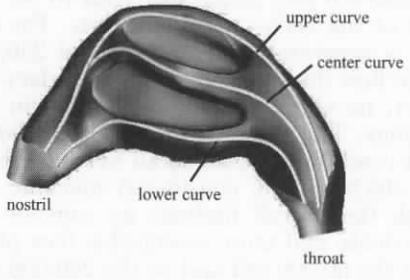

Figure 2: Prescribed geometrical curves for pressure plots

The discussion will start with concisely analysing the influence of the Reynolds number on the flow field. The detailed analysis of the impact of geometric changes on the flow structure at inspiration and expiration will be presented next. Distributions of the pressure on predefined paths as well as skin friction and streamline patterns are used to evidence the features of the various flow problems.

In the following discussion, the flow field of the NC_{111} geometry serves as a reference solution. The findings for the NC_{011} configuration will be presented to discuss the sensitivity of the flow to changes in Reynolds number. Since the spurs do not show any significant impact on the flow topology, i.e., the NC_{111} and the NC_{011} streamline patterns look more or less alike, the remaining of this paper will focus on comparing the flow fields of the NC_{111}, NC_{001}, NC_{010} and NC_{000} configurations.

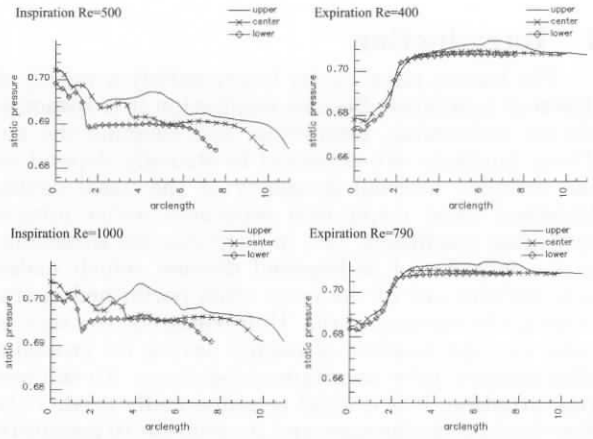

Figure 3: Static pressure distribution on three prescribed geometrical curves for the NC_{011} configuration at different Reynolds numbers

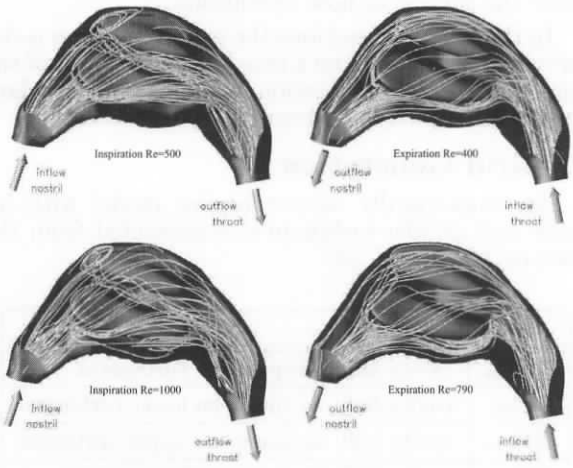

Figure 4: Streamlines for the NC_{011} configuration at different Reynolds numbers

It goes without saying that during the respiration cycle also higher Reynolds numbers occur than $Re = 400$ or $Re = 500$, respectively. To investigate the impact of volume flux, i.e., a larger Reynolds number, Figs. 3-4 show a comparison for two sets of Reynolds numbers, i.e., $Re = 500$ and $Re = 1000$ at inspiration and $Re = 400$ and $Re = 790$ at expiration, the larger values of which belong to volume fluxes of 318.31 ml/sec and 251.46 ml/sec. Pressure distributions along three prescribed geometrical curves (Fig. 3), which are located in the lower, middle, and upper channel of the nasal cavity (Fig. 2), indicate that the expiration phase is hardly impacted by the Reynolds number. There is only a slight change in the nostril pressure level. This observation is substantiated by the streamline patterns in Fig. 4. At inspiration

the Reynolds number increase results in more pronounced vortex structures, which is evidenced by the local pressure minima and maxima in Fig. 3 as well as by the streamline pattern upstream of the upper and lower turbinate in Fig. 4. The dependence of the overall flow structure on the Reynolds number in the range of $400 \leq Re \leq 1000$, however, can be considered moderate since no additional flow features are observed. For this reason, the analysis of the impact of the geometry on the flow structure is based on $Re = 500$ and $Re = 400$. Note, this comparison was performed on 60,000 and 250,000 cell meshes and in neither case the flow structures in the high Reynolds number solutions were significantly different from the low Reynolds number findings.

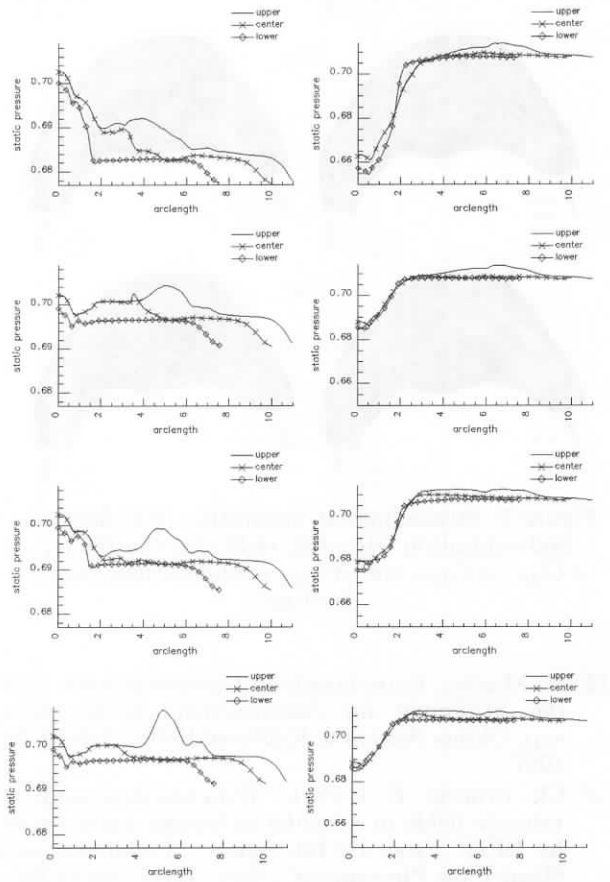

Figure 5: Static pressure distribution on three prescribed geometrical curves at inspiration (Re=500, left) and expiration (Re=400, right) for the NC_{111}, NC_{001}, NC_{010}, and NC_{000} configurations (top to bottom).

Fig. 5 contains the pressure distributions along three geometrical curves defined in Fig. 2. It is evident that at inspiration the major changes in the pressure distribution occur almost independent from the configuration approximately two to three hydraulic diameters downstream of the nostril region. This pronounced gradient is not determined by the turbinates but by the sudden expansion region, since it is also observed in the no-turbinate NC_{000} case. It goes without saying that due to the larger blockage the pressure drop is stronger in the NC_{111} problem. However, at expiration the pressure distributions for the different curves within the nasal cavity are fairly smooth and do almost coincide, whereas at inspiration the distributions possess a less monotone behavior and a clear discrepancy between the upper and the remaining paths is computed. That is, in the former case there is only a slight impact of the geometry on these distinct pressure curves, which can be interpreted as a first indication of less influence of the nasal configuration on the overall flow behavior at expiration. Only when air is inhaled the turbinates and the spurs, i.e., the NC_{111} geometry is considered, ensure a somewhat stronger acceleration near the entrance of the lower channel and cause a plateau-like pressure behavior on a lower pressure level than for the other configurations (Fig. 5). Furthermore, note the pronounced peak in the pressure distribution along the upper path when the lower turbinate is removed, i.e., in the NC_{001} and NC_{000} configurations in Fig. 5, compared to the distribution of the reference geometry NC_{111}. Although these deviations occur at inspiration and expiration it is the distribution for the NC_{000} configuration in Fig. 5 that emphasizes the stronger susceptibility of the flow field on the nose geometry at inspiration than at expiration.

The smallest cross section downstream of the nostril can be approximately identified as the first pronounced decrease in the pressure distribution for the lower geometrical curve at inspiration in Fig. 5. This pressure drop is weakened from the NC_{111} case to the NC_{000} case due to the removal of the turbinates and spurs. A second sharp pressure decrease is evident for the center curve before it enters the center channel (Fig. 5, NC_{111} case). This is related to the converging channel between the upper and lower turbinates. This pressure gradient almost vanishes when the upper turbinate is removed (Fig. 5, NC_{010} case).

Fig. 6 shows the wall shear stress distribution at inspiration and expiration. As already indicated by the pressure contours on the surface, high shear stresses occur in the nostril region for both respiration states and all nose configurations. Furthermore, also independent from the configuration considered, the larger wall shear stresses are observed in the lower part of the sudden expansion area located below the upstream tip of the lower turbinate. In other words, in the sudden expansion area the flow in the immediate vicinity of the wall does not possess any strong susceptibility to the nose geometry defined by the spurs and the turbinates. This changes when the distribution further downstream is considered. Due to the missing septum spurs steeper gradients occur in the wall shear stress distribution on the lower turbinate in the NC_{010} case than in the NC_{111} case. A similar behavior is observed when the wall shear stress distributions on the upper turbinate of the NC_{111} and NC_{001} configurations are juxtaposed. That is, the spurs smooth the streamwise distribution of the velocity gradients on the turbinates.

The streamlines in Fig. 7 evidence the vortices and recirculation regions in the flow field near the nostril and the throat. At inspiration a horseshoe-like vortex is visible upstream of the lower turbinate for the NC_{111} and NC_{010} configurations. By juxtaposing the streamline patterns of the NC_{111}, NC_{010} and NC_{001}, NC_{000} configurations in Fig. 7 it appears that especially the lower turbinate and the spurs seem to serve as guide vanes to ensure, e.g., a homogeneous velocity distribution in the upper, center, and lower channels. That is, without the lower turbinate and the spurs the flow field is characterized by massive vortices, which impact the flow distribution in the nasal cavity and change the time it takes a fluid particle to move from the nostril to the throat. At expi-

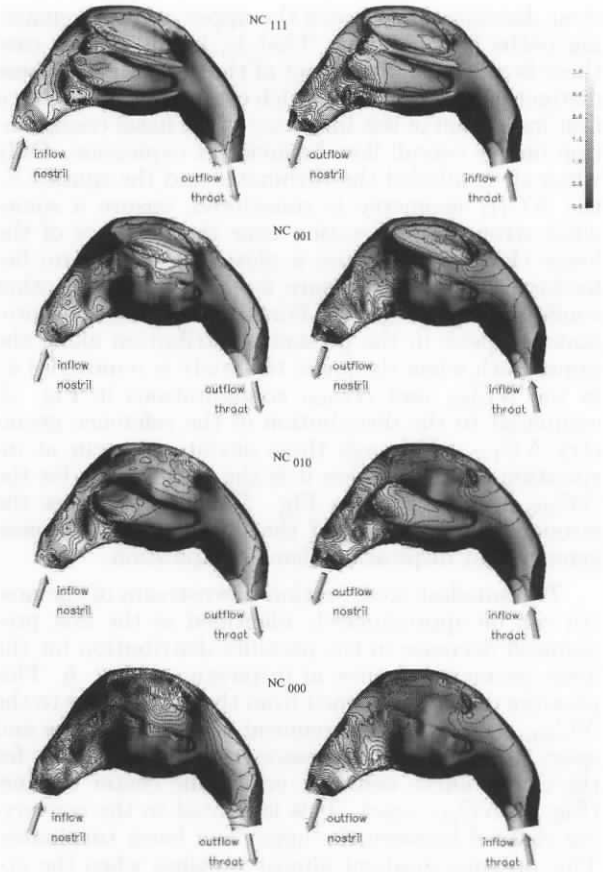

Figure 6: Skin friction distribution at inspiration (Re=500, left) and expiration (Re=400, right) for the NC_{111}, NC_{001}, NC_{010}, and NC_{000} configurations (top to bottom)

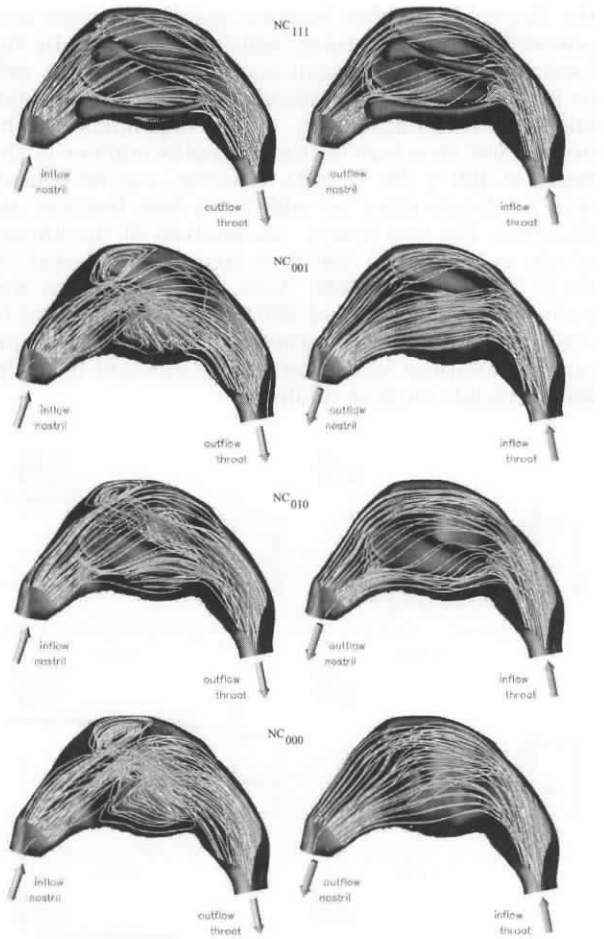

Figure 7: Streamlines at inspiration (Re=500, left) and expiration (Re=400, right) for the NC_{111}, NC_{001}, NC_{010}, and NC_{000} configurations (top to bottom)

ration clearly less vortical structures up- and downstream of the turbinates and spurs are detected emphasizing the smaller impact of the geometry on the flow field when air is exhaled.

Thus, it can be concluded that the reference geometry with turbinates and spurs appears to be optimized especially for inspiration to generate sufficient swirl to support mixing, which in conjunction with their surface area yields the correct tempering and moistening of the incoming air.

6 Conclusions

The numerical method was applied to compute the flow field of several nasal cavity configurations at inspiration and expiration to analyze the susceptibility of the flow to the geometry. The investigation shows that the inspiration phase is much more sensitive to any kind of geometry change than the expiration period. The turbinates serve as guide vanes to ensure a homogeneous velocity distribution in the lower, center, and upper channel between the nostril and the throat. The lower turbinate possesses the major impact on the velocity field and the pressure distribution since this is the part of the nose geometry that primarily interacts with the flow in the sudden expansion region.

Bibliography

[1] G. Schlöndorff. *Computer Assisted Surgery: Historical Remarks.* Computer Aided Surgery, Vol. 3, p.150-152, 1998

[2] H. Masing. *Experimentelle Untersuchungen über die Strömung im Nasenmodell.* Archiv klin. exp. Ohren-,Nasen- u. Kehlkopf-Heilk., 189:59-70, 1967

[3] Ch. Brücker, K. I. Park. *Experimental study of velocity fields in a model of human nasal cavity by DPIV.* Proc. 1st Int. Symp. "Turbulence and Shear Flow Phenomena", Sept. 12-15, Santa Barbara, California, (Eds. Banerjee, S., Eaton, K.), pp. 831-836, 1999

[4] *GridPro, The CFD Link to Design, The Graphic Manager Manual.* Programm Development Corp., 300 Hamilton Ave. Suite 409, White Plains, N.Y. 10601, USA

[5] E. Fares, M. Meinke, W. Schröder. *Numerical Simulation of the Interaction of Wingtip Vortices and Engine Jets in the Near Field.* AIAA Paper 2000-2046, June, 2000

[6] M. S. Liou, Ch. J. Steffen Jr. *A new flux splitting scheme.* J. Comp. Phys., 107:23-39, 1993

[7] I. Hörschler, Ch. Brücker, W. Schröder, M. Meinke. *Investigation of the Impact of the Geometry on the Nose Flow.* European Journal of Mechanics-B/Fluids, accepted Nov. 2005

[8] T. Colonius. *Numerically nonreflecting boundary and interface conditions for compressible flow and aeroacoustic computations.* AIAA Journal, 35/7:1126-1133, 1997

Blood Flow Measurements in Micro Vessels

Peter Vennemann, Mathieu Pourquie, Jerry Westerweel

Delft University of Technology

Laboratory for Aero- and Hydrodynamics

Leeghwaterstraat 21, 2628 CA Delft, The Netherlands - www.ahd.tudelft.nl

p.vennemann@wbmt.tudelft.nl

1 Introduction

The spatially resolved measurement of blood velocity distributions is a key-requisite in numerous applications of biomedical research. Examples are perfusion monitoring, identification of instantaneous flow patterns, derivation of shear stress distributions, or the estimation of volume flow rates. Established measurement methods like nuclear resonance imaging or ultrasound doppler velocimetry suffer from limited spatial resolution due to the utilized wavelengths. Other methods like laser Doppler imaging and time varying speckle velocimetry depend on scanning and therefore imply a temporal resolution longer than typical heart rates. Particle image velocimetry (PIV) and particle tracking velocimetry (PTV) can overcome these limitations. These methods allow for not only the determination of the velocity magnitude, but also its spatial direction. The wavelength of visible light allows a spatial resolution that is high enough for accurate wall shear stress derivations. Video rate or high speed imaging enables the resolution of typical heart rate frequencies.

The feasibility of using PIV to study blood flow in sub-millimeter blood vessels is demonstrated by studying the questions whether placental flow influences the embryonic heart development [1]. For studying this relationship experimentally, a chicken embryo can be used [1]. Figure 1 displays a chicken embryo after approximately 60 hours of incubation.

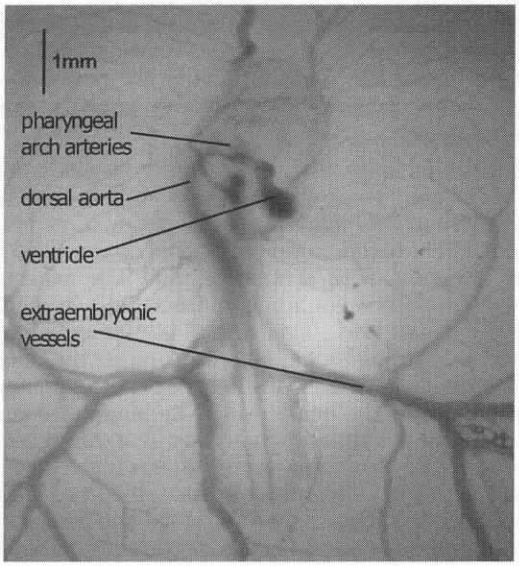

Figure 1: Chicken embryo after approximately sixty hours of incubation.

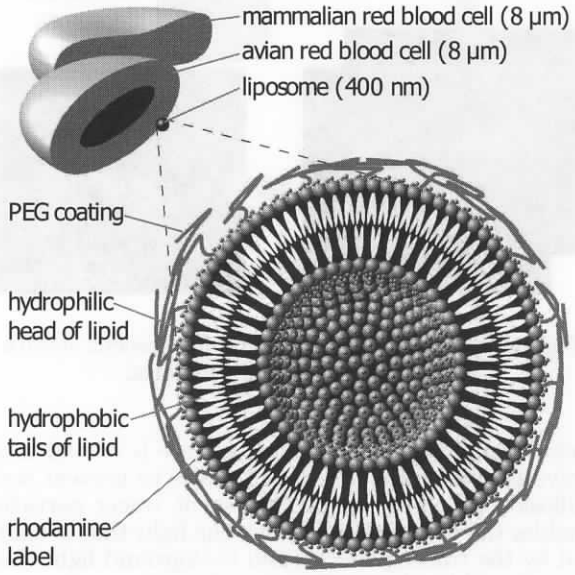

Figure 2: PEG coated liposomes are used as long circulating, biocompatible tracer particles.

The extraembryonic vessels on the right and on the left side of the embryo serve the same function as the vessels in the mammalian placenta. It has been shown that obstructing venous flow by closing one of this vessels with a clip results in severe cardiovascular malformations [1]. It is speculated that the heart development is strongly linked to specific details of the wall shear stress patterns within the forming heart. The wall shear stress acts mainly on the vascular endothelium, that is a thin layer of cells lining the whole vasculature including the heart. From *in vitro* flow studies on these cells, it is known that flow induced shear stress modulates gene expression [2], though a direct relation between abnormal placental blood flow and cardiovascular malformations is missing [1].

By combining the fluorescent visualization of gene expression with a quantitative measurement of the instantaneous flow field *in vivo* using PIV, a relationship between placental blood flow and cardiogenesis might be found.

2 Experimental Set-Up

Due to the small dimensions of the embryonic chicken heart (about 200 μm inner diameter) a μPIV system is utilized. Contrary to a conventional PIV system, the measurement plane is defined by the limited depth of focus of a microscope objective, rather than by forming a light sheet [3]. Instead of the naturally existing blood cells, fluorescent liposomes with a nominal diameter of 500 nm are used as tracer par-

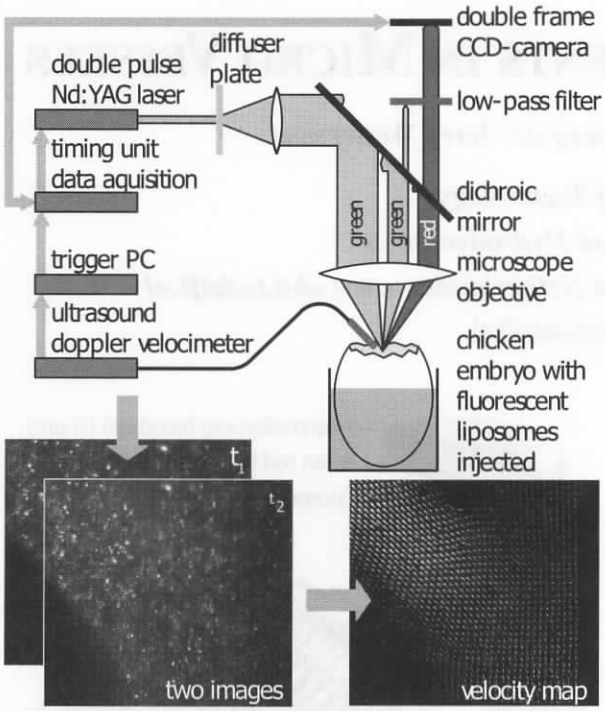

Figure 3: A μPIV set-up, using fluorescent stealth liposomes as tracer particles.

ticles (figure 2). The liposome surface is coated with polyethylene glycol (PEG) molecules to prevent wall adhesion [4]. The use of fluorescent tracer particles enables the distinction between the light that is emitted by the tracer particles and background light that is scattered by the surrounding tissue.

The experimental set-up is shown in figure 3. The PIV system is phase-locked to the cardiac cycle of the chicken embryo through the use of an ultrasound Doppler velocimeter. A PC calculates the measured velocity from the Doppler shifted signal in real time and triggers the timing unit of the PIV system with an adjustable delay. In this manner, it is possible to perform ensemble averaged PIV measurements to enhance the quality of the obtained velocity vector maps.

The laser illuminates the flow field through the objective of a Leica fluorescence microscope. The beam is widened by a diffuser plate and then reflected into the optical axis of the objective by a dichroic mirror. Background light, reflected by blood cells and tissue, is guided into the direction of illumination by the same dichroic mirror. Light with longer wavelengths, emitted by the fluorescent liposomes, passes the mirror and is imaged by a double frame CCD camera. The rest of the background light is blocked at a low-pass filter.

3 Results and Discussion

Figure 4 shows the average of fifty phase-locked vector fields in the fully expanded ventricle. The images were acquired using a 10× magnification objective. From the velocity distributions at different points in the cardiac cycle velocity profiles are extracted. From the derivative of the velocity profile, low and high shear stress domains can be identified. The maximum velocity of the velocity profile in figure 4 is shifted into the direction of the inner curvature wall. For the measurement plane of figure 4

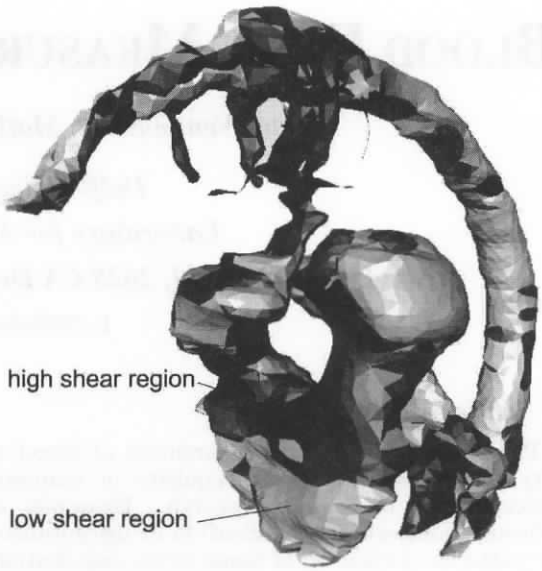

Figure 5: KLF2 gene expression pattern in the embryonic chicken heart [5]. Dark regions identify a gene expression level above a certain threshold.

the inner curvature wall is thus identified as a high shear stress region, relative to the outer curvature wall. This observation is matched by the visualization of KLF2 gene expression patterns in the embryonic chicken heart (figure 5) [5]. KLF2 is supposed to be upregulated with increasing wall shear stress. Figure 5 shows that inner curvature surfaces in general expose higher KLF2 gene expression than outer curvature walls.

4 Outlook

Further improvement, especially in the near wall region, is required for accurately calculating the wall shear stress from the flow profiles. The large diameter of particle agglomerates and the consequential low seeding density is accompanied by relatively extended interrogation areas of 32 by 32 pixels with the corresponding bias. Improvement is expected from the development of non-agglomerating particles. The spatial resolution might be enhanced dramatically by applying a two-point ensemble correlation method [6]. Multiple plane PIV measurements are necessary for a more comprehensive comparison to gene expression visualizations.

Additional work is done on the numerical simulation of the embryonic chicken heart. In fact, two ways of simulating the heart are considered. One uses a standard 3D unstructured collocated commercial flow solver (Fluent), with a moving grid. The other uses a so-called virtual boundary method on a staggered, fixed Cartesian grid. The virtual boundary is implemented by adding extra source terms to the Navier-Stokes equations which push the fluid velocity to the correct value at the heart wall. The heart wall is represented by a triangulated surface. A method related to the virtual boundary method has been used by Kovacs *et al* [8]. Two models are considered instead of one for validation purposes, since the accuracy of virtual boundary methods for the prediction of shear stress needs to be assessed. A preliminary result using a strongly simplified geometry is shown in figure 6. It shows the heart during the phase in which the cushions near the outlet are fully closed, and the cushions

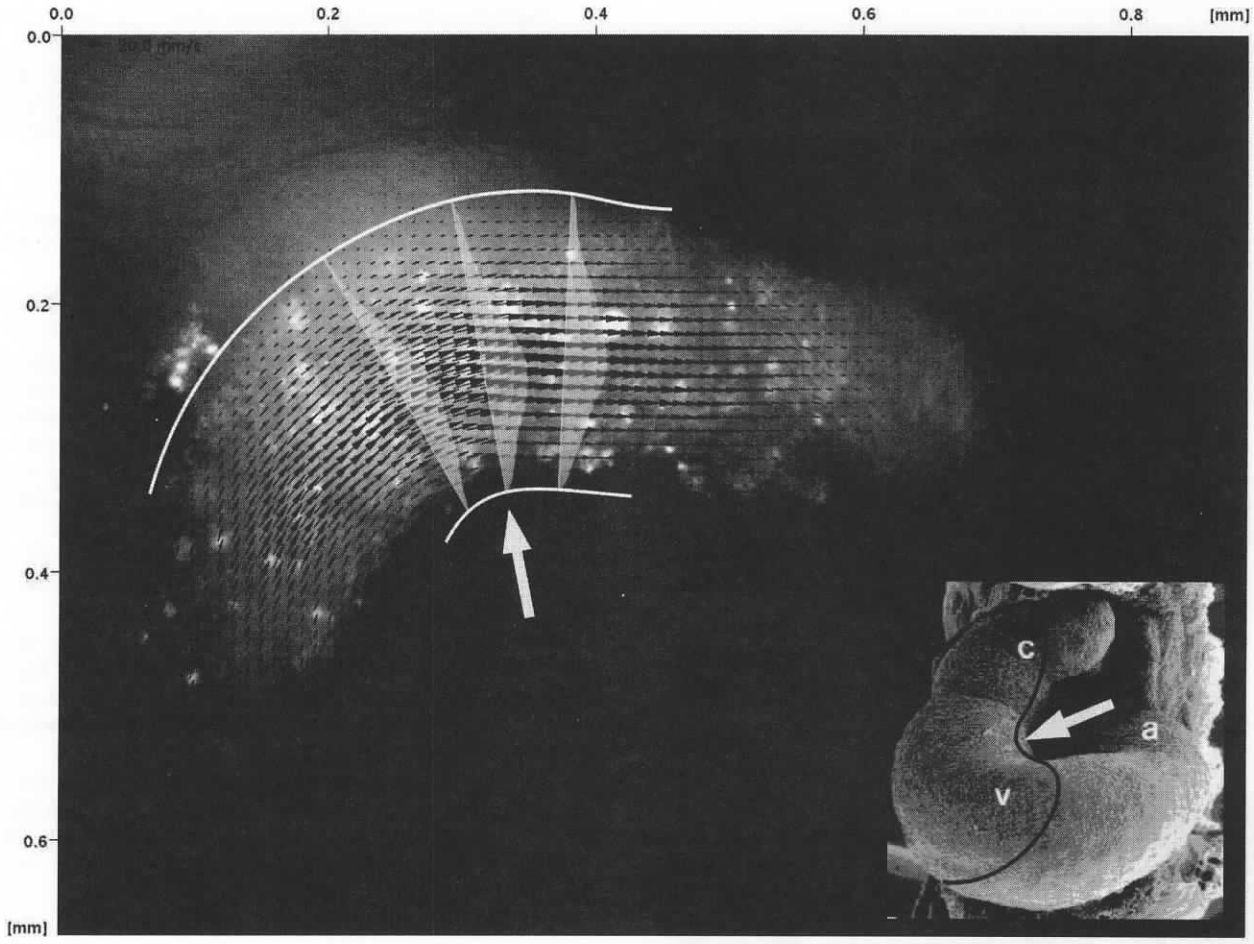

Figure 4: PIV measurement in the ventricle of a chicken embryo. The inset shows an electron micrograph of the heart [7] to illustrate the position of the measurement plane. The overlayed velocity profiles indicate that the peak velocity is shifted to the inner curvature wall. This can be explained by the low Dean number of the flow.

near the inlet are closing, giving shear stress near the inlet cushion. Light color indicates higher wall shear stress, dark indicates lower wall shear stress. The heart has the form of a distorted tube, the cushions are at the places which are constricted. The cushions near the outlet are fully closed, the cushions near the outlet (light color, high stress) are closing. A more realistic geometry was obtained by means of confocal imaging (figure 7) [5].

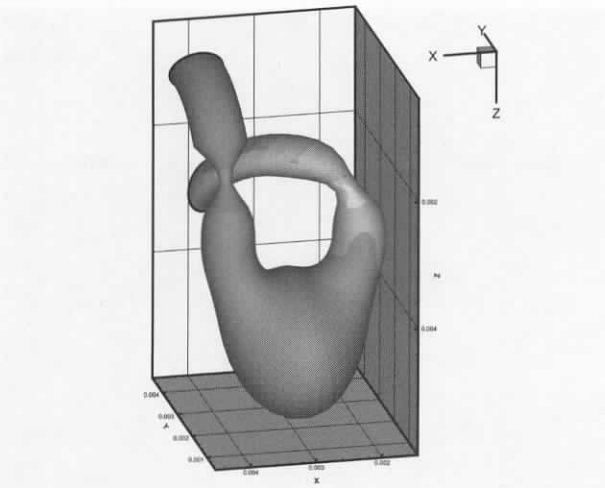

Figure 6: Numerical model of the embryonic chicken heart.

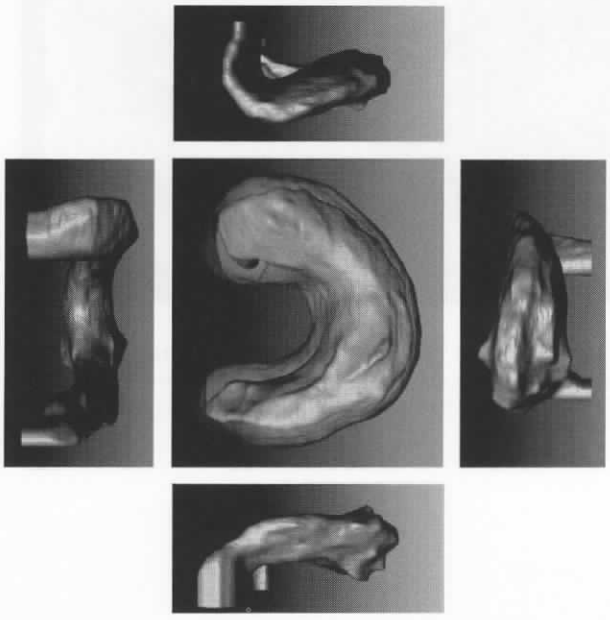

Figure 7: Reconstruction of the fully dilated chicken heart, based on confocal image scans [5].

5 Acknowledgements

This project is funded by the Dutch technology foundation STW (DSF 5695).

Bibliography

[1] Hogers, B.; DeRuiter M. C.; Gittenberger-de Groot A. C.; Poelmann R. E.: *Extraembryonic venous obstructions lead to cardiovascular malformations and can be embryolethal*, Cardiavascular Research 41, 87-99, 1999

[2] Topper, J. N.; Gimbrone Jr, M. A.: *Blood flow and vascular gene expression: fluid shear stress as a modulator of endothelial phenotype*, Molecular Medicine Today, 1357-4310, 1999

[3] Santiago, J.G.; Wereley, S.T.; Meinhart, C.D.; Beebe, D.J.; Adrian, R.J.: *A particle image velocimetry system for microfluidics*, Experiments in Fluids, 25, 316-319, 1998

[4] Lasic, D.: *Liposomes*, American Scientist 80, 20-31, 1992

[5] Groenendijk, B. C. W.; Hierck, B. P.; Vrolijk, J.; Baiker, M.; Pourquie, M. J. B. M.; Gittenberger-de Groot, A. C.; Poelmann, R. E.: *Changes in shear stress-related gene expression after experimentally altered venous return in the chicken embryo*, Circulation Research, 96, 1291-1298, 2005

[6] Westerweel, J.; Geelhoed, P. F.; Lindken, R.: *Single-Pixel Resolution Ensemble Correlation for Micro-PIV Applications*, Experiments in Fluids, 37, 375-384, 2004

[7] Männer, J.: *Cardiac Looping in the Chick Embryo: A Morphological Review With Special Reference to Terminological and Biomechanical Aspects of the Looping Process*, The Anatomical Record, 259 , 248-262, 2000

[8] Kovacs, S. J., McQueen, D. M., and Peskin C. S.: *Modelling cardiac fluid dynamics and diastolic function*, Philos Trans R Soc (A), 359, 1299-1314, 2001

GEOMETRICAL MULTISCALE MODELING OF THE CARDIOVASCULAR SYSTEM:

PROBLEMS AND PERSEPCTIVES

Alessandro Veneziani

Modeling and Scientific Computing (MOX)

Department of Mathematics "F. Brioschi", Politecnico di Milano

P.L. da Vinco 32, 20133 Milano, Italy - mox.polimi.it

alessandro.veneziani@mate.polimi.it

1 Introduction

The human cardiovascular system is formed by a closed network with a high level of inter-dependency. The distribution of blood flow inside the various vascular grounds affects the local flow patterns in each district. On the other hand, local alteration in vascular lumen induces global redistribution of the blood flow, giving rise to compensatory mechanisms that, in some cases, can ensure a sufficient blood flow in the districts downstream a stenosis. This reciprocal influence between local and systemic hemodynamics has led to the concept of *geometrical "multiscale"* modeling of the circulation (see [1, 2, 3, 4]). In these notes, we address some basic issues in developing numerical multiscale models for the circulation.

2 Basic Issues

A hierarchy of models

Blood flow dynamics in 3D can be described in terms of the Navier-Stokes equations for incompressible fluids, possibly including a non-Newton rheology. If Ω denotes a vascular district (see Fig. 1), $\mathbf{u}(\mathbf{x},t)$ and $p(\mathbf{x},t)$ represent the velocity and pressure fields respectively, ρ and μ the density and viscosity of blood, the Navier-Stokes equations reads for $\mathbf{x} \in \Omega$ and $t > 0$

$$\begin{cases} \rho \dfrac{\partial \mathbf{u}}{\partial t} + \rho\,(\mathbf{u}\cdot\nabla)\,\mathbf{u} - \nabla\cdot\left(\mu\left(\nabla\mathbf{u} + \nabla\mathbf{u}^T\right)\right) + \nabla p = \mathbf{f} \\ \nabla\cdot\mathbf{u} = 0 \end{cases} \tag{1}$$

with $\mathbf{u}(\mathbf{x},0) = u_0(\mathbf{x})$ an initial given velocity field, $\mathbf{f}$ a forcing term. System (1) has to be completed with appropriate boundary conditions. On the vascular wall Γ_{wall} we prescribe the continuity of the velocity and of the normal stresses of the blood and the wall. In the rigid case, it is enough to force null velocity conditions $\mathbf{u}(\Gamma_{wall},t) = \mathbf{0}$. On the interfaces Γ_i ($i = 1,2,3$ in Fig. 1) between the district at hand and the proximal and distal circulation we should prescribe conditions accounting for the reciprocal influence between the local and the global dynamics. How to do that in a mathematically sound way is exactly the goal of the geometrical multiscale approach. Since it is not possible to represent the whole circulation in terms of equations (1), both because of the amount of morphological data required and the computational time needed, we resort to some simplified models for the systemic circulation.

In 1775, Euler devised a model based on the realistic assumption that dynamics of blood in vessels develops essentially along the axial direction. The only component of the velocity field considered is therefore

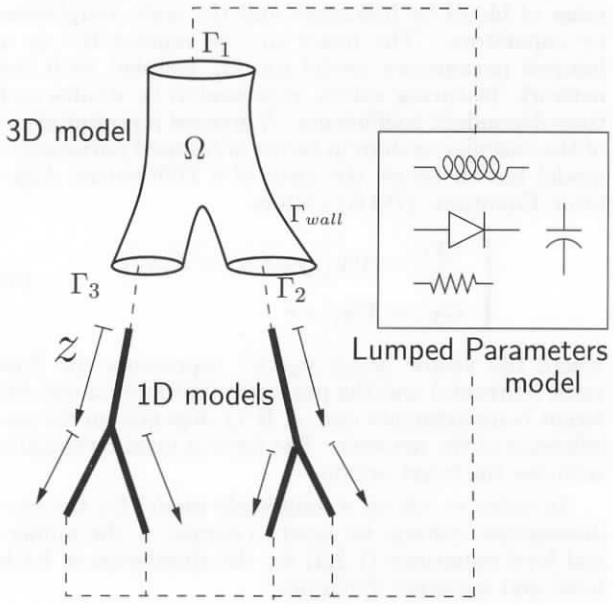

Figure 1: Schematic representation of the geometrical multiscale modeling of the vascular system, coupling 3D, 1D and lumped parameters models.

the axial one. In this way, we obtain a model where the only space coordinate is the curvilinear abscissa along the vessel (indicated by z in Fig. 1). For instance [2], if $A(z,t)$ denotes the area of an arterial (rectilinear) segment, $Q(z,t) \equiv \int_A \mathbf{u}_z da$ the flow rate and we assume that the mean pressure $P \equiv \int_A p da$ is proportional to A, from the Navier-Stokes equations we obtain the following equations:

$$\begin{cases} \dfrac{\partial A}{\partial t} + \dfrac{\partial Q}{\partial z} = 0 \\ \dfrac{\partial Q}{\partial t} + \alpha \dfrac{\partial}{\partial z}\left(\dfrac{Q^2}{A}\right) + \dfrac{A}{\rho}\dfrac{\partial P}{\partial z} + K_R\left(\dfrac{Q}{A}\right) = f \end{cases} \tag{2}$$

where α and K_R are suitable coefficients. This system has to be completed with boundary conditions, referring to A or Q. However, since this is a hyperbolic system, by combining A and Q it makes sense also to introduce the so called *characteristic variables*, whose propagation along the vessel axis is uniquely specified by the eigenvalues of the matrix associated to the quasi-linear form of (2). Boundary conditions can be prescribed therefore for these variables, yielding *non-reflecting* solutions, particularly appropriate

when one wants to specify the outgoing of simple wave from the computational domain with no reflections (see [2]).

In order to represent a 1D network, a set of arterial segment, each of them described by system (2), is built up by appropriately representing the bifurcations. Conditions prescribing the continuity of the fluxes and the relations among the branches of the bifurcation have been devised [2].

A further simplification is obtained by considering the circulatory system as a set of *compartments* whose dynamics is represented in terms of ordinary differential equations in time. A popular and expressive way to figure out this kind of models relies on the analogy between hydraulic and electric networks. On this basis, viscosity of blood is represented by resistances, mass of blood by inductors and the wall compliance by capacitors. The heart can be represented as a lumped parameters model too [3], coupled with the network, featuring valves, represented by diodes and time dependent coefficients. A general representation of the vascular system in terms of lumped parameters model has therefore the form of a Differential Algebraic Equations (DAE) system

$$\begin{cases} \dfrac{d\mathbf{y}_1}{dt} = A(\mathbf{y}_1, \mathbf{y}_2, t)\mathbf{y}_1 + B(\mathbf{y}_2) \\ G\mathbf{y}_2 = D\mathbf{y}_1 + \mathbf{c} \end{cases} \tag{3}$$

where the vector $[\mathbf{y}_1(t), \mathbf{y}_2(t)]^T$ represents the flow rates (currents) and the pressures (voltage) in the different compartments and A, B, G depends on the coefficients of the network. The forcing term $\mathbf{c}$ typically includes the heart action.

In order to set up a multiscale model for the cardiovascular system, we need to couple at the numerical level equations (1,2,3) for the simulation of both local and systemic dynamics.

Defective boundary conditions

The first problem to face comes from the different level of detail of the different model to be coupled. In fact, the Navier-Stokes equations (1) require pointwise conditions on the interface sections Γ_i. On the other hand, the simplifications behind models (2) and (3) lead to manage "average" variables on the same sections. These models can compute for instance the flow rate Q or the mean pressure P to be assigned as boundary data on Γ_i for the Navier-Stokes equations. These data are incomplete or *defective* from the mathematical viewpoint for system (1), that requires three scalar conditions on each point of the boundary. Specific methods have been devised for managing these problems in such a way that the simulations are not affected, as far as possible, by the somehow arbitrary completion of the boundary data. We address here two possible approaches.

Variational approach: A variational formulation of a differential problem is an integral representation suitable for Galerkin numerical methods, associated to an appropriate definition of the functional spaces the solution is supposed belong to. For the same differential problem, different variational formulations can be devised depending on the boundary conditions. *Essential boundary conditions* are included by selecting functional spaces fulfilling the condition assigned. The null velocity field on Γ_{wall} can be therefore included in the formulation by choosing a functional space of vector fields vanishing on Γ_{wall}. *Natural boundary conditions* are the conditions arising automatically when obtaining the variational formulation by using the Green formula $\int_\Omega \nabla \cdot \mathbf{v}\varphi d\omega = \int_{\partial\Omega} \mathbf{v}\cdot\mathbf{n}\varphi d\gamma - \int_\Omega \mathbf{v}\cdot\nabla\varphi d\omega$. The integral on the boundaries actually specifies some quantities to which it is "natural" to associate some boundary conditions. The *variational approach* for managing defective boundary conditions, proposed in [5], relies on finding an appropriate variational formulation accounting for the defective data available. The completion of the boundary data is given by the homogeneous natural conditions associated to the variational formulation chosen. Since natural conditions are supposed to weakly affect the solution, this choice should ensure that the perturbations on the numerical solution are small. For instance, for mean pressure conditions:

$$\int_{\Gamma_i} p d\gamma = P_i \tag{4}$$

where $P_i = P_i(t)$ is given, a possible variational formulation of the problem is the following. Let $L^2(\Omega)$ be the Hibert space of scalar square integrable functions in Ω, $\mathbf{H}^1_{\Gamma_{wall}}(\Omega)$ the Sobolev space of vector functions vanishing on Γ_{wall} whose components and derivatives belong to $L^2(\Omega)$, $L^2(0,T,\mathbf{H}^1_{\Gamma_{wall}}(\Omega))$ (resp. $L^2(0,T,L^2(\Omega))$) the space of functions whose $\mathbf{H}^1$ (resp. $L^2(\Omega)$) norm is a square integrable function of time over the time interval $0,T$. The variational problem reads: find $\mathbf{u} \in L^2(0,T,\mathbf{H}^1_{\Gamma_{wall}}(\Omega))$, $p \in L^2(0,T,L^2(\Omega))$ such that

$$\begin{cases} \displaystyle\int_\Omega \rho\left(\frac{\partial \mathbf{u}}{\partial t} + \mathbf{u}\cdot\nabla\mathbf{u}\right)\cdot\mathbf{v} + \mu\left(\nabla\mathbf{u} + \nabla\mathbf{u}^T\right) : \nabla\mathbf{v} d\omega \\ \qquad - \displaystyle\int_\Omega p\nabla\cdot\mathbf{v} d\omega = \sum_{i=1}^{n} P_i \int_{\Gamma_i} \mathbf{v}\cdot\mathbf{n} d\gamma + \int_\Omega \mathbf{f}\cdot\mathbf{v} d\omega \\ \displaystyle\int_\Omega q\nabla\cdot\mathbf{u} d\omega = 0 \end{cases} \tag{5}$$

for all $\mathbf{v} \in \mathbf{H}^1_{\Gamma_{wall}}(\Omega)$ and $q \in L^2(\Omega)$. In this case, we are forcing in particular that the pressure field is constant on Γ_i and that $\mu(\nabla\mathbf{u} + \nabla\mathbf{u}^T)\cdot\mathbf{n} = \mathbf{0}$ on Γ_i. These conditions are reasonable approximations in many haemodynamics problems, so this approach has been successfully used for mean pressure problems.

For flow rate conditions

$$\int_{\Gamma_i} \mathbf{u}\cdot\mathbf{n} d\gamma = Q_i \tag{6}$$

where $Q_i = Q_i(t)$ is given, the same approach can be pursued in principle, but unfortunately it requires to resort to functional spaces quite difficult to discretize for numerical purposes (see [5, 7]). For this reason, a different approach has been developed.

Lagrange multiplier approach: We still start from a variational formulation of the problem, but in this case the defective boundary conditions (in particular (6)) are considered as a *constraint* for the solution, to be forced by resorting to a Lagrangian multiplier approach. Since the linear Stokes problem can be easily regarded as a minimization of a suitable functional, the problem is reformulated in such a way that the minimization is constrained by the fulfillment of (6). In this way, the original problem is

augmented by introducing new unknowns, the multipliers λ_i, with the role of forcing the constraints. The constrained minimization yields a *saddle point problem*, in which the minimization is performed with respect to the velocity, while a maximum is searched for the multipliers (see [7]). The augmented problem for solving (6) reads: find $\mathbf{u} \in L^2(0,T,\mathbf{H}^1_{\Gamma_{wall}}(\Omega))$, $p \in L^2(0,T,L^2(\Omega))$ $\lambda_i \in L^2(0,T)$ such that

$$\begin{cases} \displaystyle\int_\Omega \rho\left(\frac{\partial \mathbf{u}}{\partial t} + \mathbf{u}\cdot\nabla\mathbf{u}\right)\cdot\mathbf{v} + \mu\left(\nabla\mathbf{u} + \nabla\mathbf{u}^T\right) : \nabla\mathbf{v} d\omega \\ \qquad - \displaystyle\int_\Omega p\nabla\cdot\mathbf{v} d\omega - \sum_{i=1}^{n}\lambda_i \int_{\Gamma_i}\mathbf{v}\cdot\mathbf{n} d\gamma = \int_\Omega \mathbf{f}\cdot\mathbf{v} d\omega \\ \displaystyle\int_\Omega q\nabla\cdot\mathbf{u} d\omega = 0 \\ \displaystyle\int_{\Gamma_i}\mathbf{u}\cdot\mathbf{n} d\gamma = Q_i \qquad (i = 1,2,\ldots n) \end{cases} \tag{7}$$

for all $\mathbf{v} \in \mathbf{H}^1_{\Gamma_{wall}}(\Omega)$ and $q \in L^2(\Omega)$.

An important drawback of this approach concerns the computational costs, in particular in the unsteady nonlinear case. Actually, saddle point problems typically require iterative approaches and in this case each iteration implies the solution of a "standard" Navier-Stokes problem (see [7, 8]), that can be quite computationally expensive. Approximate methods for solving (7) with a significant reduction of CPU time are under development [9].

Numerical schemes for coupling

Once that defective data problems can be managed and the Navier-Stokes equations are matched with 1D and lumped parameters models in a mathematically correct way (see [6] for a well posedness analysis), the multiscale model is obtained by solving together equations (1,2,3). Since the complete model reflects the different nature of the submodels in numerically ill conditioned problems, a typical approach for computations is to resort to *domain decomposition techniques* (see [4]). This means that the different sets of equations (1,2,3) are solved separately in an iterative framework and numerically coupled by managing appropriately the interface conditions.

For the sake of clarity, let us consider the coupling of 3D and 1D models. The coupling between 3D and 0D models can be faced in a similar way (see [4]). We assume that the two models are related by *interface conditions* given by the continuity of the mean pressure and the flow rate: with a self-explicative notation we set for $i = 1,2,\ldots,n$

$$\int_{\Gamma_i} p_{3D} d\gamma = P_{1D}(\Gamma_i), \quad \int_{\Gamma_i}\mathbf{u}_{3D}\cdot\mathbf{n} d\gamma = Q_{1D}(\Gamma_i). \tag{8}$$

Other interface conditions can be however devised, involving for instance the total pressure, the characteristic variables or (in the case of a 3D compliant domain) the area of Γ_i: a discussion of the different possibilities is carried out in [2], even if it is not clear so far at which extent the choice of these conditions affects the performances of the numerical solvers.

Following the domain decomposition approach, a possible scheme for solving the coupled 3D-1D problem is for instance to start from a guess for the mean pressure at the interface and to solve the 3D problem (1) with mean pressure conditions, to compute the flow rates at the interfaces and then to solve the 1D problem (2) with conditions on Q yielded by the 3D solution. The iterations continue up to the fulfillment of a given convergence criterion. At each iteration we solve therefore a defective Navier-Stokes problem (5). If only one iteration is performed, we have an *explicit coupling*, featuring low computational costs and however it can suffer from numerical instabilities, depending e.g. on the physical properties of the vascular walls.

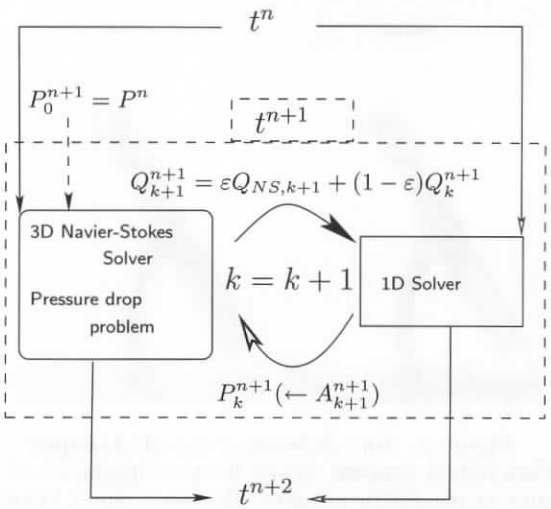

Figure 2: Coupling of 3D and 1D solvers.

In Fig. 2 we report a scheme of the 3D-1D solver. The problem has been discretized in time and the coupling is performed at time step t^{n+1}. A *relaxation parameter* ε has been introduced for accelerating the convergence. For more details, see [3, 4].

3 Numerical results

In Fig. 3, top, we report the scheme of a 3D-Lumped parameters model for the computation of the effects of a carotid-pulmonary artery shunt, as a part of a more complex paediatric surgery intervention called *modified Blalock-Taussig shunt*. Here, the specific contribution of the multiscale approach is to enable the computation of flow reversal zones, in agreement with clinical observations (see Fig. 3, bottom). A complete analysis of this case with more realistic geometries can be found in [10]. The good agreement with clinical data suggests that the multiscale approach is a reliable strategy for the computation of local and systemic dynamics.

Concerning the coupling between 1D and 3D models, as an application of the algorithm presented in Fig. 2 we consider the sequence of 1D-3D-1D models, in which the 3D domain is supposed to be rigid. This case mimics the presence of a stiff arterial segment like the one corresponding to a vascular endoprosthesis (stent). The presence of a stiffer part is supposed to introduce a backward component in the pressure wave propagating from the heart to the peripheries, yielding an overload to the heart. This is qualitatively confirmed by numerical simulations in Fig. 4.

4 Open problems and perspectives

Let us conclude with an indications of some open problems and possible developments about the geometrical multiscale approach.

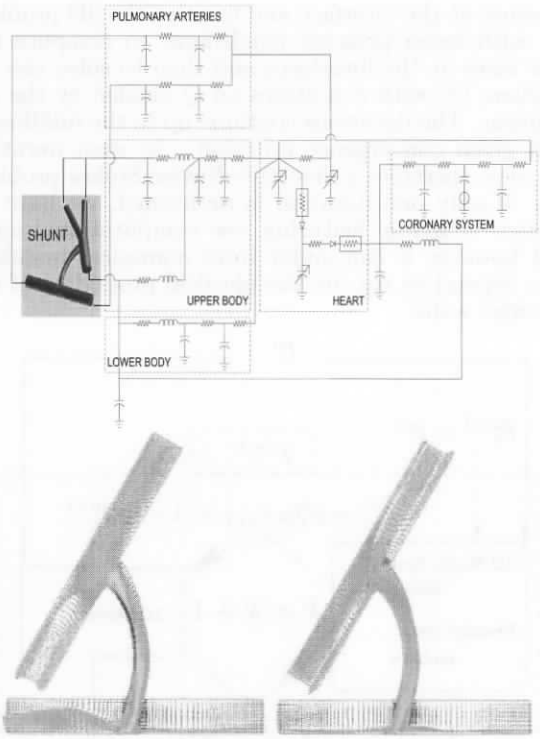

Figure 3: Top: Scheme of the 3D-Lumped Parameters coupled model for the simulation of a shunt in paediatric surgery. Bottom: Shunt velocity fields in two instants of the heart beat: flow reversal zones can be computed by the multiscale approach. Computations carried out with FIDAP.

An *extensive convergence analysis of coupled schemes* like the one depicted in Fig. 2 is still missing. The role of the different possible matching conditions between 1D and 3D models and the appropriate selection of relaxation parameters have to be investigated for devising efficient multiscale solvers, in particular for the case of a compliant 3D domain.

Another important issue is the mathematical modeling of self-regulation. In the circulation there are some mechanisms yielding great robustness to the whole system. The heart frequency grows up when the oxygen demand by the tissues and muscles is increased, for instance during exercise. The inclusion of these mechanisms in the numerical multiscale modeling of the vascular system is a relevant task to be accomplished.

A third point concerns the presence of different scales in time in the investigation of vascular pathologies. An atherosclerotic plaque can develop over time scales of months or years, induced by some anomalous stress conditions occurring on the arterial wall at each time beat (about 1 second). The devise of simple-minded models in time to be coupled with 3D models for a time-multiscale modeling is an interesting task for the investigation of the development of some pathologies.

Finally, we mention the fact that the geometrical multiscale approach is not confined to the haemodynamics context at all and it can be adopted in all the other fields in which local and global dynamics need to be simulated together, like for instance in the investigations of environmental dynamics (rivers-lakes-sea networks) or in the design of internal combustion engines.

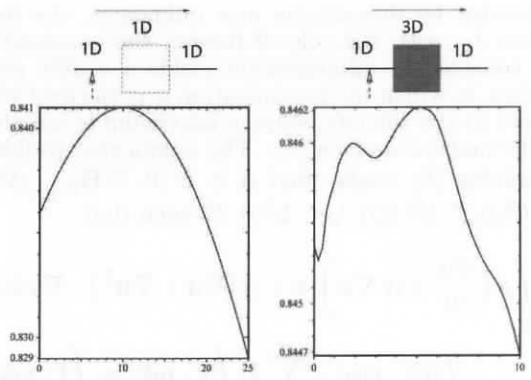

Figure 4: Left: Area in the upstream 1D model in the physiological (1D) case. Right: Area in the case of a stented artery 1D-3D-1D simulation. Observe the overload induced by the rigid domain.

Acknowledgment

These researches are carried out with the support of Italian MIUR Cofin Project "Numerical Modeling for Scientific Computing and Advanced Applications", the EU Project "HaeModel" and the Fondazione Politecnico Project "Aneurisk". I thank T. Passerini for simulations of Fig. 4 and careful reading of the manuscript.

Bibliography

[1] Formaggia L., Nobile F., Quarteroni A., Veneziani A., "Multiscale modeling of the cardiovascular system: a preminiar analysis" Comp. Vis. Science, 2, pp. 75-83, 1999.

[2] Quarteroni A., Formaggia L., "Mathematical Modelling and Numerical Simulation of the Cardiovascualr System", in N. Ayache (ed.) *Computational Models for the Human Body*, Elsevier, Amsterdam, 2004

[3] Formaggia L., Veneziani A., "Reduced and Multiscale Models for the Human Cardiovascular System", Von Karman Lecture Series, 2003

[4] Formaggia L., Veneziani A. "Geometrical Multiscale Models for the Cardiovascular System", ABIOMED Lecture Notes 2005.

[5] Heywood J., Rannacher R., Turek S., "Artificial Boundaries and Flux and Pressure Conditions for the Incompressible Navier–Stokes Equations", Int J Num Meth Fluids, 22, pp.325–352, 1996.

[6] Quarteroni A., Veneziani A., "Analysis of a geometrical multiscale model based on the coupling of Ode's and Pde's for blood flow simulations", SIAM Mult Mod Simul., 1, pp.173–195, 2003

[7] Formaggia L., Gerbeau J.F., Nobile F., Quarteroni A. "Numerical treatment of defective boundary conditions for the Navier-Stokes equation" SIAM J Num Anal, 40,pp.376–401, 2002

[8] Veneziani A., Vergara C., "Flow rate defective boundary conditions in haemodynamics simulations", Int J Num Meth Fl, 47, pp. 803-816, 2005

[9] Veneziani A., Vergara C., "An approximate method for solving incompressible Navier-Stokes problems with flow rate conditions", in preparation, 2005

[10] Migliavacca F., Balossino R., Pennati G., Dubini G., Hsiab T.Y., de Leval M.R., Bove E.L., "Multiscale modelling in bio fluid dynamics: Application to reconstructive paediatric cardiac surgery", J. Biomech, to appear, 2005

LEFT VENTRICULAR FLUID DYNAMICS

Gianni Pedrizzetti

Dept. Civil Engineering, University of Trieste, Italy

Gianni@dic.units.it

1 Introduction

The function of the human heart is that of a mechanical pump that receives the low pressure blood from the venous system and ejects it with higher pres-sure into the arterial system. The heart chambers are surrounded by muscular tissue, the myocardium, that operates in a sequence of active contractions and mainly passive relaxations. This relies on the contraction and release of the individual muscular cells, activated by a flowing electrical impulse. Given its fundamentally mechanical function, the myocardial tissue deformation and the blood flow inside the heart chambers represent a central issue of the biomechanical re-search.

The left ventricle (LV), from where the oxygenated blood is pushed into the primary circulation, is the most energetic element and plays a central role in the cardiac mechanics as well as in the diagnosis of the heart function. The LV systolic phase (LV contraction) represents the fundamental activity, an important systolic malfunction reflects immediately into the allowance of oxygenated blood in the whole body and gives rise to symptomatic pathology, however systolic dysfunction is often preceded by a weaker, possibly asymptomatic, lack of efficiency that is more difficult to detect. The cardiac phase when the LV enlarges and receives the oxygenated blood from the pulmonary venous system is called diastole. The diastolic phase is mostly (although not completely) a passive stage whose proper function is related to the elastic properties of the tissue that must allow the refilling of the chamber without a relevant increase of the blood pressure. A diastolic dysfunction is often not symptomatic, at least at relatively early stages, and represents a challenging diagnostic issue. Nevertheless it gives rise to an increasing stress of the heart tissues, lack of pumping efficiency, and may lead to heart failure sometime shortly after the appearance of evident symptoms.

Accurate diagnosis is fundamental in the cardiologic clinical practice that is focussed on the ability of an early recognition diseases. Early diagnosis of heart malfunction can be controlled by mean of a light pharmacological therapy. Cardiac pathology found at an advanced stage may produce irreversible modifications or could require a surgical approach, like valvular replacement or surgical chamber remodelling, that present a significant level of invasiveness and later drawbacks.

Cardiac diagnosis is largely based on the evaluation of the tissue mechanics by mean of medical imaging techniques like MRI, that gives good quality imaging, and echocardiography that has the advantage of a high temporal resolution and permits to differentiate the cardiac phases (some of which lasts a few hundredths of a second). Despite the allowance of imaging diagnostic tools that permit, to some extent, intraventricular flow visualization, and of some experimental and numerical studies, several aspects of the cardiac fluid dynamics are still not clear and equally unclear is their relation to physiology. The visualization of flow in the heart chambers is, in facts, still of little usage in diagnosis.

Notwithstanding this introduction there is some starting evidence that the intraventricular flow is sensibly related to the cardiac function. However several aspects of the LV flow are still known only at a very qualitative level and careful analyses and reliable tools for the quantification of the LV blood flow are still under development.

The study of the LV function requires a deep combination of methods and knowledge for either intraventricular fluid mechanics and LV tissues solid mechanics. Although this study is centred on the LV fluid dynamics, the subject cannot be developed without ac-counting for the dynamics of the surrounding tissues that represent the moving boundary of the fluid flow and give rise to a fluid-tissue interactive evolution. Fluid mechanics is characterised by a complex behaviour of a simple material, assuming the blood as a Newtonian fluid, due to the development of vortices, boundary layer separation and weak turbulence. On the opposite, the solid mechanics has a basically simpler behaviour that, in turn, presents the complexity associated with the material properties that are non-linear, time varying, and neither homogeneous nor isotropic.

2 Left ventricular flow

2.1 Generalities

The LV flow is characterised by a strong compact jet which enters the chamber through the mitral orifice during the ventricular filling (diastolic) phase. The jet enters the LV during two distinct pulses: the Early-filling wave (E-wave), during ventricular relaxation, followed by the A-wave produced by the atrial contraction (atrial systole). At the end of the diastole, also the ventricle begins to contract (LV systole), the active phase produced by the length reduction of the myocardial muscular fibres. During systole, pressure rises in the chamber, the mitral valve closes (preventing back-flow) while the aortic valve opens and blood is ejected into the primary circulation. At the conclusion of contraction

pressure is decreased until (helped by an elastic bounce-back when fibres activation is released) it becomes lower than the atrial one and filling restarts.

Notwithstanding the apparent simplicity of the cardiac cycle the fluid dynamics phenomena that participate are intense: the inflow is an impulsive jet that opens the valvular leaflets and enters a cavity a few centimetres long with a velocity near 1 m/s, it almost instantaneously reaches the ventricle moving wall and interacts with it. The diastolic entering jet has an almost irrotational core surrounded by a shear layer that rolls-up and immediately arranges into a compact ring-shaped vortex structure (the jet head) which enters the cavity. Moreover, the mitral valve is displaced with respect to the axis of the cavity, the jet is redirected to-ward one wall, and the intraventricular flow structure develops an asymmetric pattern as sketched in figure 1.

The intraventricular fluid dynamics presents a variety of complex phenomena that have an influence on the heart function. The length of the diastolic jet, with its possible impact onto some region of the endocardial tissue, as well as the arrangement of the intraventricular vortical structure, depend on several physiological or patho-physiological factors. A fundamental role is played by the geometry of the chamber and its capacity and uniformity of elastic contraction and relaxation. In addition, to mention a few, to the geometry and kinematics of the inlet orifice, that is a moving two-leaflets valve, and the relative intensity of the two (E- and A-) filling waves.

2.2 Existing results and models

The Early flow visualisations [1,2] showed that the vortex ring-like structure forming through the mitral entrance develops a large vortex located behind the longer valvular leaflet and a smaller one on the opposite side as shown in figure 1; this was confirmed by clinical imaging (echo color Doppler) and by recent studies [3] based on MRI. This stressed the importance of the asymmetric pattern to possibly facilitate the blood ejection from the ventricle to the aorta. Such a flow pattern also avoids the stagnation of fluid at the cavity apex that could induce negative physiological consequences (thrombus). However, the description so far is essentially a two-dimensional flow picture on a plane cross-section, the three-dimensional flow structure laying be-hind is less immediate.

A support for the understanding or visualising the three-dimensional flow is currently coming from the growing potential of computational fluid dynamics. The numerical solution of the ventricular flow presents several difficulties due to the moving boundary and the flow-wall interaction, which are of primary relevance in a closed cavity problem. It was stressed above how the numerical modelling of the LV flow cannot be separated from the modelling of the bounding cardiac tissues. In principle, the tissue is a mechanical element whose dynamics should be derived from the corresponding continuum equations forced by the fluid wall stresses, especially pressure. This raises some additional

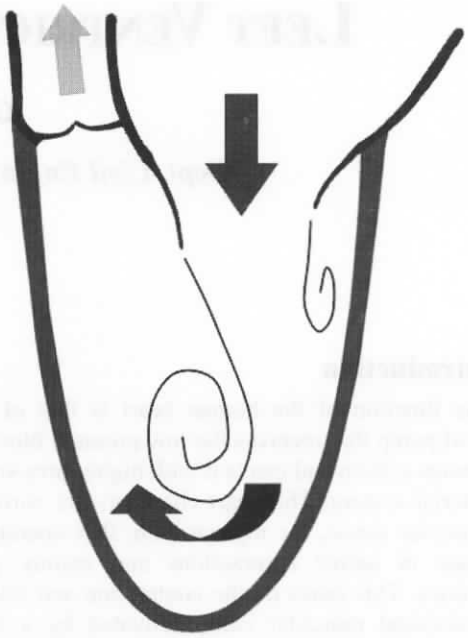

Figure 1: Sketch of the left ventricle and of the blood flow during diastole.

difficulties: the quantification of the absolute fluid pressure requires the knowledge of a reference pressure time-law somewhere nearby (or the many parameters of a complete circulation model). Most important, the elastic and contractile thick tissue properties, that are non-linear, time-varying and normally neither homogeneous nor isotropic, must be specified for the computation of wall deformation. These information are not accessible, in vivo, and are not measured in routine clinical observations, thus reliable data are not commonly available. In an alternative perspective, the dynamic of the tissue can be specified a priori and the corresponding fluid dynamics evaluated from it. This semi-coupled approach does not give information about the effective tissue response to the flow, nevertheless the tissue movement can be evaluated with relative ease from the routine clinical observation in vivo (MRI, Echocardiography) and the fluid dynamics does not change when the same boundary movement is given or it is computed by a coupled solution. Therefore the latter method is currently the most practicable for reproducing patient-specific fluid dynamics.

The first numerical LV models were based on the axisymmetric approximation, either with coupled fluid-tissue dynamics [4] or predefined tissue motion [5]. Axisymmetric flow gives some preliminary understanding of the ventricular flow but it is not realistic enough for the interpretation of most phenomena. In fact, a related study about the three-dimensional flow entering a circular eccentric orifice [6] showed how a small displacement drives the flow away from the axisymmetric solution. A fluid dynamics study on a realistic heart has been performed in [7] on the basis of MRI data, it shows the feasibility of the MRI-CFD approach al-though the flow results suffer of a limited resolution. A technique for the flow simulation based on

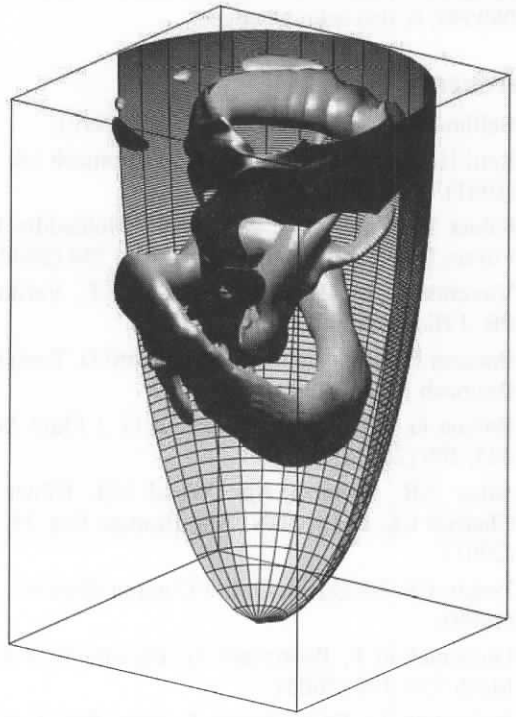

Figure 2: 3D vortex structure at end-diastole found in an idealized ventricle for parameters that correspond to those of a young healthy subject. The picture shows an iso-surface of the λ_2 parameter (intermediate eigenvalue of the squared sum of symmetric and antisymmetric parts of the velocity gradient tensor).

a simplified fluid-tissue coupling was introduced in [8]. Here the fluid problem is solved on a regular domain (typically a periodic box), with a distribution of immersed body forces that mimic, through simplified solid equations, the presence of the elastic wall. Such an approach presents some criticalities but may possibly be further exploited for simulating complex three-dimensional geometries.

The three-dimensional structure of the diastolic flow in a healthy idealised (prolate spheroid) ventricle was shown recently [9] by using an accurate mixed spectral finite-difference method. The three-dimensional intra-ventricular vortex structure is characterized by a deformed vortex ring that connects with vertical legs to the vorticity nearer the entrance, one example is shown in figure 2. The vortex flow develops some weak turbulence when the Reynolds number is large, still in the physiological range of adult or slightly dilated hearts. A further numerical analysis with the same model [10] showed that the asymmetry typically found in normal healthy ventricles corresponds to a minimum of intra-ventricular energy dissipation thus to a maximal efficiency of the LV pump.

2.3 Mitral valve modeling

The mitral valve, connecting the left atrium to the LV, is a bi-leaflet valve that open rapidly with the incoming fluid. The leaflets stay mostly open during filling with some oscillation, or partial closure, during the period between the E and A filling waves (diastasis). The geometry and the movement of the valvular leaflets have an important influence on the intraventricular flow. Recent results and models about the fluid mechanics of heart valves are given in the review [11]. The discussion reported above has intentionally avoided the description of the role of the mitral valve assuming, in a first approximation, that an orifice may mimic a fully open valve. The mathematical modelling of a fluid-valve interaction is made complicated by the large motion of the thin leaflets within the flow domain and their rapid response to the force exerted by the accelerating fluid.

A rigorous mathematical model for the fluid across the moving leaflets should be based on the equations of fluid mechanics for the flow, those of solid mechanics for the leaflets, the proper coupling relations, and tackle the problem of the solution of the resulting system. Recent numerical studies [12] began to deal with such a complete formulation numerically. These employ finite elements and a coupling strategy, to reproduce the flow in models of the aortic valve. Previous numerical approaches are based on immersed boundary methods [8] which, however, at the present stage of development introduce additional degrees of approximation.

An essential ingredient of a complete modelling is the proper mechanical description of the valvular large deformation regime and the knowledge of the actual non-linear elasticity parameters, commonly neither homogeneous nor isotropic. Approximate elastic structures have been considered so far. In general, either the valve material behaviour and its parameters are unknown and quite difficult to assess in physiological applications. For this reason, in addition to the modelling and measurement difficulties, the realistic study of fluid flows in presence of a moving leaflets valve still appears as prohibitive.

With this in mind, the need of some deeper theoretical understanding of the mitral valve motion is probably required to facilitate the description and give some basis to the modelling. An asymptotic analysis of leaflet opening is introduced in [13] for the limiting condition when the leaflet moves following with the fluid such that there is no vortex shedding from its trailing edge. This analysis corresponds to considering the fastest possible motion of a mass-less leaflet. However the close connection of simplified models to realistic valvular dynamics is still to be developed.

2 Conclusions

This brief discussion has shown that some deeper understanding of the physical phenomena involved in the LV fluid dynamics has been achieved in the last years. Nevertheless, a lot of work is still required before this subject becomes mature as a reliable support to diagnostic and therapeutic improvements.

Issue regarding the changes in the LV flow in presence of specific pathologies are still at a very early stage. The lack of activity (for infarction or ischemia) of

a region of the tissue affects the LV flow, similarly changes in geometry and elasticity (due to LV dilatation or reshaping as well as for natural or pathologic hypertrophy) are also reflected on the intraventricular flow arrangement. The physiological and patho-physiological structure of the valvular tissues also plays a fundamental role in the resulting flow.

The feasibility of using LV fluid dynamics for diagnostic purposes also requires that the medical imaging develops technologies able to visualise, or reconstruct, the LV flow. Doppler echography is the principal method currently available and suffers the limitation that only one component of the velocity vector is shows, new techniques are currently under development and will largely strengthen the potential of LV fluid dynamics for diagnostic purposes.

The therapeutic, surgical, procedures in the heart, in particular those related to the prevention of heart failure, operate a remodelling of the heart geometry. In next years it can be expected that LV fluid dynamics may become mature such to provide a reliable support for the optimisation of the new chamber design.

Acknowledgements

The developments discussed so far are due to the collaboration with my colleagues at the University of Trieste and a joint work with Federico Domenichini (Dept. Civil Engineering, University of Firenze), Giovanni Tonti (Dept. Cardiovascular Medicine, Catholic University of Campobasso) and biomedical companies, especially Esaote SpA (Genova) and Bracco Imaging SpA (Milano). Financial support by Italian MIUR, grants FIRB 2001 RBAU01Z44F and PRIN 2004089599, is also acknowledged.

References

[1] Bellhouse BJ. Cardiovas Res 6, 199 (1972).

[2] Reul H, Talukder N, Muller W. J Biomech 14, 361 (1981).

[3] Kilner PJ, Yang GZ,, Wilkes AJ, Mohiaddin RH, Firmin DN, Yacoub MH. Nature 404, 759 (2000).

[4] Vierendeels JA, Riemslagh K, Dick E, Verdonck PR. J Biomech Eng 122, 667 (2000).

[5] Baccani B, Domenichini F, Pedrizzetti G, Tonti G. J Biomech 35, 665 (2002).

[6] Bolzon G, Zovatto L, Pedrizzetti G. J Fluid Mech 493, 209 (2003).

[7] Saber NR, Gosman AD, Wood NB, Kilner PJ, Charrier CL, Firmin DN. Ann Biomed Eng 29, 275 (2001).

[8] Peskin CS, McQueen DM. J Comput Phys 81, 372 (1989).

[9] Domenichini F, Pedrizzetti G, Baccani B. J Fluid Mech 539, 179 (2005).

[10] Pedrizzetti G, Domenichini F. Phys Rev Lett 95, 108101 (2005).

[11] Yoganathan AP, He Z, Jones SC. Ann Rev Biomed Eng 6, 331 (2004).

[12] De Hart J, Peters GWM, Schreurs PJG, Baaijens FPT. J Biomech 36, 103 (2003).

[13] Pedrizzetti G. Phys Rev Lett 94, 194502 (2005).

The ERCOFTAC Best Practice Guidelines for Industrial Computational Fluid Dynamics are

Available in Electronic Form!

The Best Practice Guidelines can now be provided in electronic form.

- For a one-off payment of 2500 Euro, organisations can provide access to all members of staff by placing the Guidelines on their corporate intranet. (Security of the network must be guaranteed)
- Original, fee-paying members of the Quality and Trust Special Interest Group can receive an electronic copy, without charge, from which they are free to make paper copies.

Please contact:

A.G. Hutton
G26/X80
QinetiQ Ltd.
Cody Technology Park
Ively Road
Hants. GU14 0LX, U.K.

Tel.: +44 1252 395568
Fax: +44 1252 395275
Email: aghutton@qinetiq.com

Flow in Artificial Valves and Pulsatile Blood Pumps

Ulrich Kertzscher, Leonid Goubergrits, Klaus Affeld

Universitary Medicine Berlin, Biofluidmechanics Laboratory, Berlin, Germany

leonid.goubergrits@charite.de,
klaus.affeld@charite.de,
ulrich.kertzscher@charite.de

The function of pulsatile blood pumps is very similar to that of the natural heart: the blood chamber expands and contracts analog to the ventricle while inflow and outflow valves direct the blood flow. Initially, the valves used in blood pumps were the valves that were being developed for the replacement of the diseased natural valves. The patient with an implanted artificial valve is often endangered by thrombo-embolic complications. These complications are caused by a complex interaction between blood, material of the valve and the flow. The specific causal flow phenomenon is flow separation. In flow separation, the platelets, the thrombus generating blood cells, come into extended contact with the foreign material and may deposit and aggregate to a thrombus. Therefore the avoidance of flow separation is the objective of valve design. The danger of thrombo-embolic complications is even greater for a patient with an implanted blood pump, which contains two artificial valves. In the case of a valve replacement, the artificial valve is implanted in a vessel whose geometry may only be roughly determined and which is different for each patient. The vessel forms the duct, which has a great influence on the flow through the valve. In the blood pump, however, there is an engineering advantage: the duct can be dimensioned to the will of the designer, while in the body the size and the shape of the duct are given. An attempt to make use of this design freedom is demonstrated by the S-valve, shown in figure 1. It has a disk shaped occluder, which can tilt in order to open and close. In fact it is a Björk-Shiley valve, which is at an incline relative to the direction of the main flow, instead of the normal position, which is at a right angle to it. With this incline, one can achieve that the plane of the disk is in line with the incoming flow – the angle of attack is now zero. In this way, a flow separation at the disk can be reduced. In a straight duct, a disk in this position would not close as a result of flow reversal and for this reason the angle of attack is kept at around 30°. In the S-shaped duct the disk closes, because when the flow reverses its initial flow lines are parallel to the S-shaped duct walls and therefore inclined towards the disk plane. In the open position a flow contraction and a flow diffuser are formed. This can be designed in way that the objective, avoiding of a flow separation, is met. Figure 2 shows the results of an experiment, in which the flow and its effect on residence time and flow separation are made visible.

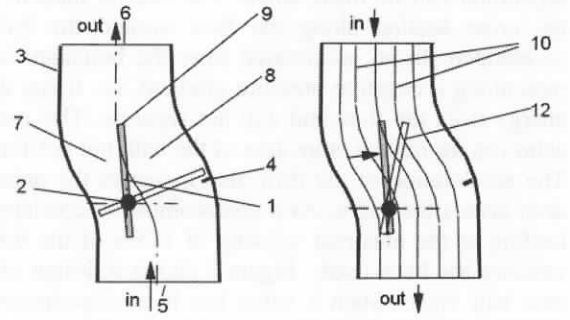

Figure 1: Schematic drawing of the S-valve. It features a disk-shaped occluder, which tilts to open and close. The duct has S-shaped centerline. In the open position on one side of the disk a contraction is formed, while on the other side a diffuser is created.

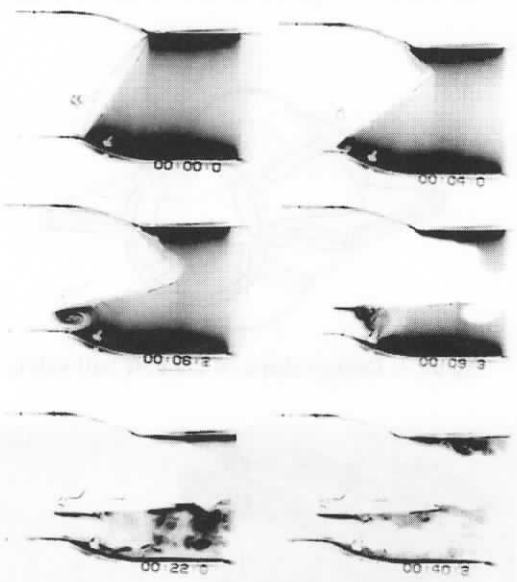

Figure 2: Experimental investigation of the flow. Firstly, the valve is filled with a fluorescent dye, which is then displaced by a clear fluid. In a few milliseconds most of the dye is washed out. This indicates that platelets will lack the residence time to deposit and form a thrombus.

As good as the flow properties of this valve are, it has also a disadvantage: it is difficult and expensive to fabricate. For its simplicity and proven design therefore the ball valve has been considered. In the form of the Starr Edwards Ball valve it was one of the first

successful cardiac replacement valves. Some of its recipients lived with the implant for more than 25 years, which still today is a very good result for a mechanical valve. However, in most of the patients the functional time was much shorter. Only today we can find an explanation for the discrepancy in performance: we assume that in some few patients there was a good match between the valve and the geometry of the aortic root. In the artificial blood pump we have, as stated above, the freedom to design a suitable duct. If a ball is used as an occluder, a different line of thought is followed: the large cross section of a ball makes it impossible to avoid a flow separation in the wake. However, the flow separation can be made small. The duct is shaped, that the cross section along the flow around the ball is accelerated. In an accelerated flow the boundary layer runs along a negative pressure gradient, i.e. it can draw energy from the flow and will not separate. This can be achieved for quite a large area of the ball, but not for all. The acceleration of the flow also increases the pressure drop across the valve. As a compromise an acceleration leading to the maximal velocity of 175% of the inflow velocity has been used. Figure 3 shows a design of the new ball valve. Such a valve has been experimentally investigated and shows the expected properties.

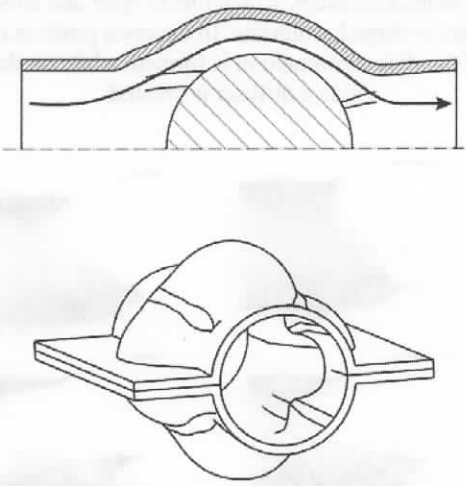

Figure 3: Design shape of the new ball valve.

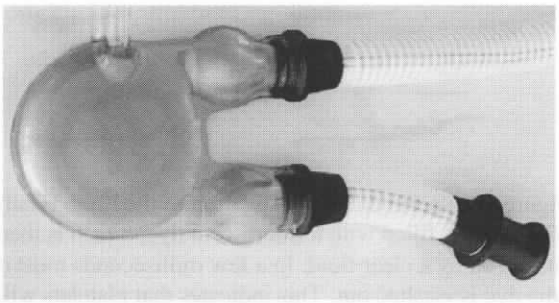

Figure 4: Ventricular assist device prototype with incorporated new cageless ball valves.

The new ball valve is very suitable for the integration in the blood pump. The valve seat, the valve guide and the valve stopper can be made part of the pump inside. In such way steps and rims can be avoided, which are otherwise difficult to avoid and which can be a site for thrombus generation. Figure 4 shows a prototype of the blood pump incorporating two ball valves.

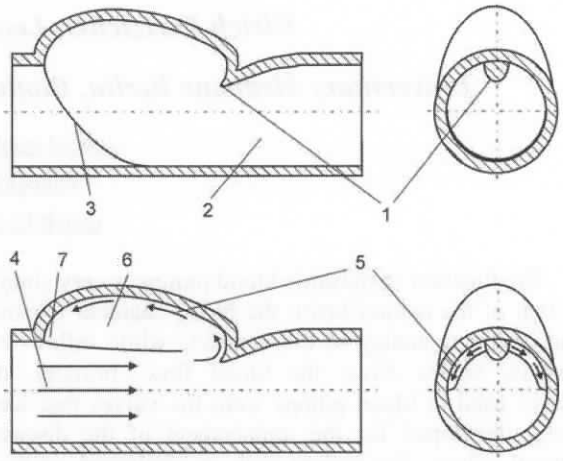

Figure 5: Principle of the new valve design with a purged flow. The leaflet above is closed and the leaflet below is open. The flow divider, 1, is a protrusion of the housing wall into duct, 2. It directs the purge flow, 5, a part of the main flow, 4, into the bulb-shaped part of the housing, 6. The purge flow turns around at the root of the leaflet, 7, and joins the main flow.

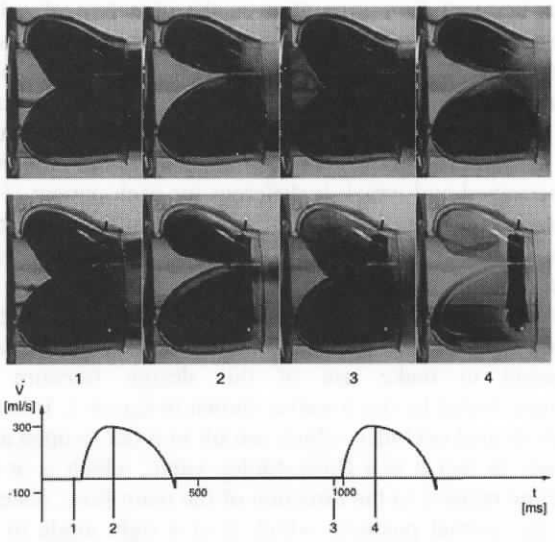

Figure 6: Experiment of washout of the trileaflet valve made of polyurethane. (Top) Four frames show washout process in the conventional valve. After 2.2 cycles the sinus space is still filled with dye. (Bottom) For comparison, washout process in the same valve with a purge flow is shown. The sinus space has been cleaned.

Another concept to avoid thrombo-embolic complications in mechanical valves is the purge flow valve (see fig. 5). In this concept, the aim is not the prevention of flow separation but the minimization of the blood residence time close to an artificial wall. The valve is designed like a natural valve and the flow separation in the sinus behind the valve is accepted. But this region

will be washed out periodically to avoid stagnant flow and hence minimize the residence time of thromboactive substances. The wash out is achieved by a purge flow, which is separated from the main flow during systole. The purge flow is caused by a flow divider. This basic concept was optimized by numerical and experimental means. The effect of the purge flow is shown in figure 6. The top of the figure shows the dye distribution in the sinus behind a conventional valve over two heart cycles. The bottom part of the figure shows the dye distribution for a valve with a purge flow. The enhanced wash out in the valve with the purge flow is clearly visible. This means a reduced danger of thromboembolic complications.

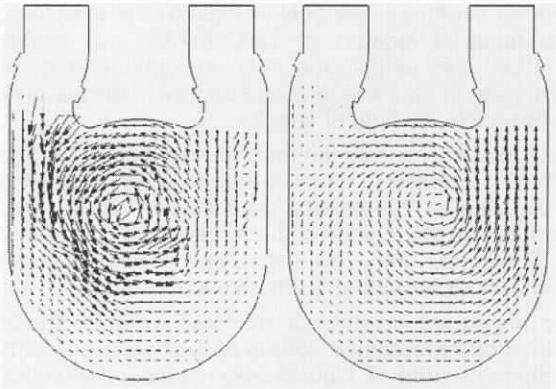

Figure 7: Left, the inflow jet of the inflow valve forms a vortex. The jet is a wall jet and runs along the inside of the blood chamber. It creates a swirling motion of the fluid and thus kinetic energy can be used for the outflow phase shown right.

The flow inside of a blood chamber is mainly determined by the inflow valve. The fluid exits the inflow valve as a jet, very much like in the natural ventricle. The jet enters a large cavity and initiates inevitably a vortex system. In the natural heart this system has a low energy, because the inflow valve has a large cross section and the inflow velocity is low. In a blood pump the velocity is higher, because the artificial valves are less perfect than the natural ones and cause a jet with a higher velocity. If the jet is directed towards the center of the blood pump, a free jet vortex system is generated, which quickly dissipates because of the complex geometry of the blood chamber and the kinetic energy is dissipated in a number of small vortices. However, if the jet forms a wall jet, the rotational energy of the inflow jet can be preserved during the inflow phase. If, in addition, the outflow valve is positioned at the right place, the energy can be used for the outflow phase. This means that blood chamber design of the blood pump is of great importance for good performance of the whole blood pump. Figure 7 shows flow field in a blood chamber designed in our group. Vector fields are obtained experimentally using particle image velocity (PIV) technique. Left is the jet at the beginning of the inflow phase and – right – at the end of this phase. The whole volume performs a swirling motion. This is desirable, because it avoids stagnant areas in the blood chamber.

References

[1] Affeld K, Goubergrits L, Holberndt O. Novel cardiac assist valve with a purge flow in the valve sinus. ASAIO J 44, M642-647 (1998).

[2] Timmel T, Goubergrits L, Affeld K. Optimization and investigation of a novel cardiac assist valve with a purge flow. Int J Artif Organs 24 (11), 777-783 (2001).

[3] Affeld K, Ziemann A, Goubergrits L. Technical obstacles on the road towards a permanent left ventricular assist device. Heart and Vessels Suppl. 12, 28-30 (1997).

[4] Goubergrits L, Affeld K, Kertzscher U. Innovative developments of the heart valves designed for use in ventricular assist devices. Expert Rev. Med. Devices 2(1), 61-71 (2005).

PhD/POSTGRADUATE POSITIONS

GRENOBLE INSTITUTE OF TECHNOLOGY (FRANCE):

Postdoctoral position in Computational Fluid Dynamics and Turbulence, starting in October 2006, in the framework of collaboration between the CNES (French National Center for Space Studies) and the MOST (MOdelling and Simulation of Turbulence) research group of LEGI laboratory (Laboratory for Geophysical and Industrial Flow Research) of Grenoble. It is aimed at the development of Large-Eddy Simulations (LES) of the turbulent flow and of thermal exchanges in the cooling passages of rocket engines. Complex flow geometries, high-Reynolds numbers and real gas effects will be considered. Coupling between statistical modelling techniques and LES will be investigated. More details on the position can be found on the Web site: http://www.cnes.fr. Proficiency in speaking French is not required.

Applicants should send (preferentially by e-mail) their Curriculum Vitae, including a detailed list of their publications, a statement of interest and the addresses of two referees to: Prof. Olivier Métais, ENSHMG, 1023, rue de la Piscine, Domaine Universitaire, BP 95, F - 38402 St Martin d'Hères Cédex, email: Olivier.Metais@hmg.inpg.fr.

VI Workshop on
Modeling of Multiphase Flows in Thermo-Chemical Systems.
Mathematical Modeling of Turbulent Combustion
September 1-3, 2006
Parchowo, near Gdansk, Poland

The Workshop is a cyclic, annual event of interdisciplinary character. The workshops on numerical modelling and experimental techniques in multiphase flows were initiated by late Prof. Z. Bilicki and since 2001 they have been organized annually by Prof. J. Cieslinski from Gdansk University of Technology and Dr. D. Butrymowicz from the Institute of Fluid Flow Machinery of Polish Academy of Sciences, Gdansk. The formula of the workshops assumed that it will have an interdisciplinary character and will attract researchers from fluid mechanics, multi-phase flows, thermodynamics and heat transfer of non-equilibrium phenomena domains.

It is proposed that the key-subject of 2006 Workshop will be devoted to the recent developments in turbulent combustion modeling. Prof. A. Boguslawski from Institute of Thermal Machinery, Czestochowa University of Technology will be responsible for the subject area. The planned scope of the Workshop ranges from advanced models of turbulence-combustion interaction like flamelet, Conditional Moment Closure and stochastic approaches through the problems of reaction kinetics, ignition and extinction modeling and two-phase combustion. Despite that the main topic is related to mathematical modeling of turbulent combustion, also some contribution of experimental works are expected allowing to evaluate a potential prospect for experimental verification of advanced mathematical models.

The organizers are interested in participation of PhD students working in the field covered by the workshop. The financial support of ERCOFTAC will enable to offer scholarships for PhD students wishing to participate in the Workshop and to present the research performed in the field of combustion.

Participation of internationally recognized foreign lecturers is aimed to stimulate the research performed in the area of combustion modeling.Invited keynote speakers are Dr. Epaminondas Mastorakos, University of Cambridge and Professor Jerzy Chomiak from Chalmers University of Technology.

The organising institutions are three working groups of the Fluid Mechanics Section of the Polish Academy of Sciences (Prof. T. Chmielniak), namely: Subsection of Multiphase Flows and Non-Newtonian Fluids (Prof. J. Cieslinski), Subsection of Turbulence (Prof. S. Drobniak) and Subsection of Internal Flows (Prof. P. Doerffer). Since 2004 the Polish Pilot Centre of ERCOFTAC (Prof. S. Drobniak) has been included as the co-organizing institution.

The Workshop was approved as the official ERCOFTAC event and will be held in Parchowo - a village 50 km west from Gdansk in the period 1-3 September 2006. All the organisational matters will be handled by the Gdansk University of Technology and the Institute of Fluid Flow Machinery of Polish Academy of Sciences, Gdansk.

The registration fee, which covers accommodation costs and lecture materials, is **200 EURO.**

Additional information about the Workshop may be found at the website:
http://www.imp.gda.pl/inst_zewn/ppw/index-en.html

Registrations should be directed to:
Dr. Dariusz Butrymowicz
Institute of Fluid-Flow Machinery
of Polish Academy of Sciences
Gen. Fiszera 14, PL-80-231, Gdansk, Poland
butrym@imp.gda.pl

The Workshop was granted the **2000 EURO** scholarship from ERCOFTAC authorities. The organisers intend to give a certain number of scholarships to PhD students who would like to participate in the Workshop. Requests for the grants should be directed to Prof. J.T. Cieslinski (jcieslin@pg.gda.pl), chairman of the Subsection of Multi-phase Flows and Non-Newtonian Fluids until **June 1st 2006**.

Thermal Problems in Hard and Soft Tissue Biomechanics

Maciej Stanczyk
Institute of Fundamental Technology Research
Polish Academy of Sciences, Warsaw, Poland
mstan@ippt.gov.pl

1 Introduction

In the present contribution the overview of recent research activities in IFTR PAS concerning heat transfer analysis in biomechanics is given. The description is divided into two main parts that cover respectively some specific thermal problems in orthopaedics and selected results of the modelling of soft tissue heat transfer phenomena.

2 Exothermic Bone Cement Polymerisation

Cemented prosthesis implantation is a well-established orthopaedic technique, used mainly to fix artificial joints in bone. The polymethylomethacrylate (PMMA) bone cement is used to fill the cavity in the bone at the implantation site. The implant is then fixed in the cement which undergoes the process of in-situ polymerisation, which takes approx. 5–10 min. and yields a stiff cement mantle between the bone and the implant. This layer transfers the mechanical loads from the implant to the bone and helps to reduce the unwanted "stress shielding" effect.

The cementation fixation method is not perfect and loosening of the prosthesis is not uncommon. Figure 1 depicts the cemented component of the knee implant that had to be extracted and replaced with a new one. PMMA cement layer debonded from the bone and remains attached to the metal implant. The figure yields two important insights about the cementing technique. First: the cement layer is very irregular and its thickness can hardly by predicted or prescribed in advance. Second: the location of the joint implant (at the end of a long bone) will often make it necessary that the cement contacts the irregular surface od the trabecular bone rather than the smooth cortical bone. While it is desirable from mechanical point of view, it may be highly unwanted for the thermal reasons.

During the process of polymerisation a certain amount of latent heat is released. Since exposition to elevated temperature may cause necrosis of the bone tissue, which may be detrimental to the stability of the implant, the investigation of the temperature distribution in bone is undertaken.

Two separate problems were approached. First is to study the kinetics of the heat release during the PMMA polymerisation and propose suitable theoretical model. Second was to investigate the temperature distribution in the region most exposed to adverse thermal conditions i.e. domain of interpenetration of cement and trabecular bone.

2.1 Kinetics of the PMMA Polymerisation

Introduction

The subject of this study was to develop a mathematical model of bone cement polymerisation for prediction of heat generation rate in the cement mantle.

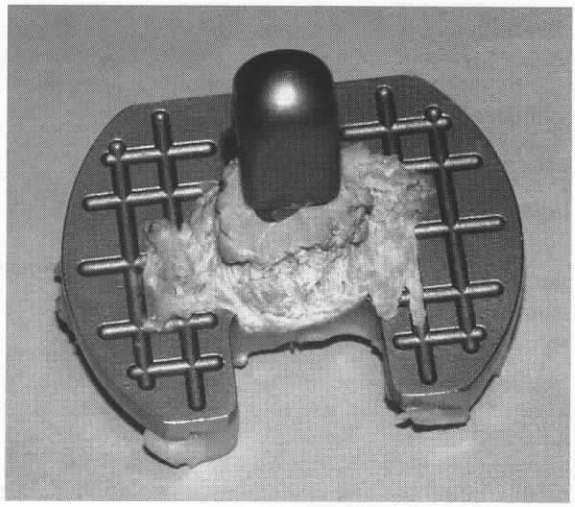

Figure 1: An explanted tibial component of the cemented knee joint prosthesis. Irregular lumps of PMMA bone cement were removed along with the implant and are visible in the center.

The detailed account of the model can be found in [7].

Models that are frequently used in the biomechanical literature have the following form:

$$\frac{\partial w}{\partial t} = \varphi(w, T, t) \tag{1}$$

where w is a measure of the polymerisation process, usually called the polymerisation fraction. The heat generation rate q [W/m^3] is proportional to the polymerisation rate:

$$q = L\frac{\partial w}{\partial t} \tag{2}$$

where L is a latent heat of polymerisation.

The function φ defines the kinetics of the polymerisation and is usually defined in such a way so that agreement with experiments is obtained. There are however not many theoretical constraints on the form of this function and indeed the formulae proposed by various authors are different. Huiskes proposes a prescribed function of time only [3], Baliga et al. [2] used the second order polynomial in w multiplied by the fifth-order polynomial in temperature, while Mazzullo et al. [5] proposed a power function in w multiplied by exponential function of temperature. The goal of the present study was to derive an appropriate model of polymerisation without a-priori assuming the form of the relation.

Chain growth model

The presented model rests on the following assumptions:

1. The material is treated as a collection of *chains*. Every chain is composed of a number of *meres*. Each chain is therefore characterised by its length as measured in the number of constituent meres.
2. Each chain is characterised by a number of *active centres* $\in \{0, 1, 2\}$ that determine the potential of the chain to bind to other chains.
3. The chains with nonzero number of active centres can bind together to form a new chain. The length of the resulting chain is the sum of the lengths of the chains that formed it. The number of active centres of the chain is the sum of numbers of active centres of these chains minus two. The act of formation of the binding between two chains liberates an elementary amount of heat Q_e.
4. The susceptibility of the chain to a chemical reaction is dependent on the temperature and chain length only.
5. No depolymerisation is allowed (hence chains may not break up forming smaller chains).

According to the first assumption the material is described in terms of the sequence of functions $N_i(n,t)$ which denote the number of chains of length n and i active centres at time t, divided by the number of all the meres occupying the unit volume of the cement. The following conservation equation holds:

$$\sum_{i=0}^{2}\sum_{n=1}^{\infty} nN_i(n,t) = 1 \tag{3}$$

The required polymerisation kinetics equations now take on the form:

$$\frac{\partial N_i(n,t)}{\partial t} = C_i(n,t,T) - D_i(n,t,T) + G_i(n,t,T) \tag{4}$$

where $i = 0, 1, 2$ and $n > 0$. By C we denote the rate of creation of particular chain species (by reactions between smaller chains); D is the rate of the disappearing of particular chains (as they are used up in the reactions to form longer chains); G reflects the polymerisation initiation effect, which will be not discussed in detail here.

The detailed formulae for the C and D functions are then derived on the basis of the assumptions described above. Once they are known, the heat generation rate can be obtained as

$$q = Q_e N \sum_{i=0}^{2}\sum_{n=1}^{\infty} \frac{\partial N_i(n,t)}{\partial t} \tag{5}$$

with N being the number of meres per unit volume. The last equation is derived from the fact that the heat generation rate is proportional to the time derivative of the number of chemical bindings (assumption 3) that can be readily expressed using the functions $N_i(n,t)$.

The polymerisation problem is coupled to the heat conduction problem as the rates C and D are temperature-dependent (assumption 4). The actual calculation using the presented model can only be approximate, even for isothermal conditions. This is caused by the fact that the number of separate chain species described by the model is not finite. This also appears to be the most significant shortcoming of the model.

2.2 Study of PMMA Polymerisation at the Bone-Cement Interface

Introduction

The goal of this study was to estimate the temperature history in the course of bone cement polymerisation in the immediate vicinity of the bone. During surgery, in certain areas (e.g. in the proximal region in the hip implantation) the cement is pressed between the implant and the surface of the trabecular bone. It can be expected that while in the doughty, semi-solid state, the cement will penetrate the intertrabecular spaces. This may lead to the significant increase in the heat exchange rate between the two materials and, in consequence, increase the maximum temperature in bone, and decrease the temperature in the cement mantle (prolonging the polymerisation time and leading to the presence of unwanted monomer leftover. The detailed account of the presented analysis can be found in [9].

Modelling

In order to reproduce the temperature distribution during the polymerisation the numerical model was constructed. To obtain the necessary description of the geometry of the cement-bone junction, the physical model was manufactured using the bovine bone sample and the bone cement mixture. The sample was then scanned in micro tomograph. The resulting representation was then filtered, segmented and converted to the mesh of finite elements suitable for commercial FE system ABAQUS. It consisted of $35 \times 35 \times 119$ cubic elements. An outline of the mesh is shown in fig. 2.

The long axis of the sample is perpendicular to the cement-bone boundary. The side walls of the sample were assumed adiabatic, as well as the 'cement side' wall. On the 'bone-side' wall the third order (convective) boundary convection was assumed. The initial temperature of the entire region was assumed equal 300 K.

The polymerisation process was modelled by the polymerisation-fraction-based kinetics equation of the following form (see [5]):

$$\frac{\partial w}{\partial t} = a \exp\left(-\frac{E_a}{RT}\right) P(T, w) \tag{6}$$

where a and E_a are model constants and the function P is a given in [5, 9].

The calculations comprised simultaneous solution of both the heat conduction and polymerisation kinetics equations within the sample volume. Figure 3

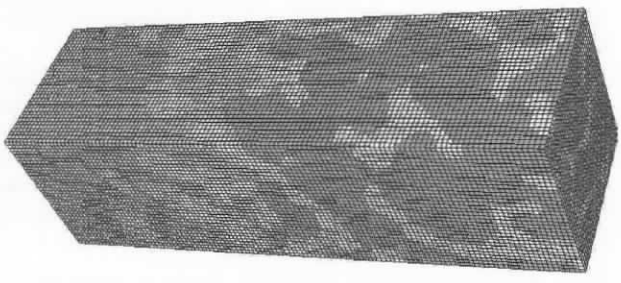

Figure 2: A fragment of the mesh used in FE simulation. Yellow denotes cement and green—marrow spaces. White is bone tissue. After [9].

depicts one of the obtained results: the distribution of the polymerisation fraction (hence the progress of polymerisation) at several time moments. It can be seen here that the polymerisation in the immediate vicinity of bone is retarded and incomplete. Since increase in w is probably related to the transition of mechanical properties of the cement, then residual stress may arise as an effect of the polymerisation inhomogeneities depicted in fig. 3.

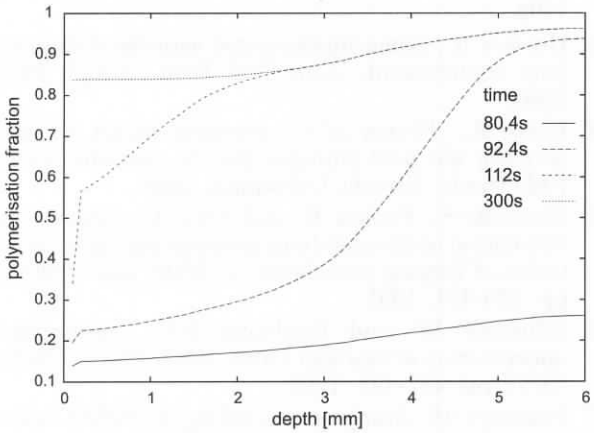

Figure 3: Distribution of area-averaged polymerisation fraction at several time instants. Depth = 0 denotes the deepest cement penetration into the bone, depth = 5 is in the bulk of the cement.

Resulting distributions showed a fair agreement with other studies in terms of the average temperature and monomer leftover. The maximum temperature of 64°C predicted in bone is higher than results obtained from models that neglect interpenetration (57°C in model using the same polymerisation kinetics, [5]). It is however smaller than the maximum temperature obtained from simple model of interpenetration on a generic interface, provided by Huiskes in [3] (78°C). Probable reason for this discrepancy is the fact that the polymerisation model in [3] was temperature-independent and therefore did not take into account the cooling effect of the bone trabeculae on the power output of the cement.

The average monomer leftover calculated in the bulk of cement is similar to the values reported in the literature (around 5%), while the maximum is significantly higher (up to 15%). To the best of our knowledge, there are no other models in the literature including both the monomer leftover effect, and inhomogeneity of the polymerisation.

3 Modelling of Heat Transfer in Perfused Tissue with a Vascular Model

3.1 Introduction

This study aimed at developing a method to include the effect of discrete blood vessels in the soft tissue heat transfer calculations, that would be less computationally expensive than approaches known in the literature. The presented attempt is based on the fact that most of the thermally-significant blood vessels in human body exist in the form of closely juxtaposed counter-current artery-vein pairs. Therefore, it is the counter-current artery-vein vessel pair segment that is the primitive building block of the blood vessel system, not the single vessel segment. In that respect, the proposed approach is different from e.g. the method described in [4, 10], where a more general

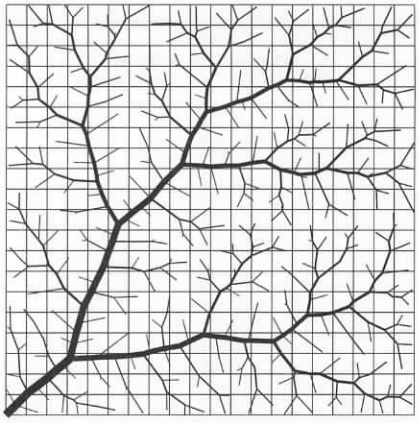

Figure 4: Vessel geometry used in simulation

view is taken and the feeding and draining vessel tree are modelled entirely separately. A detailed description of the method can be found in [8].

3.2 Method

The considered approach consists of three basic steps: generation of the vessel tree geometrical description, generation of the tissue mesh and subdivision of the tree, and calculations of the tissue and blood temperature distributions. These steps will now briefly be described here.

The geometrical description of the tree is generated by means of the growth algorithm, developed by Schreiner and Buxbaum in [6], based on the minimum blood volume criterion. For a given domain, one generates the vessel tree step-by step in such a way that two conditions are satisfied at every stage of generation:

- a general form of Murray's law is satisfied: $r^{\gamma}_{parent} = \sum r^{\gamma}_{daughter}$: a relationship between the radii of the parent and daughter vessels in a bifurcation (γ is a constant ≈ 3),
- for a given inlet pressure of the vessel tree, and all terminal pressures being equal, all terminal flows are also equal (provided certain assumptions on the blood flow in the tree hold true), see [6].

The regular tissue finite element mesh is then introduced and the existing vessel description is subdivided in such a way that each vessel pair segment is contained in exactly one tissue element. The solution of the vessel blood temperature problem is then approximated by means of the set of interconnected one-dimensional regions (intervals), where linear interpolation of temperature between the vessel pair segment connecting points is assumed. Each vessel pair segment contributes four unknowns: inlet and outlet arterial and blood temperatures. Two segment equations are finite-difference forms of energy conservation equations for counter-current vessels (see also [1]), and two others express the conservation of arterial blood temperature as the flow splits in the bifurcation and mixing of the blood in the venous system bifurcation (where two veins meet).

For the tissue, standard finite element procedure is assumed. The heat exchanged between the blood and tissue contributes to the source term in the tissue finite elements that contain blood vessel segments. Present implementation allows calculations of blood and tissue temperatures in a two-dimensional domain. Example simulation has been conducted on

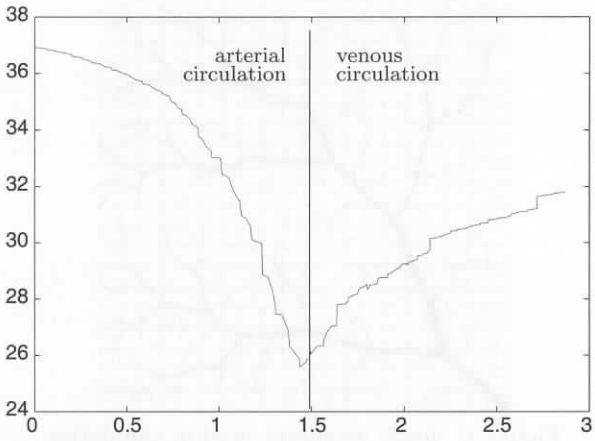

Figure 5: Blood temperature in the circulatory loop.

the square region of tissue containing the countercurrent vessel tree shown in fig. 4.

As an example result, in fig. 5 we present here the steady-state temperature of the blood travelling from the arterial root to the venous root via the circulatory loop embedded in tissue, against the distance travelled (in arbitrary units). Tissue temperature at the vicinity of root segments (left and right sides of the figure) is equal to the temperature of the arterial blood inflow, while at the vicinity of the arterio-venous capillary junction (where the blood temperature is the lowest) it is 25°C.

Venous mixing leads to discontinuities in blood temperature (as seen on the right side of the fig. 5) and discontinuities in heat flow to the artery (from the countercurrent vein), which manifests itself in discontinuous slope of blood temperature in the arterial part of the circulation (as shown on the left side of the fig. 5).

Comparison of the proposed method with other methods available in the literature, notably with the more general method presented in [4, 10] is a subject of ongoing study.

Bibliography

[1] Baish J.W., Ayyaswamy P.S. and Foster K.R., Small-scale temperature fluctuations in perfused tissue during local hyperthermia, *J. Biomech. Eng.*, 108, pp. 246-250, 1986.

[2] Baliga B.R., Rose P.L. and Ahmed A.M., Thermal modeling of polymerizing polymethylmethacrylate, considering temperature-dependent heat generation, *J. Biomech. Eng.*,114, pp. 251-259, 1992.

[3] Huiskes R., Some fundamental aspects of human joint replacement, *Acta Orth Scan.*, Suppl. 185, 1980.

[4] Kotte A., *Design of a numerical model for describing the heat transfer due to vascular trees*, PhD thesis, Utrecht University, 1998.

[5] Mazzullo S., Paolini M. and Verdi C., Numerical simulation of thermal bone necrosis during cementation of femoral prostheses, *J. Math. Biol.*, 29(5), pp. 475-494, 1991.

[6] Schreiner W. and Buxbaum P.F., Computer-optimization of vascular trees, *IEEE Trans. BME*, 40(5), pp. 482-491, 1993.

[7] Stańczyk M., Study on modelling of PMMA bone cement polymerisation, *J. Biomech.*, 38(7), pp. 1397-1403, 2005.

[8] Stańczyk M., *Vascular Model of Heat Transfer in Perfused Tissue*, IFTR PAS, CoE Abiomed, Warsaw, 2005, in press.

[9] Stańczyk M. and van Rietbergen B., Thermal analysis of the bone cement polymerisation at the cement-bone interface, *J. Biomech.*, 37, pp. 1803-1810, 2004.

[10] van Leeuven G., *Numerical simulation of heat transfer in hyperthermia*, PhD thesis, Utrecht University, 1998

PhD/POSTGRADUATE POSITIONS

GRENOBLE INSTITUTE OF TECHNOLOGY (FRANCE):

Postdoctoral position in Computational Fluid Dynamics and Turbulence, available immediately, in the framework of a French research network dealing with the development of efficient modelling tools for unsteady simulations of turbulent flows at high Reynolds numbers. It is aimed at designing advanced coupling procedures between Large-Eddy Simulations (LES) techniques and statistical modelling approaches based on Reynolds Averaged Navier-Stokes (RANS). The development of efficient immersed boundary conditions will furthermore allow simulating complex flow geometries. A particular focus will be placed on flows involving heat transfers with applications to thermal-hydraulics, heat exchangers, cooling devices of combustion chambers. The work will take place in Grenoble at the LEGI laboratory (Laboratory for Geophysical and Industrial Flow Research). Proficiency in speaking French is not required.

Applicants should send (preferentially by e-mail) their Curriculum Vitae, including a detailed list of their publications, a statement of interest and the addresses of two referees to: Prof. Olivier Métais, ENSHMG, 1023, rue de la Piscine, Domaine Universitaire, BP 95, F - 38402 St Martin d'Hères Cédex, email: Olivier.Metais@hmg.inpg.fr.

Note: For information, one half of page in the Bulletin is allocated for announcing PhD/postgraduate positions in the form of two or three lines of text per announcement. For submission, please contact the Editor at ercoftac@epfl.ch.

SPECIAL INTERESTING GROUP ON TURBULENCE MODELLING – SIG 15

12TH ERCOFTAC WORKSHOP ON REFINED TURBULENCE MODELLING

TECHNICAL UNIVERSITY BERLIN, GERMANY

OCTOBER 12-13, 2006

http://www.cfd.tu-berlin.de/ercoftac-workshop06.html

BACKGROUND

Computational Fluid Dynamics (CFD) has developed to a key technology which plays an important role in design, development and optimization in engineering practice. The ERCOFTAC Workshops on Refined Turbulence Modelling aim to bring together scientists, researchers, users and developers from industry and from the academic field. Similar to the previous workshops in Lyon (1992,1993), Lisabon (1994), Karlsruhe (1995), Chatou/Paris(1996), Delft (1997), Manchester (1998), Helsinki (1999), Darmstadt (2001), Poitiers (2002) and Gothenburg (2005), some fundamental phenomena, but also some industrially relevant problems have been chosen as test cases for this workshop.

TEST CASES

The workshop focuses on four test cases involving numerous features of scientific and engineering relevance (three-dimensionality, unsteady wake regions, periodicity, separation and reattachment, swirling effects, turbulent mixing, etc.):

CASE 11.1:

Flow over a wall-mounted, 2-D hump with oscillatory zero-mass-flux jet or suction through a thin slot (Exp.: Greenblat et al., 2005)

Coordinator S. Saric: Saric@sla.tu-darmstadt.de

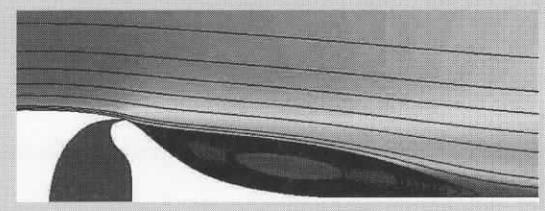

CASE 11.2:

Flow over a 3-D hill (Exp.: Simpson et al., 2002)

Coordinator M. Leschziner: Mike.Leschziner@imperial.ac.uk

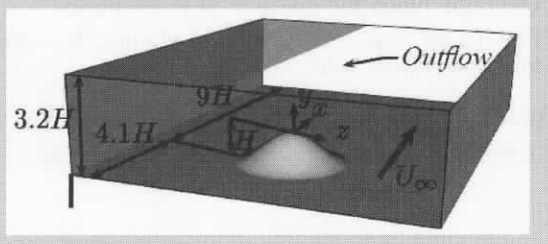

CASE 12.1:

Tip-gap turbulent flow in a low-speed, linear compressor cascade (Exp.: Tang and Simpson 2004)

Coordinator F. Menter: Florian.Menter@ansys.com

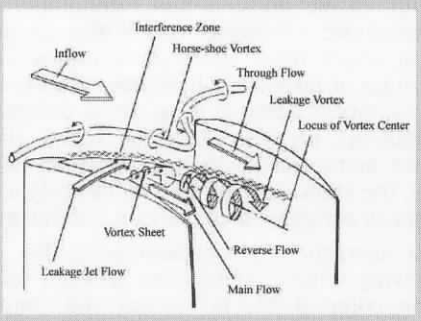

CASE 12.2:

Flow and mixing in a model of swirl combustor (Exp.: Palm et al., 2005)

Coordinator S. Jakirlic: S.Jakirlic@sla.tudarmstadt.de

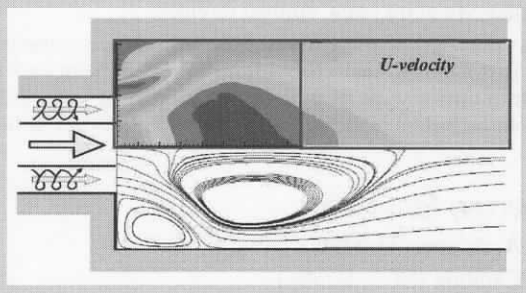

SIG-15 STEERING COMMITTEE

Prof. K. Hanjalic, Dr. S. Jakirlic, Prof. B.E. Launder, Prof. D. Laurence, Prof. M.A. Leschziner, Dr. R. Manceau, Dr. F. Menter, Prof. W. Rodi and Dr. S. Wallin

LOCAL ORGANIZING COMMITTEE

Prof. F. Thiele, O. Frederich and D. Eschricht

IMPORTANT DATES

Results submission: September 1, 2006

Registration: September 1, 2006

CONTACT:

Prof. F. Thiele, Hermann-Foettinger Institute for Fluid Mechanics, Technical University Berlin, Mueller-Breslau Strasse 8, D-10623 Berlin, Germany, Frank.Thiele@cfd.tuberlin.de

Conference on Turbulence and Interactions - TI2006 IGeSA Porquerolles, France May 29 - June 2, 2006

http://www.onera.fr/congres/ti2006/

Scientific Scope

Turbulence is a nonlinear phenomenon which is encountered in most fields dealing with the description of the universe and technology, ranging from astrophysics to engineering. While, for turbulent motion in simple flows, many observations related to the dynamics of turbulence have been reported during the last century, leading to an accurate understanding of interactions between different scales (isotropic turbulence, homogeneous shear, pure strain, solid body rotation), the knowledge of the nonlinear dynamics of turbulence in complex interactions is still incomplete.

Complex interactions are understood at this point in the following senses: interactions between scales and modes in compressible turbulence and coupling of turbulence with other physical mechanisms such as acoustics, heat and mass transfer, radiation, structure vibrations-deformation, multiphase dynamics, etc.

The advanced research themes have many industrial applications in civil and military aviation, terrestrial transportation, engine design, environmental management and new control devices.

The purpose of the present Conference, co-organised by ERCOFTAC, is to provide researchers from various communities with an updated panorama of knowledge about turbulence and its interactions with other fields.

Invited Speakers

N. A. Adams (TUM, Garching)
C. Cambon (ECL, Écully)
J.-P. Dussauge (IUSTI, Marseille)
D. A. Gosman (Imperial College, London)
Y. Kaneda (Nagoya University, Nagoya)
O. Simonin (IMFT, Toulouse)
G. Tryggvason (WPI, Worcester)
D. Veynante (ECP, Châtenay-Malabry)
F. Waleffe (Univ. of Wisconsin, Madison)
Y. K. Zhou (LLNL, Livermore)

Organizing Committee

Michel Deville (EPFL, Lausanne)
Thiên-Hiêp Lê (ONERA, Châtillon)
Pierre Sagaut (UPMC, Paris)

Scientific Committee

Y. Andreopoulos (CCNY, New York)
D. Carati (ULB, Bruxelles)
P. Comte (LEA, Poitiers)
P. A. Davidson (Univ. of Cambridge, Cambridge)
M. Deville (EPFL, Lausanne)
R. Friedrich (TUM, Garching)
T. B. Gatski (LEA, Poitiers)
B. Geurt (Univ. of Twente, Enschede)
T.-H. Lê (ONERA, Châtillon)
E. Leriche (EPFL, Lausanne)
J. Magnaudet (IMFT, Toulouse)
Ph. Petitjeans (ESPCI, Paris)
T. Poinsot (IMFT, Toulouse)
P. Sagaut (UPMC, Paris)
N. Sandham (Univ. of Southampton, Southampton)

Calendar

13 January 2006: Deadline for Extended abstracts (from selected abstracts)

6 March 2006: Notification to Authors

9 May 2006: Deadline for Submission of Camera-Ready Papers

Registration and Fees

Registration on TI2006 website.

Fees are 327 euros or 294 euros (for "young "scientist, member of ERCOFTAC).

Accommodation

The conference is hosted by the IGeSA Centre, at the village of Porquerolles.

- Full board with double room (two beds) including breakfast, lunch and dinner = 54 Euros/person
- Full board with single room including breakfast, lunch and dinner = 61,50 Euros/person

For hotels see:
www.provenceweb.fr/e/var/porquerolles/hotels.htm

COUPLED HEAT TRANSFER PROCESSES IN A DOUBLE WALL INFANT INCUBATOR

A.J. Nowak [1], M.K. Ginalski [1], L.C. Wrobel [2]

[1] Institute of Thermal Technology, Silesian University of Technology, Konarskiego 22, 44-100 Gliwice, Poland

[2] School of Engineering and Design, Brunel University, Uxbridge UB8 3PH, United Kingdom

ginalski@itc.polsl.pl

Abstract

The main objective of this study is to investigate the major physical processes taking place inside an infant incubator, after modifications have been made to the interior chamber. Additional screens (double walls) are used in the modern incubators to decrease radiation heat losses from the infant child. However, these improvements affect the flow and temperature fields inside the incubator. The present study investigates the effect of these modifications on the convective heat flux from the infant's body to the surrounding environment inside the incubator. Due to the geometrical complexity of the model, CAD applications were used to generate a computer-based model. All numerical calculations have been performed using the commercial CFD package Fluent, together with in-house routines used for managing purposes and User-Defined Functions which extend the basic solver capabilities. The results obtained were numerically verified as well as compared with results published in the literature.

1 Introduction

Infant incubators are nowadays widely used in the modern neonatal units [1] to save newborns lives and to provide them with appropriate environmental conditions. These conditions are absolutely crucial for newborn proper grow in the very early stage of the life. In this paper results of the numerical modelling of the fluid flow and energy/heat transfer processes occurring in the incubator are discussed. Understanding of these phenomena is essential for the correct design of comfortable, safe and effective medical equipment. Because of the very complex nature of those physical phenomena the whole available information regarding that subject was up-to-now obtained rather through experimental techniques tested only on neonates animals [2] and adults [3]. Some of these tests were carried out even 40-50 years ago [4]. All that information must be treated as general guidelines and used with certain factor of uncertainty. Because of that it seems to be essential to develop relevant numerical algorithms capable of examining, with appropriate accuracy, the heat and fluid flow processes and their results within an incubator environment. In this study a commercial CFD (Computational Fluid Dynamics) package known as Fluent is applied to build a computational model and calculate results.

The Computational Fluid Dynamics is the methodology which models involving fluid flow and heat transfer with conjugated phenomena such as mass transfer processes, chemical reactions etc. Although the human body has not only a complicated physical shape, but it also has complex thermo-physiological properties, the rapid advances in computer technology and relevant software allow to investigate processes taking place within neonate incubator. This study presents the major mechanisms of heat transfer between a newborn infant and environment within modern incubator. This incubator is provided with the additional over-head screens aiming to decrease radiation heat losses from the infant's body. In order to validate the usefulness of this design modification, the mass flow and heat transfer mechanisms are analysed before and after the proposed modification.

2 Numerical model

Mathematical model of the coupled fluid flow and heat transfer processes in the double-wall incubator is based on the classical continuity, momentum and energy equations. The following main assumption are made:

- Steady-state model is considered.
- Airflow through the incubator is laminar and viscous.
- Original shapes and general dimensions of the infant incubator as well as the newborn baby have been set according to available data [1, 4-6].
- The amount of heat lost by a premature baby due to conduction is very small compared to the total heat exchange between the child and the surrounding environment. For this reason, this process was neglected in this study [4-6].
- The impact of the water evaporation process from the newborn's body on the internal incubator thermal conditions was examined using the Discrete Phase Model available in Fluent [7].
- Heat exchange due to respiration has been included and subtracted from the total amount of heat generated by the newborn's body.
- The Discrete Ordinate Model [7] was used to model the radiation process between the infant and the surrounding environment.

Essential contributions to the total heat transfer between a newborn infant and its environment are given by the thermal radiation and water evaporation. In this paper, only surface radiation described by the brightness of the relevant surface elements, i.e. the infant's skin and walls of the incubator, has been considered.

The last section of the mathematical model includes the equations which describe the evaporation of sweat particles from the surface of the body. Once the trajectory of a particle is computed, Fluent keeps track of the heat, mass and momentum gained or lost by the particle stream that follows that trajectory [2]. These quantities can be incorporated in the subsequent continuous phase calculations. Therefore, while the continuous phase always impacts on the discrete phase, it is also possible to incorporate the effect of the discrete phase trajectories on the continuous phase.

3 Solution procedure

In order to make the calculation process fully automatic, a managing program was created to deal with all the essential stages of the numerical simulation, step by step. Particularly, after the creation of the model geometry in the CAD package *CATIA*, the pre-processor *GAMBIT* is used to generate the numerical grid. In the next step, the managing in-house program reads information regarding boundary conditions, material properties and initial parameters. Following this step, the *FLUENT* main solver is launched and calculations are performed. Once a grid has been read into Fluent, all remaining operations are performed within the solver.

4 Results and discussion

The heat transfer rate from the newborn child to the surrounding environment is directly related to the temperature and air velocity within the incubator. Moreover, based on this information, Fluent calculates the heat losses from the infant's body and provides results of heat losses due to convection, radiation and evaporation.

The simulation confirms the air movement conforms to the basic working principles of the Caleo™ Infant Incubator [8]. Figures 1-2 and 7-8 show clear differences in flow and temperature fields between the two cases analysed. In the incubator with the internal screen, the main air stream from the inlets separates into two. One of these streams starts circulating and warms up the baby. The second stream warms up only the internal screen and after mixing with the stream from the inlets located on the opposite side of the incubator, it moves directly to the outlets. The analysis also shows that the circulating air creates a zone around the baby where the air velocity is almost zero. Due to this fact, convection heat losses from the child to the surrounding air in this region are greatly reduced. This process can be seen in Figures 3-4, which shows the distribution of the convective heat flux on the infant's body (negative values on the scale indicates heat flux provided to the baby). The upper part of the chest and the head of the child are in direct contact with the circulating air. Therefore, heat transfer due to convection is larger in those areas.

The distribution of the radiative heat flux on the newborn's skin is presented in Figures 5-6. A reduction of the heat loss due to radiation can be seen in Figure 6. This fact indicates that incubators with internal screens (double walls incubators) significantly decrease the radiative heat losses from the infant's body.

The last stage of the analysis examines the evaporation process from the infant's skin. Evaporation of moisture greatly decreases the temperature of the skin. Therefore, the impact of this energy balance component is very important for the thermal comfort of the infant. Relevant numerical values of evaporation heat losses are presented in Table 1. In extremely low birth weight infants, evaporation is a major source of heat loss. Evaporative heat flux from the infant's body is steadily distributed and the influence of radiation and convection is almost unnoticeable. Using a high ambient humidity in the incubator reduces the loss of heat by evaporation. However, in this study, this process was only examined for air with ambient humidity of 50%.

Incubator with over-head screen	Incubator without over-head screen
Heat transfer rate due to convection	
0.02 W	0.015 W
Heat transfer rate due to radiation	
0.356 W	0.451 W
Heat transfer rate due to evaporation	
1.720 W	1.714 W
Total heat transfer rate from the newborn's body	
2.08 W	2.18 W
Heat generated by the newborn's body	
1.25 W	1.25 W
Deficit of heat	
-0.62 W	-0.715 W

Table 1: Comparison of the performance of two types of incubators

5 Conclusions

As shown in this work, modern numerical methods can successfully be used in biomedical engineering to solve complex heat and mass flow problems with high accuracy. The procedure described in this study is very efficient and flexible. New designs, materials and technologies can be examined first by using numerical models, which will save time and money in the complete design cycle of new products.

The possibility of interfacing two different types of software, such as CAD and CFD, was also examined in this paper. In order to generate the complex incubator and human body geometries, a powerful CAD application (CATIA) was employed. A STEP file was then used to transfer the geometry created by the CAD application to the CFD software. Models transferred from CAD applications are much more accurate compared with models created directly in CFD packages. Therefore, a heat transfer analysis which is strongly dependent on the model geometry can be performed with higher accuracy.

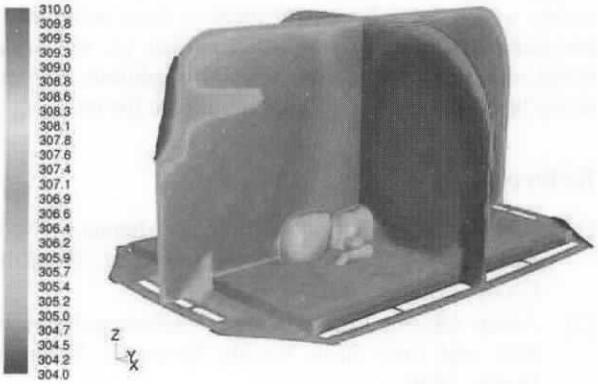

Figure 1: Temperature distribution within an infant incubator without the over-head screen (K).

Figure 2: Temperature distribution within an infant incubator with the over-head screen (K).

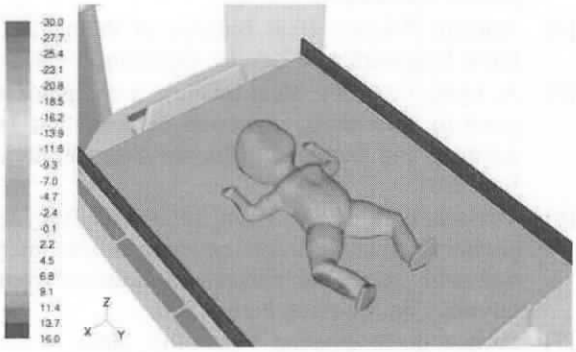

Figure 3: Contours of the convective heat flux plotted on the newborn's skin nursed inside the incubator without the over-head screen (W/m2).

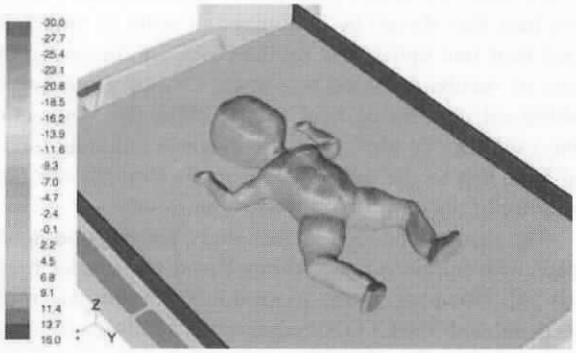

Figure 4: Contours of the convective heat flux plotted on the newborn's skin nursed inside the incubator with the over-head screen (W/m2).

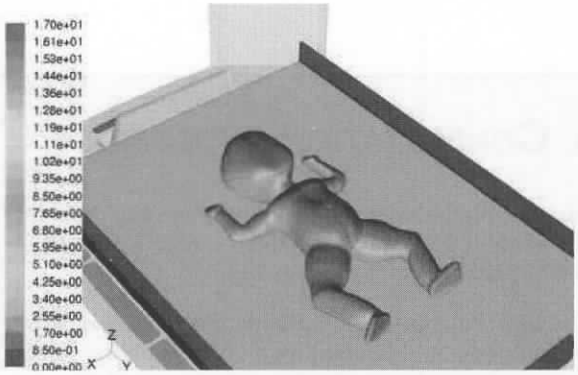

Figure 5: Contours of the radiative heat flux plotted on the newborn's skin nursed inside the incubator without the over-head screen (W/m2).

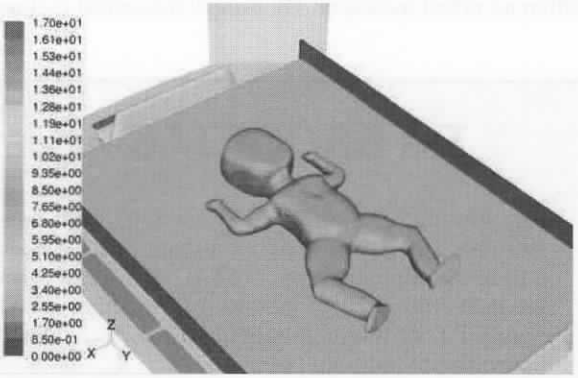

Figure 6: Contours of the radiative heat flux plotted on the newborn's skin nursed inside the incubator with the over-head screen (W/m2).

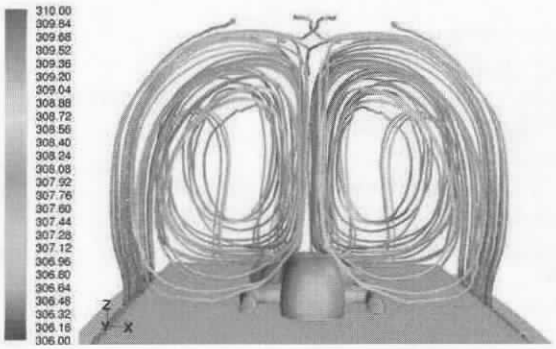

Figure 7: Path lines colored by total temperature inside the incubator without over-head screen (K).

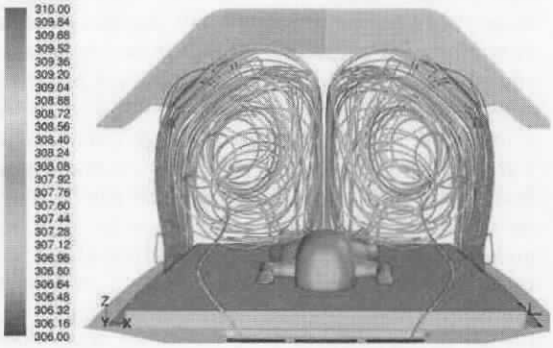

Figure 8: Path lines colored by total temperature inside the incubator with over-head screen (K).

Unlike previous studies, using the procedures presented in this paper, individual cases can be examined. This includes identical twin infants placed in the same incubator or some extremely ill premature newborns. It is also possible to examine several special cases and use the results to create a system of graphs or equations, which can then be used for the determination of the heat transfer rate from the infant's body to the surrounding environment within an infant incubator.

From the thermal point of view, the Caleo™ infant incubator is a well-designed neonatal unit. The temperature and velocity fields show that the characteristic geometry and the specific way the air flows within the incubator are unique and very efficient. An additional over-head screen not only reduces radiative heat flux, but also changes the airflow inside the incubator in such a way that convective heat fluxes are reduced. Convective heat flux should be minimized in order to reduce the total heat rate that is lost by the child. Moreover, in this type of incubator, there is a possibility of providing an additional amount of heat to the child (by convection only) that can be useful for significantly reducing the total heat lost to the environment or to increase the temperature of the newborn's body, if necessary.

The results obtained in this study are in good agreement with previous calculations based on simpler methods [4]. However, much more detailed information can be generated via CFD simulations. Therefore, it can be assumed that the algorithm presented here is efficient and possesses the necessary capabilities for calculating the thermal factors present during the neonatal care within an infant incubator. By using a numerical method, we can save time and money during the design process of new infant incubators, while maintaining levels of accuracy which are at least equivalent to those achieved in previous studies using simplified models [5, 6]. Additional measurements in real hospital conditions are currently being undertaken to further validate the models.

References

[1] J.M. Rennie, N.R.C. Robertom. A Manual of Neonatal Intensive Care. Arnold Hodder Headline Group, London 2002.

[2] Albert Okken, Joahim Koch. Thermoregulation of Sick and Low Birth Weight Neonates. Springer, Berlin, 2000.

[3] Yunus A. Cengel. Heat transfer a practical approach. McGraw-Hill, 2001

[4] Joachim Wasner. Heat Balance of Premature Infants. Dragwerk AG, Lubeck, Germany, 1994.

[5] A. Lyon, C. Oxley. Heat Balance, a computer program to determinate optimum incubator air temperature and humidity. Elsevier Science, Ireland Ltd. 2001.

[6] V. Bach, F Telliez, G. Krim, J.P. Libert. Body temperature regulation in the newborn infant: interaction with sleep and clinical implications. Neurophysiol Clin, Elsevier, Paris, 1996.

[7] Product documentation. Fluent Inc., 2000.

[8] Commercial information provided by Dräger Polska, 2002.

The ERCOFTAC Industrial Consultation Initiative

Part of the remit of the ERCOFTAC Industrial Advisory Committee (IAC) is to pose the big flow, turbulence and combustion (FTAC) questions from the industrial point of view and then promote and enable FTAC research programmes which match innovation to industrial need.

In order to strengthen its role in this area, the IAC is initiating a dialogue with industry so as to establish their priority needs. After consultation and analysis, these needs will be translated into targeted research programmes. Researchers will then be encouraged and supported by the IAC to pursue such programmes using funds from the EU and other sources. As a first step, a questionnaire is being circulated to European industrial organisations with interests in flow, turbulence and combustion. This can be found on the ERCOFTAC web page (www.ercoftac.org, under the left side menu window, «Industrial Consultation Initiative»). The response to this questionnaire will be analysed and themes which need further development will be identified. Workshops will then be held in each country to explore these themes with the aim of refining them into key elements of industrial need which can then be readily translated into targeted research programmes.

The IAC welcomes the participation of all industrial organisations in this initiative and we invite key technical personnel to spend a few minutes completing the questionnaire (www.ercoftac.org, under the left side menu window, «Industrial Consultation Initiative»).

Please return to:

A. G. Hutton
Deputy Chairman of the Industrial Advisory Committee
G26/X80
QinetiQ Ltd.
Cody Technology Park
Ively Road
Hants. GU14 0LX
U.K.
Tel.: +44 1252 395568
Fax: +44 1252 395275
Email: aghutton@qinetiq.com

MODELLING HEAT TRANSFER IN HUMANS

A. Frijns, G.M.J. van Leeuwen, A.A. van Steenhoven

Deptartment of Mechanical Engineering, Eindhoven University of Technology
P.O. Box 513, 5600 MB Eindhoven, The Netherlands

a.a.v.steenhoven@tue.nl

Abstract

Temperature plays an important role in the functioning of biological systems. To predict tissue temperatures, the influence of blood flow must be accounted for. The collective effect of blood vessels in a tissue volume may be reasonably successfully described by a heatsink. This is for instance the case in our study of using scalp cooling to prevent hair loss induced by chemotherapy. In the calculation of overall temperature distributions the thermoregulatory mechanisms of vasoaction, sweating and shivering need to be considered. Models get increasingly sophisticated, but accurate predictions for individuals (rather than average behaviour) remain difficult because of the many influencing factors. A predictive tool for individual patients, including effect of anaesthesia, is being developed for use during hypothermic (cardiac) surgery.

1 Introduction

Temperature influences the functioning of biological (sub)systems. For humans, the core temperature varies within narrow bounds around about 37°C. Changes in temperature can have significant consequences for the behaviour of individual cells and the body as a whole. The temperature dependence of biological processes can be used to clinical effect. Examples are hyperthermia treatment against cancer; cooling of the head to prevent hair loss as a side effect of chemotherapy; and cooling of patients during major surgery to protect the brain. Intervention can also be necessary to maintain or restore normal temperature, e.g. during or after exposure to harsh environmental conditions. Conversely, the functioning of cells influences temperature and hence temperature measurements can be used in diagnosis. Mathematical models have a role both in treatment and diagnosis. They can aid in predicting the time course of temperatures or in giving information on the temperature where (invasive) thermometry is lacking.

Heat transfer within the body takes place by means of conduction and convection. Convective transfer by blood plays a key role. Problematically, densities of blood vessels are very high and hence it is hard to compute a detailed temperature distribution in even a small part of the body while accounting for all of the blood vessels individually. Fortunately, the effects of the blood vessels can be described collectively with some success. In 1948, Pennes [13] devised his bio heat equation, also known as heatsink equation, in which the effects of all vessels are lumped together:

$$\nabla k_{\mathrm{tis}} \nabla T - W_{\mathrm{b}} c_{\mathrm{b}} \left(T - T_{\mathrm{art}}\right) + M = c_{\mathrm{tis}} \rho_{\mathrm{tis}} \frac{\partial T}{\partial t} \qquad (1)$$

Here, k_{tis}, ρ_{tis} and c_{tis} are respectively the thermal conductivity, density and specific heat of the tissue. In the heatsink term, c_{b} is the specific heat of blood, W_{b} the volumetric blood perfusion of the tissue [kg m^{-3} s^{-1}], and T_{art} the temperature of the arterial blood entering the volume. Finally, M is the volumetric rate of (metabolic) heat generation [W m^{-3}]. The bio-heat equation (1) describes the blood to tissue heat transfer as if it all takes place in the capillaries: blood reaches the capillaries with the temperature of the major supply artery. Subsequently, in the returning veins heat transfer with the tissue is again assumed negligible. The bio-heat equation has established itself as the most used continuum description of tissue heat transfer. Relatively good accuracy is achieved for highly perfused tissue (such as brain) because at high perfusion a relatively large proportion of the blood-tissue heat transfer does take place in the smallest vessels. But of course, heat transfer between tissue and blood does take place in vessels of all sizes. Because of this, firstly, the optimum continuum description also includes terms qualitatively different to the heatsink (effective conductivity, directed perfusion), and, secondly, large blood vessels can cause significant temperature inhomogeneities unpredictable by any continuum model. Especially in local hyperthermia therapy these inhomogeneities are extremely relevant and much effort has been put in the development of accurate thermal models that account for individual vessels. Much effort is put in the development of accurate models to take those effects into account and they are recently reviewed in van Leeuwen and van Steenhoven [10]. Here we will focus on the more global models, using the Pennes bio-heat equation.

2 Scalp cooling to prevent hair loss due to chemotherapy

Chemotherapy often makes cancer patients lose some or all of their hair. Although temporary, this hair loss is a much feared side effect of the therapy. Cooling the scalp during chemotherapy treatment can prevent or reduce hair loss (Protière, [14]) thanks to two mechanisms. The first is a reduction in skin blood flow during cooling, which reduces the delivery of the drugs. The second is

slower cell metabolism due to the lower temperature, resulting in less susceptibility to the drug. The success of scalp cooling varies strongly (Grevelman, [4]) which can be attributed to a lack of insight in the temperature dependence of these mechanisms and resulting uncertainty over the best cooling protocol. This is compounded by possible local variations in skin temperature and blood flow during cooling. Hence, a computer model is being developed which will describe all aspects of scalp cooling. The model includes sub-models to describe drug transport, heat transfer and hair follicle damage. Experiments are being conducted to find the necessary physiological and biological relations (Janssen et al., [6]). With the model complete, it will be possible to optimize the design and cooling protocol of scalp coolers. Here we will show some intermediate results.

The numerical model describing heat transfer in the head uses the Pennes heatsink (although perfusion in this case raises temperatures) equation. It was shown before that temperatures in a cooled neonatal head predicted with the Pennes model agreed well with predictions made including detailed discrete vasculature (Van Leeuwen et al., [8]). The head is approximated by a sphere, with layers representing different media: brain, skull, fat, skin, and hair (van Lenthe et al., [11]). Normal temperature profiles were first calculated, with metabolism and perfusion fixed at their basic values (Janssen et al., [7]). Subsequently the head was cooled by addition of a cap that was continuously supplied with cooling fluid with a temperature of -8°C. The normal tissue temperatures were used as the reference temperatures in the temperature dependent metabolism and blood flow relations and new steady state solutions were calculated. For typical tissue characteristics and hair layer thickness (see Fig. 1) the skin temperature drops from 34°C to about 18°C. It was shown that the thicknesses and thermal conductivities of the fat and hair layers are the most important parameters that influence skin temperature and perfusion. A hair layer thickness of 2 mm instead of the basic 1 mm decreased the skin temperature drop by 3.5°C, while instead a 0.5 mm layer increased the temperature drop by 8.2°C. In the former case the perfusion was still one third of that without cooling, but in the latter case the perfusion was less than one seventh. For the clinic, this means that a good fit of the cap is essential.

The large variation in perfusion reduction suggests that temperature is a major factor determining the amount of drugs delivered to the hair follicles. The temperature/perfusion model provides the necessary boundary conditions for a physiology based Pharmacokinetic (PBPK) model (Gustafson et al., [5]). Accounting for perfusion and temperatures of the scalp skin, the total amount of drugs that are delivered to the hair follicles can be estimated. The subsequent relations between drug delivery, extra cellular concentration, temperature, and hair follicle damage will be experimentally determined in the near future. The combination of sub-models will result in a complete model that can help in optimizing scalp cooling for hair loss prevention.

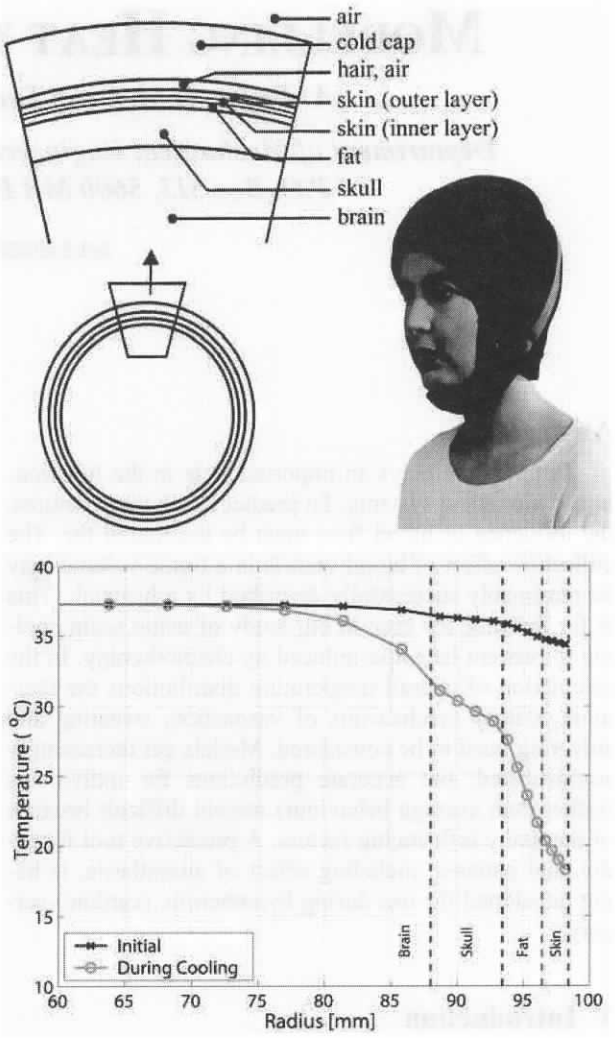

Figure 1: Upper left: configuration of the head model. Upper right: a typical scalp-cooling helmet. Down: temperature distribution in the head before and during cooling.

3 Human thermoregulation

The human body, when healthy, maintains its core temperature of about 37°C within small margins. The core consists of the brain and the internal organs in the trunk. Temperatures in the remaining parts of the body - `the periphery': surface tissue and the limbs - are much less constant. When environmental conditions vary, core temperature is maintained partly by behaviour (e.g. clothing), and partly by the body's thermoregulatory system.

Several models have been developed to describe whole-body heat transfer, from just two nodes describing core and periphery (e.g. Gagge et al., [3]) to multi-segment, multi-layered models. A recent model is that developed by Fiala et al. [1,2], which we adapted for our purposes (van Marken Lichtenbelt et al., [12]). The anatomy in Fiala's model consists of ten elements, see Fig 2, refining the earlier six segment model by Stolwijk [17]. Heat exchange with the environment takes place at the skin, and in the lungs/respiratory tract. The heat exchange by convection between skin or clothes surface and ambient air is described by a combined convection

coefficient that considers both natural and forced convection. Also the heat losses due to radiation and evaporation are taken into account. Within the body, elements are made up of concentric tissue layers and heat transfer is modelled using the Pennes equation, with perfusions under control of the thermoregulatory system. By increasing or reducing blood flow to the skin, the body can increase or lower the skin temperature and hence its heat transfer to the environment. The thermoregulatory relations (Fiala et al., [2]) for blood flow, as well as those for shivering and sweating were found by using regression analysis on measured data from a large number of experiments.

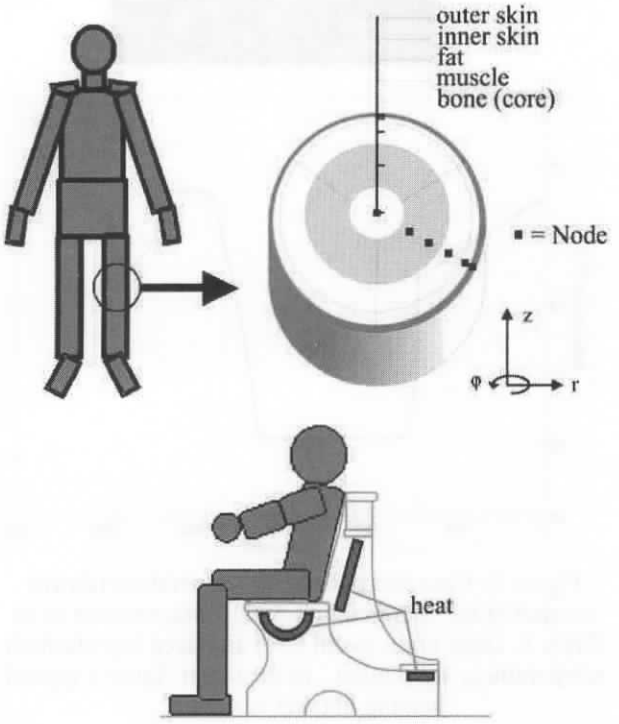

Figure 2: Top: Schematic representation of the model anatomy. The model is built from cylinders and a sphere for the head; the elements are divided in concentric layers and the layers, apart from the core are divided in sectors. Down: A schematic representation of the contact area of a person sitting on a pew with heat sources.

One informative use of the whole body model is the evaluation of different heating systems in monumental churches. Large temperature variations are damaging for the paintings, but high ceilings and poor insulation make the energy cost of constant heating in winter prohibitive. A possible way to save paintings and energy and still provide thermal comfort to churchgoers is by heating locally instead of heating the entire hall. This might be done by installing heating elements in the pews. In order for the heating system to work as effectively as possible experimental and numerical investigations are under way. The effect of radiative heaters in the pews is measured and calculated. A remarkable finding is the large influence of posture changes (sitting, standing) during the service.

4 Cardiac Surgery

Cooling is widely used to reduce metabolic demand and protect vital organs during open heart surgery. During cardiac surgery with cardiopulmonary bypass - the majority of cardiac surgical interventions - cooling is performed by means of the heart lung machine (HLM). The procedure consists of six distinct phases as detailed below:

1) The patient is anaesthetized. Due to anaesthetics the patient's metabolic rate is lowered and the threshold for vasoconstriction shifts to lower core temperatures. Furthermore the anaesthetics often contain vasodilatators. This leads to a lowering of the core temperature by approximately 2°C.
2) The first stage of the actual surgery: the thorax is opened.
3) The body is connected to a HLM which takes over the functions of heart and lungs. The HLM contains a heat-exchanger in which blood exchanges heat with water. In this stage the patient is cooled by adjusting the water temperature.
4) The main cardiac surgical procedure takes place and the body is kept at a constant low temperature. The temperature depends on the surgical intervention and can be near 30°C but also as low as 16-18°C.
5) On nearing completion of the surgical procedure the body is warmed at a steady rate by adjusting the water temperature of the heat exchanger. Rewarming must take place slowly in order to prevent cell damage. Because of their higher perfusion, core body parts (thorax and brain) react faster on rewarming than peripheral parts (arms and legs).
6) Once the core organs have reached the target temperature the patient is disconnected from the HLM and consequently control over the core temperature is relinquished. This often results in a phenomenon known as afterdrop: the core temperature temporarily drops. This effect is considered to be a result of the large temperature difference between the core and peripheral regions at the moment of decoupling (Sessler, [15]).

Patients who experience a large afterdrop need longer to recover and may experience more post-operative complications than patients who do not. Clinicians try to minimize the afterdrop as much as possible. Often forced-air heating blankets that are draped over the patient's legs are used in the rewarming phase. In this way the temperature gradient between the core and the periphery decreases. For the prevention of the afterdrop effect more knowledge about heat transfer in the anaesthetized human body during cardiac surgery is needed. We are building a numerical thermal model of the patient that can be used by clinicians to determine the optimal warming protocol in order to avoid afterdrop.

If the normal thermoregulatory model can be thought of to consist of two layers, describing respectively the physics of the system and the changes in this system by thermoregulation, then anaesthesia adds a third layer, describing the changes in thermoregulatory relations by anaesthetics and other drugs (van Leeuwen et al., [9]).

The most obvious change due to anaesthetics that should be implemented is a lowering of the thermoregulatory thresholds for vasoconstriction and shivering. Because a perioperative phase in which the effects of anaesthetics gradually wear off may need to be modelled, a variable was introduced that is a measure for the level of anaesthesia, Ca ($0 < Ca < 1$). There is currently only one variable Ca in the model, but it could be useful to consider using multiple anaesthetic variables in the case of multiple agents, and/or to have different Ca's for different tissue types in the body, reflecting different rates of uptake. Temperature shift parameters were introduced that shift the normal thermoregulatory thresholds. Because the thermoregulation should be the same as normal for Ca = 0, these shifts were made dependent on the depth of anaesthesia.

Apart from the anaesthesia, several particular conditions that are pertinent during (cardiac) surgery need to be accounted for in the computations. E.g. the open thorax and the immediate effect of heating blankets. With respect to the latter, the heat transfer coefficient of Bair Hugger blankets (Arizant Healthcare, Eden Prairie, MN, USA) was experimentally determined from measurements of the time evolution of the temperature of a solid aluminium cylinder wrapped in a Bair Hugger blanket.

Time [min]	Simulation
0-70	Supply anaesthetics: Ca=1, T_{room}=18°C, shivering prohibited
70-160	Cooling patient till 30°C, Ca=1, shivering prohibited
160-210	Rewarming till 37°C , using heating blanket, Ca=0
210-270	Decoupling from heart lung machine, using heating blanket, Ca=0

Table 1: Characteristics of the surgical procedure simulated with the model

With the 'in progress' model we simulated the temperature course during a cardiac operation (Severens et al., [16]). The procedure is characterized by the values in Table 1. In the simulation shivering is impaired during the first two phases. During the last two phases (t=160-270 min.) we assume that shivering is re-establishing. Also vasomotion is returning to a normal level. In Figure 3 the results for core and peripheral temperatures are shown. This result shows the main temperature characteristics as also observed in literature, like the slower reaction of the periphery compared to the core to the arterial blood temperature changes prescribed by the HLM and the characteristic afterdrop after decoupling the HLM.

Uncertainties in the model exist about the moment shivering actually starts and the chosen values in the vasomotion relations during surgery. Clinical data is now being collected to validate and refine the control equations - vasodilatation, vasoconstriction and shivering - for patients that undergo open heart surgery.

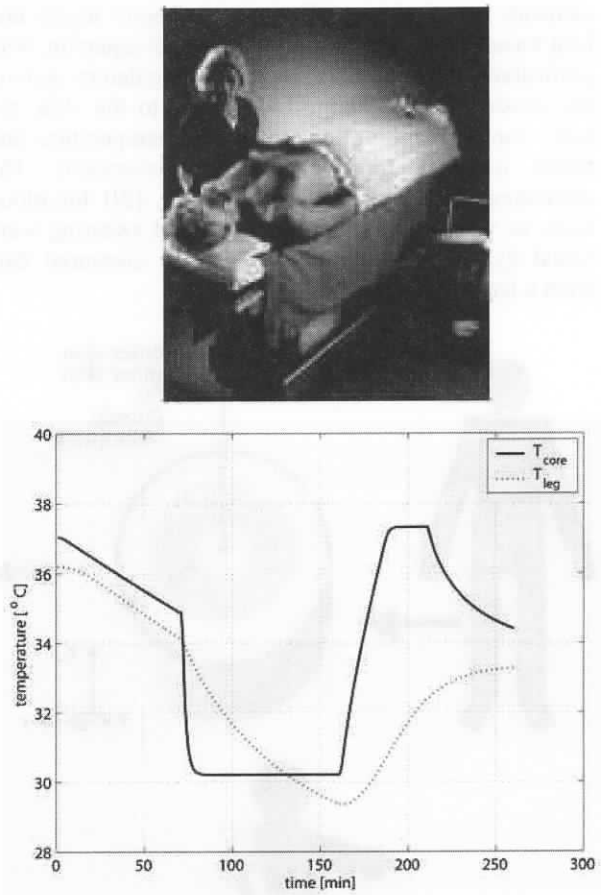

Figure 3: Core and peripheral temperature (down) computed for the operation with characteristics as in Table 1. Deep brain (solid line) and deep leg (dashed) temperatures are plotted. In the upper figure a typical heating blanket is shown.

4 Conclusion

Intricate biological and physical processes determine temperatures in humans. With the appropriate assumptions and simplifications usable predictions can be made. To make precise predictions for individuals in specific conditions extensive data acquisition is essential. For detailed temperature distributions this will include acquisition of tissue and vessel anatomy. For overall behaviour this could mean many individual parameters influencing thermoregulation.

Acknowledgements

The PhD-students ir. F.E.M. Janssen and ir. N.M.W Severens perform most of the work presented here. The projects are carried out in close collaboration with medical partners. The human thermoregulation is investigated together with dr. W.D. van Marken Lichtenbelt (Human Biology, Maastricht University), the scalp cooling together with dr. W.P.M. Breed (former Catharina Hospital) and the rewarming of patiens after cardiac urgery together with prof. B.A.J.M. de Mol (Academic Medical

Center, Amsterdam). The church-heating problem is analysed together with ir. D. Limpens-Neilen and dr. H.L. Schellen (FAGO, Eindhoven University of Technology). We are fortunate that in building our own models we could build on the model developed by dr. Fiala, now at De Montfort University (UK).

References

[1] D. Fiala, K.J. Lomas, M Stohrer, A computer model of human thermoregulation for a wide range of environmental conditions: The passive system, J. Appl. Physiol., 87:1957-1972, 1999.

[2] D. Fiala, K.J. Lomas, M Stohrer, Computer prediction of human thermoregulatory and temperature responses to a wide range of environmental conditions, Int. J. Biometeorol., 45:143-159, 2001.

[3] A.P. Gagge, J.A.J. Stolwijk and Y. Nishi, An effective temperature scale based on a simple model of human physiological regulatory response, ASHRAE Trans, 77:247-257, 1971.

[4] E.G. Grevelman and W.P.M. Breed, Prevention of chemotherapy-induced hair loss by scalp cooling, Ann. Oncol., 16: 352-358, 2005.

[5] D.L. Gustafson, J.C. Rastatter, T. Colombo and M.E. Long, Doxorubicin pharmacokinetics: Macromolecule binding, metabolism, and excretion in the context of a physiologic model, J. Pharm. Sci., 91: 1488-1501, 2002.

[6] F.E.M. Janssen, G.M.J. Van Leeuwen and A.A. Van Steenhoven, Biological and physiological mechanisms of scalp cooling to prevent chemotherapy induced alopecia, Proc. Ercoftac Workshop/Abiomed Advanced Course on Blood Flow Modelling and Diagnostics, Abiomed Lecture Notes 6, Editor: T.A. Kowalewski, Warsaw, 405-414, 2005.

[7] F.E.M. Janssen, G.M.J. Van Leeuwen and A.A. Van Steenhoven, Modelling of temperature and perfusion during scalp cooling, Phys. Med. Biol., 50: 4065-4073, 2005.

[8] G.M.J. Van Leeuwen, J.W. Hand, J.J. Lagendijk, D.V. Azzopardi and A.D. Edwards Numerical modeling of temperature distributions within the neonatal head Pediatr. Res. 48: 351–356, 2000.

[9] G.M.J. Van Leeuwen, F.E.M. Janssen, W. van Marken Lichtenbelt, B.A.J.M. de Mol, A.A. van Steenhoven, Modelling patient temperature for improved thermal management during surgery, Proc. ASME -ZSIS International Thermal Science Seminar II; Editors: Bergles, A.E. et al., Bled, Slovenia, 363-368, 2004.

[10] G.M.J. Van Leeuwen and A.A. Van Steenhoven, Heat transfer in humans- local and whole-body, Proc. Ercoftac Workshop/Abiomed Advanced Course on Blood Flow Modelling and Diagnostics, Abiomed Lecture Notes 6, Editor: T.A. Kowalewski, Warsaw, 205-242, 2005.

[11] G.H. Van Lenthe, J. de Hoogh, W.P.M. Breed, A.A. van Steenhoven, Numerical modeling of scalp cooling to prevent hair loss induced by chemotherapy, Proc. 12th International Heat Transfer Conference; Editors: J. Taine, Grenoble, Vol.4: 555-560, 2002.

[12] W.D. Van Marken Lichtenbelt, A.J.H. Frijns, D. Fiala, F.E.M. Janssen, A.M.J. van Ooijen , A.A. van Steenhoven, Effect of individual characteristics on a mathematical model of human thermoregulation, Thermal Biol., 29, 577-581, 2004.

[13] H.H. Pennes, Analysis of tissue and arterial blood temperature in the resting human forearm, J. Appl. Physiol., 1:93-122, 1948.

[14] C. Protière, K. Evans, J. Camerlo, Efficacy and tolerance of a scalp--cooling system for prevention of hair loss and the experience of breast cancer patients treated by adjuvant chemotherapy, Support. Care Cancer, 10:529-37, 2002.

[15] D.I Sessler, Perioperative heat balance, Anesthesiology, 92: 587-596, 2000.

[16] N.M.W. Severens, WD. van Marken Lichtenbelt, G.M.J. van Leeuwen, A.A. van Steenhoven and B.A.J.M. de Mol, Heat transfer in cardiac surgery-a numerical and experimental approach, Proc. Ercoftac Workshop/Abiomed Advanced Course on Blood Flow Modelling and Diagnostics, Abiomed Lecture Notes 6, Editor: T.A. Kowalewski, Warsaw, 439-450, 2005.

[17] J.A.J. Stolwijk, A mathematical model of physiological temperature regulation in man, NASA contractor report CR-1855, Washington DC, 1971.

PhD/POSTGRADUATE POSITIONS

J.M. BURGERS CENTRE FOR FLUID MECHANICS (THE NETHERLANDS) :

Postdoctoral position in Two-Phase Flow and Heat Transfer in Furnace tubes. The position for two years is available in the multiphase pipe flow group of the Kramers Laboratory at Delft University of Technology. Staff and students at the Kramers Laboratory are involved in numerous projects on multiphase flow, both experimental and numerical. The project with the vacancy is part of a long-term research program on the improvement of the flow regime dependent two-phase pipe flow models for use in industrial design and operation. Running projects deal with two-phase gas lift enhancement, liquid loading of gas wells, oil/water well logging, long liquid slugs in stratified flow and dispersed two-phase flow simulations in tubes.

More details on the position can be obtained from Prof. René Oliemans (r.v.a.oliemans@tnw.tudelft.nl). For further information on the Multi-Scale Physics Department, Delft University, and the Burgers Centre, please look at the web sites: http://msp.tudelft.nl, http://tudelft.nl, and http://jmburgerscentrum.org. Applications from both The Netherlands and abroad are welcome.

10TH INTERNATIONAL WORKSHOP ON THE PHYSICS OF COMPRESSIBLE TURBULENT MIXING

PARIS, FRANCE

17-21 JULY 2006

http://www-iwpctm10.cea.fr/

THEME

This workshop aims to communicate updated information on fundamental aspects of turbulent mixing in flows subject to destabilizing acceleration in both compressible and incompressible fluids. Specific topics include (but are not limited to):

- Rayleigh-Taylor instability
- Richtmyer-Meshkov instability
- Mixing layers
- Coherent structures
- Experimental, numerical and theoritical studies
- New numerical and experimental technics
- Direct numerical simulation, large-eddy simulation and turbulence models
- Associated 2D and 3D models and flows
- Applications

This workshop will gather both oral and poster presentations as well as presentations of general interest given by invited speakers.

LOCAL ORGANIZING COMMITTEE

D. Besnard (CEA)
S. Bouquet (CEA)
J.-F. Haas (CEA)
M. Legrand (CEA) Chairman
J. Redondo (Universitat Politecnica de Catalunya, Barcelona)
M. Vandenboomgaerde (CEA)

ACCOMODATION

Accomodation will not be managed by workshop organizers, but a list of various hotels will be provided.

PROGRAM AND VENUE

Scientific sessions will run from Monday morning until lunchtime Friday. The oral presentations will be given in a tiered lecture theatre, equipped with all the necessary projection equipment, and posters will be displayed in one or two rooms to allow viewing during the breaks, as well as in dedicated poster sessions.

Oral and poster presentations will be given in the ENSTA-Ecole Nationale Supérieure de Techniques Avancées (National Institute for advanced Technologies, www.ensta.fr).

REGISTRATION

Registration will open in February 2006. The registration fee is not yet finalized. Preliminary figures suggest the conference fee, including a reception on the Sunday, lunches and the conference dinner, is likely to be about 550 euros per person, with a reduction for students. The registration deadline has been fixed very early (April 2006).

SPONSORSHIP

ERCOFTAC (www.ercoftac.org)
Commissariat à l'Energie Atomique/DAM Ile de France (www.cea.fr)
AWE plc (www.awe.co.ukl)

CONTACTS

A special electronic address is devoted to the Local Organizing Committee: iwpctm10@cea.fr.

All your E-mails concerning the Workshop have to be sent exclusively to this electronic address.

Mailing address:

Michel Legrand
IWPCTM 10 Local Organizing Committee Chairman
Commissariat à l'Energie Atomique
Centre DAM Ile de France
BP 12
F-91680 Bruyères le Chatel, France
Phone : +33.1.69.26.57.09
Fax : +33.169.26.70.94

For further information please visit the workshop web page at: http://www-iwpctm10.cea.fr

NEXT ERCOFTAC EXECUTIVE MEETINGS

The ERCOFTAC Executive meetings will be held on the following dates:

SCIENTIFIC PROGRAMME COMMITTEE AND INDUSTRIAL ADVISORY COMMITTEES:

May 4, 2006
Florence, Italy

October 26, 2006
Athens, Greece

EXECUTIVE COMMITTEE MEETING:

May 5, 2006
Florence, Italy

MANAGING BOARD AND GENERAL ASSEMBLY MEETING:

October 26, 2006
Athens, Greece

Please note that the meetings in **Florence** are on Thursday and Friday.

For further information contact Dr. Thierry Ursenbacher at the ERCOFTAC Coordination Centre (contact details inside the back page of the Bulletin).

BULLETIN THEMES AND PC REPORTS

PAST AND FUTURE

The ERCOFTAC Bulletin aims to publish news of, and of interest to, the ERCOFTAC Community every 3 months. Every second issue (March and September) is dedicated to a scientific theme. Pilot Centres are supposed to report occasionally on their activities, and the non-theme issues (June and December) since March 1996 should contain two Pilot Centre reports.

We list below the Themes and PC reports of past and planned future issues from 2003 to 2006. PC chairmen are asked to note when their report is due. A complete list of Bulletin themes can be found in the Bulletin section of the ERCOFTAC web server.Those interested in organising a theme issue or in contributing to planned theme issues are invited to contact the Coordination Centre.

2003

March	*Theme:*	Complex Flow Problems (I. Eames)
June	*PC reports:*	Germany South Nordic Spain (R. Castilla)
September	*Theme:*	Aeroacoustics (B. Boersma)
December	*PC reports:*	France South PC FranceWest PC Germany North PC

2004

March	*Theme:*	Geophysical and Environmental Turbulence Modeling (J. Redondo)
June	*PC reports:*	France PEPIT PC (delayed) Netherlands PC
September	*Theme:*	New Developments in Numerical Methods for CFD (D. Laurence & Ch. Hirsch)
December	*PC reports:*	Belgium PC Switzerland PC France PEPIT PC

2005

March	*Theme:*	Combustion (A. Turan)
June	*PC reports:*	Polish PC
September	*Theme:*	Design Optimisation (W. Haase, F. Menter)
December	*PC reports:*	Czech Republic PC Greek PC Italian PC (short report)

2006

March	*Theme:*	Bio Fluids (A. Van Steenhoven)
June	*PC reports:*	Germany West PC Italian PC UK PC
September	*Theme:*	Turbulence and Compressible Flow (P. Comte)
December	*PC reports:*	German South PC Nordic PC

Special Interest Groups

1. Large Eddy Simulation (LESig)
B.J. Geurts, University of Twente, NL
☎ 31.53.489.4125
Fax 31.53.489.4888
b.j.geurts@math.utwente.nl

2. Turbulent Boundary Layers
J. Morrison, Imperial College London, UK
☎ 44.171.594.5067
Fax 44.171.184.8120
j.morrison@ic.ac.uk

4. Turbulence in Compressible Flows
P. Comte, ULP, Strasbourg, F
IMFS
☎ 33.3.90.242.894
Fax 33.3.88.614.300
comte@imfs.u-strasbg.fr

5. Environmental CFD
H. Morvan, University of Nottingham, UK
☎ 44.115.846.6374
Fax 44.115.951.3898
Herve.Morvan@nottingham.ac.uk

8. Turbomachinery
M. Casey,
Universität Stuttgart, D
☎ 49.711.685.3516
Fax 49.711.685.3280
casey@itsm.uni-stuttgart.de

10. Transition Modelling
E. Dick,
Universiteit Gent
Gent, B
☎ 32.9.264.3301
Fax 32.9.264.3586
erik.dick@ugent.be

12. Dispersed Turbulent Two Phase Flow
M. Sommerfeld, Martin-Luther Universität, Halle-Wittenberg, D
☎ 49.3461.462.879
Fax 49.3461.462.878
Martin.Sommerfeld@iw.uni-halle.de

14. Stably Stratified and Rotating Turbulence
J.M. Redondo, UPC, Barcelona, E
☎ 34.93.401.7984
Fax 34.93.401.6090
redondo@fa.upc.es

15. Turbulence Modelling
K. Hanjalic, University of Technology, Delft, NL
☎ 31.15.278.1735
Fax 31.15.278.1204
hanjalic@wt.tn.tudelft.nl

20. Drag Reduction and Flow Control
K.S.Choi, Nottingham University, UK
☎ 44.115.9513.792
Fax 44.115.9513.800
Kwing-So.Choi@nottingham.ac.uk

21. Vortex Dynamics
D. Dritschel, Univ. of St-Andrews, Scotland
☎ 44.1334.463721
Fax 44.1334.463748
dgd@mcs.st-and.ac.uk

24. Variable Density Turbulent Flows
F. Anselmet, IMST, Marseille, F
☎ 33.4.91.505.439
Fax 33.4.91.081.637
Fabian.Anselmet@irphe.univ-mrs.fr

28. Reactive Flows
A. Tomboulides
Aristotle Univ. of Thessaloniki
Thessaloniki, GR
☎ 30.2310.991.306
Fax 30.2310.991.304
ananiast@enman.auth.gr

30. Wind over Waves
G. Stelling, Delft
University of Technology, NL
☎ 31.15.278.5426
Fax 31.15.278.4842
g.s.stelling@citg.tudelft.nl

32. Particle Image Velocimetry
M. Stanislas, Ecole Centrale de Lille, Villeneuve d'Asq, F
☎ 33.3.20.337.170
Fax 33.3.20.337.169
stanislas@ec-lille.fr

33. Transition Mechanisms, Prediction and Control
A. Hanifi, FOI, Stockholm, S
☎ 46.8.5550.4334
Fax 46.8.5550.3481
ardeshir.hanifi@foi.se

34. Design Optimisation
R. Schilling, TU München, D
☎ 49.89.289.16295
Fax 49.89.289.16297
schilling@lhm.mw.tum.de

35. Multipoint Turbulence Structure and Modelling
C. Cambon, ECL Ecully, F
☎ 33.4.72.186.161
Fax 33.4.78.647.145
cambon@mecaflu.ec-lyon.fr

36. Swirling Flows
M. Braza, IMFT, Toulouse, F
☎ 33.5.61.285.839
Fax 33.5.61.285.899
braza@imft.fr

37. Bio-Fluid Mechanics
A.A. van Steenhoven
Eindhoven Univ. of Technology, NL
☎ 31.40.2472.722
Fax: 31.40.2433.445 a.a.v.steen hoven@wtb.tue.nl

38. Microfluids and micro heat transfer (MicroSIG)
M. Favre-Marinet, LEGI, Institut National Polytechnique de Grenoble, Grenoble, F
☎ 33.4.76.825.049
Fax 33.4.76.825.271
michel.favre-marinet@inpg.fr

39. Aeroacoustics
B.J. Boersma, University of Technology, Delft, NL
☎ 31.1.5278.7979
Fax 31.1.5278.2947
b.j.boersma@wbmt.tudelft.nl

101. Quality and Trust in Industrial CFD (IAC SIG)
A.G. Hutton, QinetiQ, Farnborough, UK
☎ 44.1252.395.568
Fax 44.1252.395.322
ahutton@QinetiQ.com

102. ERCOFTAC Database Interest Group (Dbig)
ad interim
D. Laurence, UMIST, Manchester, UK
☎ 44.161.200.3704
dominique.laurence@manchester.ac.uk

The following activities have ceased: 3, 6, 7, 9, 11, 13, 16, 17, 19, 18, 22, 23, 25, 26, 27, 29 and 31.

This page lists the Special Interest Groups currently believed to be active and gives one contact person for each one.

Please notify any corrections to the Coordination Centre in Lausanne.

ERCOFTAC PILOT CENTRES

Austria-Hungary-Slovenia
Prof. H. KUHLMANN
Institute of Fluid Mechanics and Heat Transfer
Vienna University of Technology
Resselgasse 3/1/2
A - 1040 VIENNA
☎ 43.1.58801.32212
Fax 43.1.58801.32298
h.kuhlmann@fluid.tuwien.ac.at

Belgium
Prof. E. DICK
Universiteit Gent
Department of Flow, Heat and Combustion Mechanics
Sint Pietersnieuwstraat 41
B - 9000 GENT
☎ 32.9.264.3301
Fax 32.9.264.3586
erik.dick@ugent.be

Czech Republic
Prof. J. PRIHODA
Institute of Thermomechanics AS CR
5 Dolejskova
CZ - 18200 PRAHA 8
☎ 420.286.890.383
Fax 420.286.584.695
prihoda@it.cas.cz

France - Centre Henri Bénard
Dr. C. CAMBON
Ecole Centrale de Lyon
L.M.F.A. - B.P. 163
F - 69131 ECULLY Cedex
☎ 33.4.72.18.6161
Fax 33.4.78.64.7145
cambon@ mecaflu.ec-lyon.fr

France South
Dr. M. BRAZA
IMF Toulouse
UMR CNRS/INPT-N° 5502
Av. du Prof. Camille Soula
F - 31400 TOULOUSE
☎ 33.5.61.28.5839
Fax 33.5.61.28.5899
braza@imft.fr

France West
Dr. J.-P. BONNET
LEANP, CNRS
BP 30179
F - 86962 Futuroscope - Chasseneuil
☎ 33.5.49.36.6031
Fax 33.5.49.53.6001
jean-paul.bonnet@univ-poitiers.fr

Germany North
Dr. C. WAGNER
DLR
Inst. für Strömungsmechanik
Bunsenstrasse 10
D-37073 GÖTTINGEN
☎ 49.551.709.2261
Fax 49.551.709.2404
claus.wagner@dlr.de

Germany South
Dr. F. MENTER
ANSYS Germany
Staudenfeldweg 12
D - 83624 OTTERFING
☎ 49.8024.905.415
Fax 49.8024.905.417
florian.menter@ansys.com

Germany West
Prof. N. PETERS
RWTH-Aachen
Templergraben 64
D - 52056 AACHEN
☎ 49.241.809.4609
Fax 49.241.809.2923
n.peters@itm.rwth-aachen.de

Greece
Prof. N. VLACHOS
Dept. of Mechanical & Industrial Engineering
Univ. of Thessaly,
Athens Ave. - Pedion Areas
GR-38334 VOLOS
☎ 30.24.210.74094
Fax 30.24.210.74085
vlachos@uth.gr

Italy
Prof. F. MARTELLI
University of Florence
Dept. of Energy
Via Santa Marta 3
I - 50139 FIRENZE
☎ 39.055.479.6237
Fax 39.055.479.6342
martelli@ing.unifi.it

Nordic
Dr. S. WALLIN
Dept. of Mechanics
KTH
S - 10044 STOCKHOLM
☎ 46.8.790.7172
Fax 46.8.796.9850
stefan.wallin@foi.se

Poland
Prof. S. DROBNIAK
Tech. Univ. of Czestochowa
Thermal Machinery Inst.
al. A. Krajowej 21
PL-42 200 CZESTOCHOWA
☎ 48.34.3250.507
Fax 48.34.3250.555
imc@imc.pcz.czest.pl

Spain
Prof. E. ONATE
Universitat Politecnica de Catalunya - C.I.M.N.E.
Edificio C-1- Campus Norte
Gran Capitan s/n.
E - 08034 BARCELONA
☎ 34.93.401.6035
Fax 34.93.401.6517
onate@cimne.upc.es

Switzerland
Prof. P. MONKEWITZ
EPFL - STI - ISE - LMF
ME B2 485, Station 9
CH - 1015 LAUSANNE
☎ 41.21.693.5322
Fax 41.21.693.5307
peter.monkewitz@epfl.ch

The Netherlands
Prof. G. OOMS
J.M. Burgerscentrum
Mekelweg 2
NL - 2628 CD DELFT
☎ 31.15.278.3216
Fax 31.15.278.2979
g.ooms@wbmt.tudelft.nl

United Kingdom
Prof. A.B. CROWLEY
Cranfield University (RMCS)
Shrivenham, Swindon
UK - Wilts, SN6 8LA
☎ 44.1793.78.5277
Fax 44.1793.78.4196
a.b.crowley@cranfield.ac.uk

Chairman

Prof. R.V.A. OLIEMANS
Multiphase Flow B.V.
Noord Houdringelaan 30
NL - 3722 BR Bilthoven, The Netherlands
☎ +31.30.229.1719
Fax +31.15.278.2838
oliemans@globalxs.nl

Seat, Administration and Development Office

Prof. Ch. HIRSCH
ERCOFTAC
Av. Franklin Roosevelt 5
B - 1050 - Brussels / Belgium
☎ +32.2.643.3572
Fax +32.2.647.9398
ado@ercoftac.be

Coordination Centre

Dr. T. URSENBACHER
ERCOFTAC - Coordination Centre
EPFL STI ISE ERCOFTAC
ME B2 495, Station 9
CH - 1015 Lausanne / Switzerland
☎ +41.21.693.5305
Fax +41.21.693.5307
ercoftac@epfl.ch

The ERCOFTAC Best Practice Guidelines for Industrial Computational Fluid Dynamics

The Best Practice Guidelines (BPG) were commissioned by ERCOFTAC following an extensive consultation with European industry which revealed an urgent demand for such a document. The first edition was completed in January 2000 and constitutes generic advice on how to carry out quality CFD calculations. The BPG therefore address mesh design; construction of numerical boundary conditions where problem data is uncertain; mesh and model sensitivity checks; distinction between numerical and turbulence model inadequacy; preliminary information regarding the limitations of turbulence models etc. The aim is to encourage a common best practice by virtue of which separate analyses of the same problem, using the same model physics, should produce consistent results. Input and advice was sought from a wide cross-section of CFD specialists, eminent academics, end-users and, (particularly important) the leading commercial code vendors established in Europe. Thus, the final document can be considered to represent the consensus view of the European CFD community.

Inevitably, the Guidelines cannot cover every aspect of CFD in detail. They are intended to offer roughly those 20% of the most important general rules of advice that cover roughly 80% of the problems likely to be encountered. As such, they constitute essential information for the novice user and provide a basis for quality management and regulation of safety submissions which rely on CFD. Experience has also shown that they can often provide useful advice for the more experienced user. The technical content is limited to single-phase, compressible and incompressible, steady and unsteady, turbulent and laminar flow with and without heat transfer. Versions which are customised to other aspects of CFD (the remaining 20% of problems) are planned for the future.

The seven principle chapters of the document address numerical, convergence and round-off errors; turbulence modelling; application uncertainties; user errors; code errors; validation and sensitivity tests for CFD models and finally examples of the BPG applied in practice. In the first six of these each of the different sources of error and uncertainty are examined and discussed, including references to important books, articles and reviews. Following the discussion sections, short simple bullet-point statements of advice are listed which provide clear guidance and are easily understandable without elaborate mathematics. As an illustrative example, an extract dealing with the use of turbulent wall functions is given below:

- Check the lower limit of y^+. In the commonly used applications of wall functions, the meshing should be arranged so that the values of y^+ at all the wall-adjacent integration points is only slightly above the recommended lower limit given by the code developers, typically between 20 and 30 (the form usually assumed for the wall functions is not valid much below these values). This procedure offers the best chances to resolve the turbulent portion of the boundary layer. It should be noted that this criterion is impossible to satisfy close to separation or reattachment zones unless y^+ is based upon y^*.
- Check the upper limit on y^+. In the case of moderate Reynolds number, where the boundary layer only extends to y^+ of 300 to 500, there is no chance of accurately resolving the boundary layer if the first integration point is placed at a location with the value of y^+ of 100.
- Check the resolution of the boundary layer. If boundary layer effects are important, it is recommended that the resolution of the boundary layer is checked after the computation. This can be achieved by a plot of the ratio between the turbulent to the molecular viscosity, which is high inside the boundary layer. Adequate boundary layer resolution requires at least 8-10 points in the layer.
- Exercise care when calculating the flow usingdifferent schemes or different codes with wall functions on the same mesh. Cell centred schemes have their integration points at different locations in a mesh cell than cell vertex schemes. Thus the y^+ value associated with a wall-adjacent cell differs according to which scheme is being used on the mesh.
- Check that the correct form of the wall function is being used to take into account the wall roughness. An equivalent roughness height and a modified multiplier in the law of the wall must be used.

All such statements of advice are gathered together at the end of the document to provide a 'Best Practice Checklist'. The examples chapter provides detailed expositions of eight test cases each one calculated by a code vendor (viz FLUENT, AEA Technology, Computational Dynamics, NUMECA) or code developer (viz Electricité de France, CEA, British Energy) and each of which highlights one or more specific points of advice arising in the BPG. These test cases range from natural convection in a cavity through to flow in a low speed centrifugal compressor and in an internal combustion engine valve.

Copies of the Best Practice Guidelines can be acquired from

Prof. A.G. Hutton
QinetiQ
Building 880
Ively Road
Farnborough GUI401X
UK
☎ 44.1252.395.568
Fax 44.1252.395.322
Email: aghutton@qinetiq.com

The price per copy (not including postage) is:

Non-ERCOFTAC Members	150EUR (discount price for academics 75EUR)
ERCOFTAC Members	100EUR (discount price for academics 50EUR)